SYNTHESIS AND CHARACTERIZATION OF SILVER PHOSPHATE FROM LYOTROPIC LIQUID CRYSTALLINE MESOPHASE TEMPLATE AS A PHOTOCATALYST

A THESIS SUBMITTED TO

THE GRADUATE SCHOOL OF ENGINEERING AND SCIENCE

OF BILKENT UNIVERSITY

IN PARTIAL FULFILLMENT OF THE REQUIREMENTS FOR

THE DEGREE OF

MASTER OF SCIENCE

IN

CHEMISTRY

By

Nüveyre Canbolat

July 2018

SYNTHESIS AND CHARACTERIZATION OF SILVER PHOSPHATE FROM LYOTROPIC LIQUID CRYSTALLINE MESOPHASE TEMPLATE AS A PHOTOCATALYST

By Nüveyre Canbolat

July 2018

We certify that we have read this thesis and that in our opinion it is fully adequate, in scope and in quality, as a thesis for the degree of Master of Science.

_____

Prof. Dr. Ömer Dağ (Advisor)

_____

Prof. Dr. Ayşen Yılmaz

_____

Assoc. Prof. Dr. Emrah Özensoy

Approved for the Graduate School of Engineering and Science:

_____

Ezhan Karaşan

Director of the Graduate School

ABSTRACT

SYNTHESIS AND CHARACTERIZATION OF SILVER PHOSPHATE FROM LYOTROPIC LIQUID CRYSTALLINE MESOPHASE TEMPLATE AS A PHOTOCATALYST

Nüveyre Canbolat

M.S. in Chemistry

Advisor: Ömer Dağ

July 2018

Increasing energy demands and environmental problems are the driving forces of the current literature. Over the years, many new compounds have been synthesized and also morphological control of the well-known compounds have been the major topics to improve/contribute to the solutions of energy demand and environmental issues. One of these issues is finding an efficient and stable photocatalyst for some of the environmental problems. Ag_3PO_4 has been a target material for dye degradation and water splitting processes. Silver phosphate has a suitable band gap for photo-oxidation process under visible light irradiation. However, it has stability and reusability problems that needs to be resolved to effectively use as an efficient photo-catalyst. Because of that, many research worked on the synthesis and stability issues of this material. In this thesis, the work focuses on surfactant:Ag(I):H_3PO_4 lyotropic liquid crystalline mesophase to synthesize mesoporous Ag_3PO_4.

Two different surfactants (small, 10-lauryl ether, $C_{12}EO_{10}$ and large pluronic, triblock copolymer, P123, $HO(CH_2CH_2O)_{20}$-$(CH(CH_3)CH_2O)_{70}$-$(CH_2CH_2O)_{20}H$), two different silver salts ($AgNO_3$, SN and $AgCF_3SO_3$, AgOTf) and two different phosphate precursors (H_3PO_4 and LiH_2PO_4) have been used throughout this investigation. Solutions were prepared in water or ethanol by first dissolving surfactant, then adding stoichiometric ratio of $AgNO_3$, and H_3PO_4. To achieve clear and homogenous solution, a small amount of HNO_3 is added to the above solution. Without HNO_3, some yellow precipitation occurs that needs to be filtrated out. According to XRD patterns, SEM images, and N_2 adsorption-desorption isotherms, the yellow precipitate is bulk Ag_3PO_4. Decanted solution and normal acidified solution compares well with each other and the results are similar in

further steps of the synthesis. Therefore, adding small amount of HNO_3 to the solution overcomes the precipitation of bulk Ag_3PO_4 and used in further steps of the synthesis.

Then, the solutions can be spin or drop-cast coated over glass slides to form the mesophases and thin/thick films. The films diffract at small angles, indicating the formation of the mesophase. However, the mesophases are not stable and gradually transform into soft mesocrystals that diffract at small and high angles. Later step is to determine a desired calcination temperature for mesoporosity. Therefore, first a high temperature (over 300˚C) treatments have been applied to burn all surfactant in the films. This ensures mesoporosity, but it also results some bulk formations; silver metal forms at high temperatures. Therefore, the calcination or heat treatment temperature has been gradually reduced down to room temperature (RT). At RT, soft mesocrystal forms that can be heat treated at various low temperatures (70-150˚C) to form Ag_3PO_4 in many different morphologies; these samples have no silver metal. All Ag_3PO_4 samples, obtained under different conditions, were tested in Rhodamine-B (Rh-B) dye degradation by visible light irradiation with a good activity. But the catalyst is not stable under catalytic conditions. To solve this problem, some samples were prepared under vacuum to convert surfactants carbons to coat the surface of the catalyst by carbon that stabilized the catalyst.

In the last section of the thesis, cation exchange method has been developed to convert pre-formed mesoporous $LiMPO_4$ (M = Mn, Co, and Ni) to Ag_3PO_4. Mesoporous Ag_3PO_4 has been obtained from all precursors but the ones obtained from $LiCoPO_4$ performed the best in photo-degradation of dye under visible light and the ones obtained from $LiMnPO_4$ is almost inactive. Therefore, this part needs further studies to understand details of these observations.

Introducing carbon and cation exchange methods seem to be effective solutions for the stability problem of this photocatalyst. All synthesis products are tested in the photodegradation experiment and compared with each other. This thesis is partially clarified; how to synthesize mesoporous Ag_3PO_4, what the behavior of silver in system is, and how to stabilize the catalyst. Furthermore, the cation exchange process opens a new horizon for the Ag_3PO_4 synthesis.

Keywords: ***Ag_3PO_4, Lyotropic Liquid Crystalline Mesophase, Soft Mesocrystal, Photocatalyst, Cation Exchange.***

ÖZET

GÜMÜŞ FOSFATIN LİYOTROPİK SIVI KRİSTALLERİN MEZOFAZ BAZLI BİR FOTOKATALİZÖR OLARAK SENTEZİ VE KARAKTERİZASYONU

Nüveyre Canbolat

Kimya Yüksek Lisans

Tez Danışmanı: Ömer Dağ

Temmuz 2018

Artan enerji ihtiyaçları ve çevre sorunları araştırma çalışmalarını yönlendirmektedir. Yıllar içinde, birçok yeni bileşik sentezlenmiştir ve aynı zamanda iyi bilinen bileşiklerin morfolojik kontrolü, enerji ve çevre sorunlarının çözümüne katkıda bulunmak için hedef olmuştur. Bunlardan birisi de daha verimli ve uygun bir foto katalizör bulunmasıdır. Son zamanlarda, Ag_3PO_4 görünür ışık altında foto oksidasyon işlemi için uygun bant aralığına sahip boya bozulması ve suyun hidrolizi için kullanılır olmuştur. Bununla birlikte, etkili bir foto katalizör olarak etkin bir şekilde kullanılması için çözülmesi gereken kararlılık ve yeniden kullanılabilirlik sorunlarına sahiptir. Bu nedenle, birçok araştırma grubu bu materyalin sentezi ve kararlılığı konularında çalışmaktadır. Bu tez çalışması, yüzey aktif madde:Ag(I):H_3PO_4 liyotropik sıvı kristalin mezofazlardan yararlanılarak mezogözenekli Ag_3PO_4 sentezine odaklanmıştır.

Burada iki çeşit yüzey aktif madde (küçük, 10-lauryl ether, $C_{12}EO_{10}$ ve büyük pluronik triblok kopolimer, P123, $HO(CH_2CH_2O)_{20}$-$(CH(CH_3)CH_2O)_{70}$-$(CH_2CH_2O)_{20}H$), iki faklı gümüş tuzu ($AgNO_3$, GN and $AgCF_3SO_3$, AgOTf) ve iki farklı fosfat öncüsü (H_3PO_4 and LiH_2PO_4) kullanılmıştır. Çözeltiler ilk olarak yüzey aktif maddeyi su ya da etanol içerisinde çözüp, sonra stokiyometrik oranda gümüş nitrat ve fosforik asit eklenerek hazırlanmıştır. Homojen ve temiz bir çözelti elde etmek için az miktarda HNO_3 eklenmiştir. HNO_3 eklenmediği zaman, çözelti içerisinde oluşan sarı çökeltiler filtre ederek çözeltiden ayrılmıştır. XRD, SEM ve N_2 tutma-bırakma tekniklerin sonuçlarına göre, bu çökenlerin büyük Ag_3PO_4 kristaller olduğu anlaşılmıştır. Filtre edilen çözelti ve normal asitli çözeltilerin sonuçları birbirleriyle karşılaştırıldığı zaman aralarında çok büyük farklılıkların olmadığı anlaşılmıştır. Sonuç olarak, az miktarda HNO_3 eklenmesi bu sarı çökeltilerin oluşumunu durdurmuştur, bu nedenle diğer sentezlerde nitrik asit kullanılmıştır.

Çözelti hazırlandıktan sonra cam slaytların üstüne çevirmeli kaplama ya da döküp kaplama yöntemleri kullanılarak ince ve kalın filmler hazırlanmıştır. Bu filmlerin düşük açıdaki kırınımları mezofazın oluşumunu desteklemiştir. Fakat, bu faz çok kısa bir zaman içerisinde yumuşak mezokristallerine dönüşmektedir. Bunu da XRD de düşük ve yüksek açıda oluşan kırınımlar bize göstermektedir. Daha sonraki adım ise mezogözeneklerin oluşması için kalsinasyon sıcaklığının belirlenmesi işlemidir. Bunun için 300˚C seçilmiştir, çünkü tüm yüzey aktif madde bu sıcaklıkta yanarak istenilen mezogözenekler elde edilir. Ancak istenilen gözenekler tüm madde de homojen olarak oluşmamaktadır. Bazı bölgeler de gümüş metali ve büyük Ag_3PO_4 kristalleri görülmektedir. Bu yüzden, bu sıcaklığı düşürerek gözlemlere devam edildi. Oda sıcaklığında oluşan yumuşak mezokristallerin düşük sıcaklıklar da Ag_3PO_4 oluşumunun gözlenmesi sayesinde, sıcaklık aralığının 70-150˚C arası olduğu belirlenmiştir ve bu sıcaklık aralığında farklı morfolojilerde gümüş fosfatların oluştuğu saptanmıştır. Bunlar Rhodamine-B (Rh-B) boyası kullanılarak boya bozulması deneyinde görünür ışık altında test edilmiş ve sonuçlar oldukça tatmin edicidir. Kararlılık sorunu için yüzey aktif maddede bulunan karbonları aktifleştirmek için yakma işlemini vakum altında yapılarak gümüş fosfatlar karbon ile kaplanmıştır.

Son olarak, önceden oluşturulmuş mezogözenekli $LiMPO_4$'ü (M = Mn, Co ve Ni) Ag_3PO_4'e dönüştürmek için katyon değişim yöntemi geliştirilmiştir. Üsteki maddelerden mezogözenekli Ag_3PO_4 elde edilmiştir, ancak $LiCoPO_4$'ten elde edilenler görünür ışık altında boyanın ışıl bozunumunda en iyi sonucu verirken $LiMnP0_4$'ten elde edilenler neredeyse aktif değildir. Bu nedenle, bu gözlemlerin ayrıntılarını anlamak için daha fazla çalışmaya ihtiyaç vardır ve bu yöntemin yeni ufuklar açacağı ön görülmektedir.

Foto katalizörün karalılık problemi için aktif karbon ve katyon değişim yöntemlerinin tanıtımı etkili bir çözüm olarak görünmektedir. Tüm sentez ürünleri ışıl bozunumu deneyinde test edilmiş ve birbirleriyle karşılaştırılmıştır. Bu tez, mezogözenekli Ag_3PO_4'ün sentezlenmesinin, sistemdeki gümüşün davranışının ve katalizörün nasıl kararlı hale gelebileceği kısmını kısmi olarak açıklığa kavuşturmuştur.

Anahtar Kelimeler: ***Ag_3PO_4, Liyotropik Sıvı Kristal Mezofaz, Yumuşak Mezokristal, Foto katalizör, Katyon Değişimi.***

ACKNOWLEDGEMENT

Chemistry is coming from the observation of natural process; which is chemical reactions. Reactions of compounds creates our lives, colors, and all of living and unliving species. This amazing field gives me inspire to think and research on chemistry. When I participated to Prof. Dr. Ömer Dağ's group, I did not know about how to control my ideas in these big oceans. It is not possible to figure out everything. His excellent experience leads me shaping my research style systematically. He also helped to teach me how to ask and find a question as a scientist, then work hard to find reasonable answers without hesitation. Therefore, I would like to thank to him for all contributions throughout my life and this thesis. I am grateful to him in order to upgrade my passion to chemistry.

I want to thank my other two examining committee members; Prof. Dr. Ayşen Yılmaz and Assoc. Dr. Emrah Özensoy for their feedback and valuable time on my thesis.

I also would like to thank Associate Prof. Dr. Emrah Özensoy for photodegradation experiments' set up and procedures by sharing his lab, and his group members, Muhammad İrfan, Sean W. McWhorter, Merve Balcı, and Elnaz Ebrahimi. His graduate lectures inspired me to think differently and figure out new aspects.

I express my sincere appreciations to my all group members, Gülbahar Saat, Simge Uzunok, Assel Amirzanova, Işıl Uzunok, Irmak Karakaya, Ezgi Yılmaz, Mete Turgut, Guvanch Gurbandurdyyev, Nesibe Akmanşen, Gökçin Özin and other all alumni to give me unforgettable and precious memories in Dağ's group.

I want to give my thanks to Menekşe Liman, Elif Pınar Alsaç, Özge Bayrak, Bengisu Başbay, Zeynep Kap, Simay Aydonat, Damla Sürmeli and my all undergraduate friends for their emotional supports. Also, I express my thanks to Dr. Merve Uygunoğlu for her sincere friendship and emotional support.

I would like to thank Prof. Dr. Zeki Cemal Kuruoğlu for his emotional support and loving Quantum and Statistical Mechanics.

My special thanks and appreciate goes to my surgeon; Prof. Dr. Cavit Çöl for his patience, and support. During my master work and thesis, he gives me inspire to continue my normal life and not give up by calling me as a Professor.

I would like to thank to TUBİTAK (under 215Z193 project) for financial support.

Lastly but most importantly, I would like to thank to my mother, father, sister and brother. Without them, I could not exist and handle to scientific research. My mom always supports me emotionally, and inspirationally. My father always supports my strange ideas about chemistry, and he forced me to study Chemistry. My sister and brother always support me to laugh and to keep me alive. Without my family, I cannot come to this stage of my life.

To my remarkable family…

Contents

LIST OF FIGURES

LIST OF TABLES

CHAPTER 1

1.Introduction

1.1. Semiconductor electrode

There are three basic classification of solid materials; these are metals, polymers, and ceramics. Composites are combination of two or three of the above solids. This classification is based on their chemical compositions. [1] The solid materials have special properties such as magnetic, electronic, and optical. One concern of this thesis is the electronic properties of our target material, namely silver phosphate (Ag_3PO_4). Electronic properties of solid can be best understood by using band theory. According to band theory, semiconductors have occupied valance band (VB) and unoccupied conduction band (CB) with a gap, known as band gap (denoted as E_g). [1]

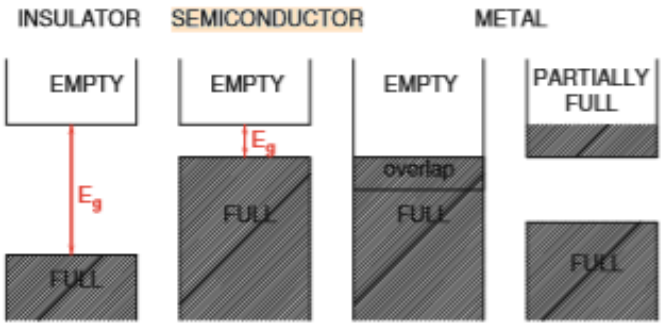

Figure 1.1.1. Energy band diagrams of insulators, semiconductor and metals [2][1]

[1] Reprinted by permission from [RightsLink]: [Springer Nature] Massimo Fischetti, and William G. Vandenberghe, Advanced Physics of Electron Transport in Semiconductors and Nanostructures [Copyright] 2016.

The solid materials can also be electronically classified into three types that are insulator, semiconductor, and conductor, see Figure 1.1.1. Semiconductors will be the main topic of this section. Semiconductor electrochemistry is an important field since Brattain and Garrett's experiments on the germanium. [3] They measured electrical potential of p- and n-type germanium in KOH, KCl, and HCl aqueous solution by redox couples, which describe a system of germanium electrode. [4] After stating basic principle of semiconductor electrochemistry, many of them have been used as electrodes in photo-electrochemistry applications and solar cells. Semiconductors are materials in which the valance and conduction bands are separated by energy band gap, see Figure 1.1.1. Figure 1.1.2 shows different representation of band diagram of semiconductors [3] that can be doped by an acceptor (p-type) or a donor (n-type) to enhance their electrical responses for various purposes.

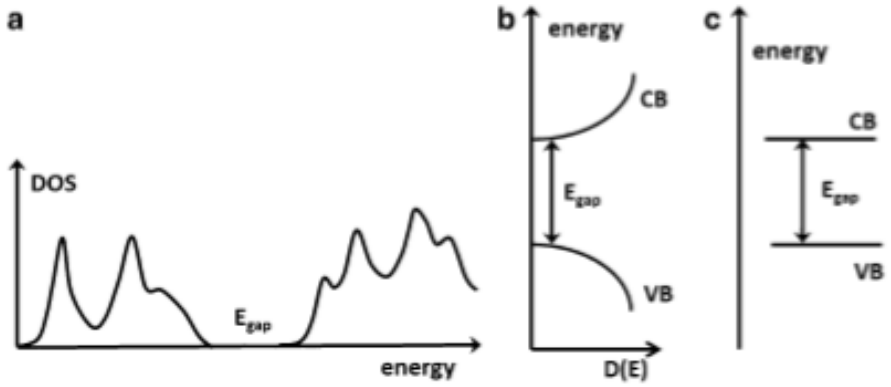

Figure 1.1.2. (a) Density of state (DOS) curve for a typical semiconductor; (b) parabolic approximation near band edges; (c) simplified band gap. [3][2]

[2] Reprinted by permission from [RightsLink]: [Springer Nature] Sixto Giménez, and Juan Bisquert, Photoelectrochemical Solar Fuel Production [Copyright] 2016.

Semiconductors are used for diodes, transistors and microelectronic circuit, and many other electrical devices, because of their unique electronic properties, [1] They may also have photocatalytic properties for many chemical reaction, carried by using sun-light. Generalized behavior of a semiconductor/electrolyte junction is that, when a photon with an energy of E_g or higher is absorbed by the semiconductor, an electron is excited across the VB to empty CB, creating free electron and hole in the semiconductor. Both electron and hole can be used for a chemical reaction. Giménez defined the photocatalysis as a process of exo-energetic oxidation involving illuminated oxides such as TiO_2. [3] By contrast, light-driven reactions that are endo-energetic, such as water splitting, should be referred to as photosynthetic reactions, although the term photocatalysis is widely misused in this context. The confusion is often compounded when a so-called sacrificial agent is used as an electron donor in order to generate hydrogen from illuminated solid. In this case, the generation of hydrogen may be exo-energetic. In other words, the electron in the CB is thermodynamically capable of reducing protons to hydrogen molecule. In this case, we are again dealing with photocatalysis and not photosynthesis. [3]

1.2. Silver Phosphate

Silver phosphate is an important semiconductor photo-catalyst that was investigated firstly by Wyckoff in 1925. His work showed that silver phosphate structure is R_3X crystal type from XRD data. In his paper, he noted Ag_3PO_4 is a colorless or light yellow cubic crystal. [5] Later Wyckoff and Helmholtz studied the crystal structure of silver phosphate in 1936, see Figure 1.2.1. [6] They evaluated some points related to crystallographic details. Then, in 1977, Calvo and Faggiani contributed a new parameter for this cubic structure. [7]

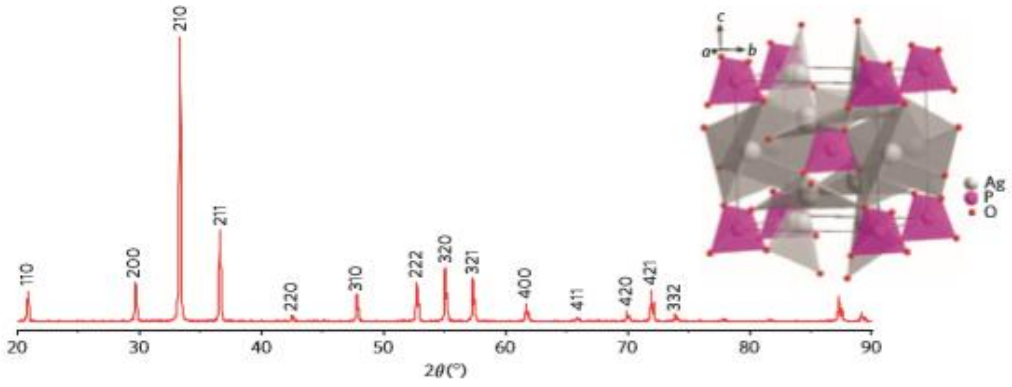

Figure 1.2.1. XRD pattern of bulk silver phosphate powder. [8][3]

Figure 1.2.1 shows the crystal structure and XRD pattern of cubic silver phosphate, first established by Wyckoff et. al. [5] [6] [7] After these contributions, there is limited investigations on silver-phosphate for a long time. Recently, Yi's group showed that silver-phosphate is a highly photo-active semiconductor with a convenient band gap

[3] Reprinted by permission from [RightsLink]: [Springer Nature] [Nature Materials] Zhiguo Yi, Jinhua Ye, Naoki Kikugawa, Tetsuya Kako, Shuxin Ouyang et al. An orthophosphate semiconductor with photooxidation properties under visible-light irradiation [Copyright] (2010).

energy towards dye degradation processes. Figure 1.2.2 shows a detailed band diagram of Ag_3PO_4. They also noted that silver phosphate can absorb energy with a wavelength shorter than 530 nm. Their study demonstrated that it has an indirect band gap of 2.36 eV [9] and direct band gap of 2.43 eV. [8] They did also DFT calculations to estimate the photochemical behavior, see Figure 1.2.2. According to this study, the bottom of the conduction band is hybridized silver 5s5p and phosphorous 3s orbitals, and the top of the valence band has hybridized silver 4d and oxygen 2p orbitals. [8] They also deduced that phosphorous in materials seems to adjust the band structure and redox power, which results in the high photooxidation by silver phosphate under visible-light irradiation, compared to Ag_2O that has a narrow band gap with a black color. [8]

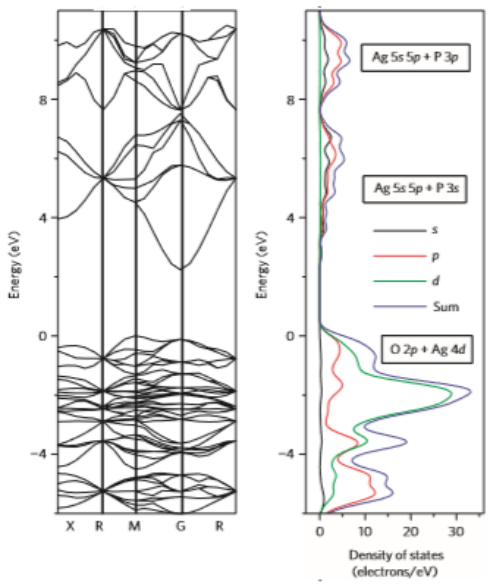

Figure 1.2.2. Energy Band Diagram and density of state curves of silver phosphate from Ref. [8][4]

[4] Reprinted by permission from [RightsLink]: [Springer Nature] [Nature Materials] Zhiguo Yi, Jinhua Ye, Naoki Kikugawa, Tetsuya Kako, Shuxin Ouyang et al. An orthophosphate semiconductor with photooxidation properties under visible-light irradiation [Copyright] (2010).

1.2.1 Photodegradation of dye molecules under visible light

Currently and in the near future, environmental pollution is becoming a huge problem for human lives. The most important substance of life is water (nature of life) and its pollution is threatening survival of life. [10] Dyes are used in many industrial areas such as textile, photography etc. Dye effluents are the contaminant of waste water with high toxicity, unacceptable color, high chemical oxygen demand content, and resistance to photochemical and biological degradation. [11] In recent years, motivation of the researchers is to solve environmental problems by dye degradation using semiconductors and light. Many studies and research groups demonstrated photodegradation of dye molecules by commonly used photocatalysts. To illustrate this, generally, TiO_2 based photocatalysts have been widely used under ultra-violet light illumination. However, doping of titania with other transition metals have modified the band structure to efficiently use titania under visible light illumination [12]. $Bi_{24}O_{31}Cl_{10}$ is an example of a p-block metal as a visible light photocatalyst [13]. Visible light irradiation is important for cost effective applications due to solar light as a light source. However, TiO_2 has a relatively wide band gap of 3.2 eV and limits efficient utilization of sunlight. Therefore, recent studies focused on the synthesis of visible light photocatalyst using other materials or doping TiO_2 with other metals. [14] A general dye degradation experiment is typically carried out using Rhodamin B (Rh-B) and methylene blue (MB), which are extensively used in industry. In this thesis, Rh-B dye has been used for photo-degradation experiments. Photo-degradation mechanisms have been discussed using many types of photocatalysts. The degradation mechanism is based on photooxidation process via production of hydroxyl radicals and superoxide ion radicals in the media, and holes in the

semiconductor, used as photocatalyst. [15] The following steps for the photo-degradation process are common in all photo-degradation process; the photo-catalyst absorbs the visible light and produce oxidative valance band holes and reductive conduction band electrons, where the electrons produce superoxide radicals by reacting with O_2, and oxidative holes contribute water oxidation to form hydroxyl radicals to oxidize organic dye. [9] This general mechanism is also valid for the silver phosphate photo-degradation of dye molecules under visible light. The only difference is that the silver ion acts as a scarifying agent and it is reduced to silver metal. This is major drawback of Ag_3PO_4 that decompose during the photo-catalytic process.

1.2.2. Photocatalysis of dyes using Ag_3PO_4

In 1925, Wyckoff investigated the cubic structure of yellow powder, silver phosphate. He obtained the Ag_3PO_4 crystals by precipitating from an aqueous solution of $AgNO_3$ and $NaNH_4HPO_4$. [5] Usually, the difference in the synthesis methods is the source of phosphate or orthophosphate ion. So far, $Na_2HPO_4.12H_2O$, Na_2HPO_4, H_3PO_4, Na_3PO_4, KH_2PO_4 etc. [7] [16] [17] [18] [19] have been used as phosphate source. However, there are also some modification methods to incorporate a second semiconductor such as titania, graphene etc. Preparation of these coupled semiconductor systems differs significantly. Even though silver phosphate has an appropriate energy band gap for dye degradation and water splitting application as a semiconductor, the biggest problem is its stability and reusability. Although it has an excellent photocatalytic activity, the catalyst also degrades after several use in a photocatalytic process. Therefore, silver phosphate has been modified to increase its durability by incorporating some other materials.

One study showed that titania nanotube-silver phosphate synthesis increased the photocatalytic property and stability. [19] In another study, silver phosphate-titanium dioxide nanocomposite fiber was hydrothermally synthesized to improve the photocatalytic activity and stability by showing 3 cycles of methylene blue dye degradation experiment.. [20]

After Yi's work, the silver phosphate photocatalytic activity studies focused on investigating its structure and bleaching mechanism of Ag_3PO_4 under visible light irradiation. [8] These investigations inspired us to demonstrate a new synthetic strategy for the silver phosphate using lyotropic liquid crystalline media for the synthesis of porous Ag_3PO_4.

In 2011, Cao-Thang Dinh published a new paper on a uniform colloidal silver phosphate. They synthesized silver phosphate with oleylamine to produce nanocrystals with a capped surface. They controlled the size in the range of 8-16 nm and noted that these nanocrystals enhanced the photoactivity under visible light. [21] However, their activity result is not any better than Yi's. In 2012, Qinghua showed the synthesis of porous microcubes of silver phosphate. [21] He noted that the value of surface area is 5.6 m^2 g^{-1} and the irradiation time for Rh B dye is 24 min only in first cycle. The stability problem was not mentioned. [22] Around the same time, Jin-Ku published a paper related to controlled synthesis of silver phosphate crystals. He showed silver phosphate with different morphology by collecting SEM images, see Figure 1.2.2.1. [23]

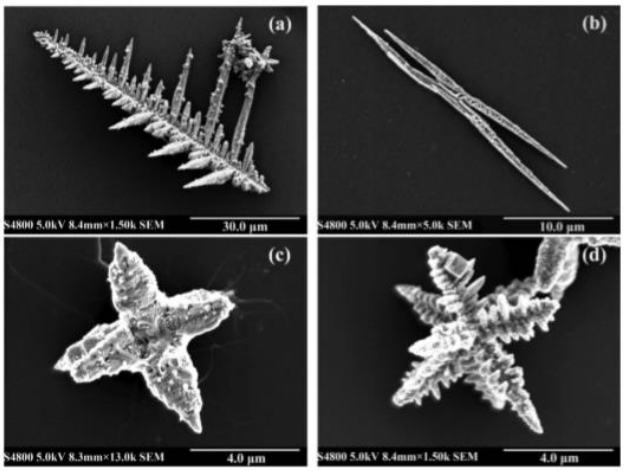

Figure 1.2.2.1. SEM images of Jin-Ku synthesis silver phosphate crystals. [23][5]

Another paper by Yingpu showed that the cubic and spherical silver phosphate have different photoactivity, 3 and 6 min for methylene blue dye degradation, respectively. The surface area of cubic structure was 2.32 m^2g^{-1} and spherical one was 2.55 m^2g^{-1} therefore the surface area may not be the reason for a better activity from the cubic crystals. [24]

Then, in 2012, Yingpu Bi et.al. synthesized silver phosphate on silver nanorods, and they found that the best photocatalytic activity is obtained from the Ag_3PO_4 on Ag-nanorods structure, see Figure 1.2.2.2. They showed that 2D structure minimized the probability of electron-hole recombination. [25]

[5] Reprinted by permission from [RightsLink]: [Royal Society of Chemistry] [CrystEngComm] Jin-Ku Liu,Chong-Xiao Luo,Jian-Dong Wang,Xiao-Hong Yang,Xin-Hua Zhong Controlled synthesis of silver phosphate crystals with high photocatalytic activity and bacteriostatic activity [Copyright] (2012).

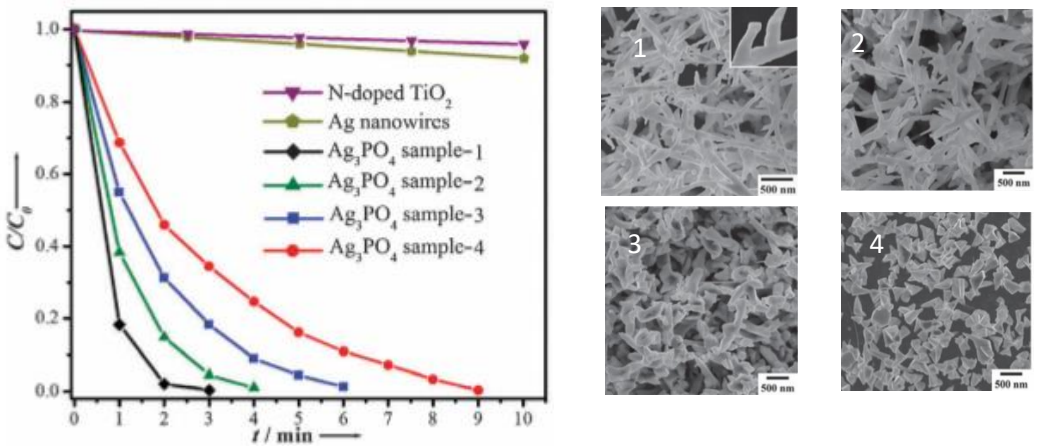

Figure 1.2.2.2. The C/C_0 vs. time graph of Yingpu silver phosphate with SEM images of them. [25][6]

The annealing temperature was investigated by Shuang between 100 and 500˚C. They did not find any transition from silver phosphate to silver or silver oxide, implied an excellent thermal stability of silver phosphate bulk crystals and also a better photocatalytic activity by annealing sample at 400˚C. [26]

The other studies are related to increase the photocatalytic activity of silver phosphate by introducing mesoporous silica, graphene, C_3N_4. [27] [17] [28] The list of synthesis methods, characterizations, and the enhanced photocatalytic activity studies is increasing exponentially since 2010. The common consensus is that silver phosphate is an excellent semiconductor photo-catalyst for dye degradation but, the problem of reusability (or stability) still need to be resolved.

[6] Reprinted by permission from [RightsLink]: [Royal Society of Chemistry] [Phys. Chem. Chem. Phys] Yingpu Bi, Hongyan Hu, Zhengbo Jiao,Hongchao Yu, Gongxuan Lu and Jinhua Ye Two-dimensional dendritic Ag3PO4 nanostructures and their photocatalytic properties [Copyright] (2012).

By checking above studies for a standard photo degradation of dye molecules, we found that every research group choose different mole ratio of dye and amount of silver phosphate. Adding more silver phosphate in a similar dye concentration solution clearly showed better results. Silver phosphate is known to show excellent photocatalytic behavior, but these papers may not be a good reference because of lack of knowledge about mechanism of degradation process.

1.3. Unique synthesis method

By inspecting all silver phosphate synthesis methods, we found that the synthesis is commonly based on precipitation in an aqueous solution; see section 1.2.2. In this thesis, a similar method will also be employed to obtain bulk crystals, but our synthesis method is based on the salt-surfactant lyotropic liquid crystalline templating. We will discuss the synthesis method and its advantages in the next section.

1.4. Liquid Crystals

Freidrich Reinitzer observed an interesting and different phase transition under polarizing microscope in 1889 from carrot extract and collaborated with Otto Lehmann to investigate the new transition more precisely. After these observations, they discovered liquid crystalline phase in their compound; cholesterol. [29] They introduced liquid crystals as a new type of state of matter to science community. Liquid crystals are liquid like and crystalline at the same time; therefore; they have typical properties of liquid (fluidic) and solid in terms of electrical, optical, and magnetic properties. [30] Thus, liquid crystalline state is among three states of matters as a mesophase, intermediate state, in terms of the orientational order and perfect three dimensional ordered structure like solid crystal and

the absence of long range order like liquids and amorphous solids. [31] This leads to molecular arrangement and visualization under the polarized optical microscope (POM). These are stated by Otto Lehmann, and Ernst Haeckel in 1917 and named Kristallseelen (crystal souls). [29]

Molecular arrangement of mesophases, liquid crystals, are divided into four mesophases types; i) nematic a view of isotropic surface, ii) cholesterics observed as a helical structure, iii) smectics outlook is focal conic texture, and iv) columnar as a hexagonal phase. [30] These phases display unique images under POM, see Figure 1.4.1. These division classified related to heat and solvent. [32] Thermotropic liquid crystals exist in a temperature interval and stable below melting point and above freezing point, however, lyotropic liquid crystals (LLC) are depend on a combined action of polar or amphiphilic and nonamphiphilic compound and concentration of certain solvents, such as water, ethanol etc. [33] [34] The main consideration in this thesis is LLC mesophase that can also be used as a templating media.

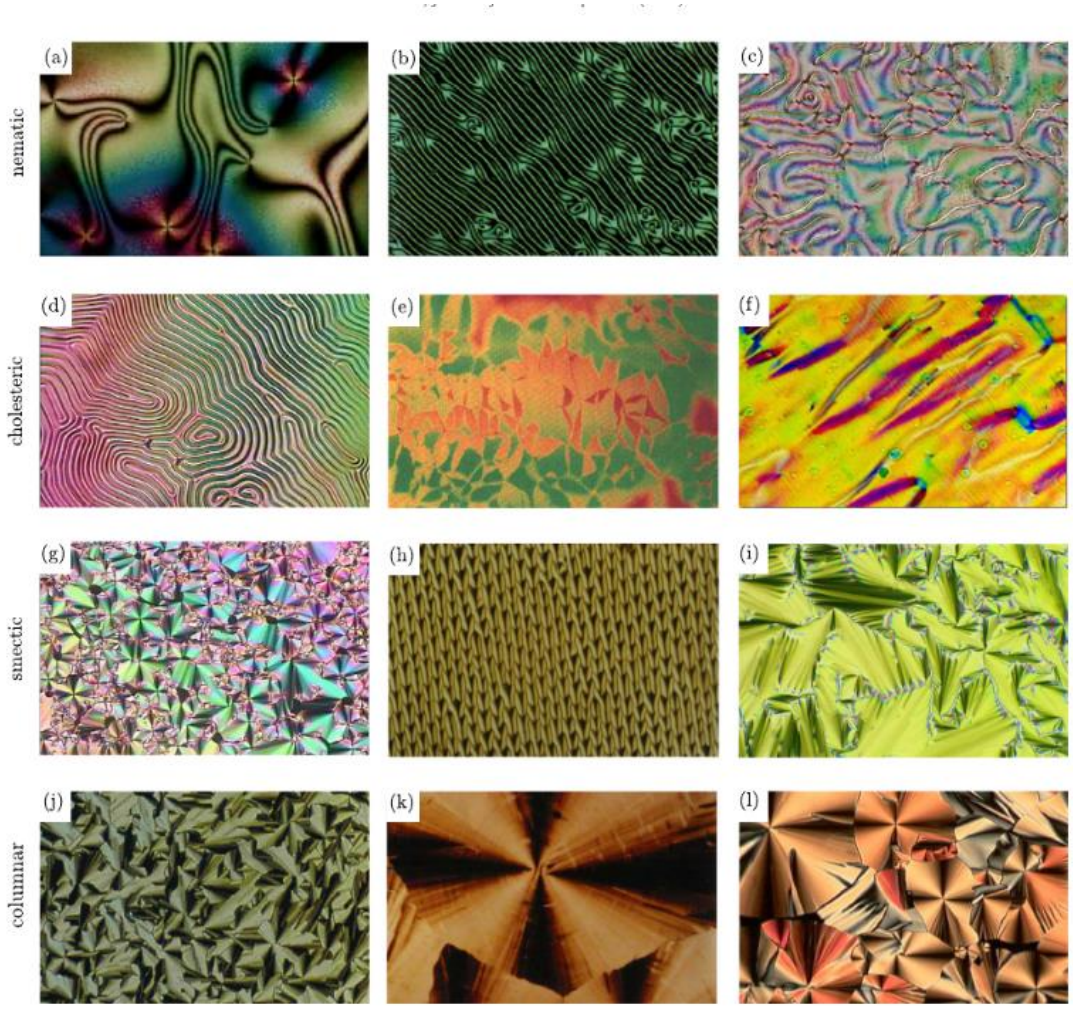

Figure 1.4.1. Liquid crystals types of mesophases under polarized microscope. [30][7]

1.4.1. Lyotropic liquid crystalline templating

Lyotropic liquid crystalline (LLC) phase form upon weak interaction of surfactant and solvent. Surfactants are amphiphilic molecules that contain both polar (head group) and nonpolar (tail group) parts. In an appropriate solvent (such as water), they self-assemble into micelles at a critical concentration (known as critical micelle concentration [35]);

[7] https://doi.org/10.1016/j.molliq.2018.01.175 under Creative Commons Attribution License.

micelles are aggregates of surfactant molecules with head groups in the aqueous media and tail groups inside the micelles. Self-assembly of micelles at higher surfactant concentration leads the formation of LLC mesophases that have unique structures, such as hexagonal (H_1), cubic (bicontinuous V_1 and micella I_1), and lamellar (L_1). With increasing surfactant amount, the LLC mesophases change from lamellar (increasingly densely packing) to hexagonal (rod-like structures with indefinite length), and finally to a cubic (monodomains) mesostructures. [32] [36] The structure of a cubic and hexagonal mesophase are shown in Figure 1.4.1.1. If the solvent is a nonpolar solvent, reverse micelles and reverse LLC mesophases can be formed, where tail groups are in the out-side and interaction with the solvent molecules and hydrophilic heads are hiding from the solvent media. Surfactant based LLC mesophases have been used as organic templates for synthesis of mesoporous molecular sieves in 1992, silicates, and latter many other porous materials have been synthesized. [37] [38] [39] [40]

In 2001 Dag's group discovered that poly (ethylene oxide) type non-ionic surfactants and many transition metal salts, later some alkaline and alkaline earth metal salts and non-volatile acids (such as H_3PO_4 and H_2SO_4) form stable LLC mesophases. [40] [32] [41] [42] [43] The salt-surfactant and acid-surfactant mesophases are stable to very high temperatures (60-150^o C). The reason of high stability has been explained by strong hydrogen bonding between the solvent and surfactant. Above mesophases can be considered as a network of hydrogen bonding, ion-dipole interaction between the micelle of surfactants and the solvent (salts and acids), in between these domains the salts species remains either solvated by water molecules or in the molten (melt) phase. [44] In such a small space salts species are in the liquid phase due to confinement effect. [45] Moreover,

the mesophases can be dissolved in water or any other solvent to obtain their clear solutions that can be spin-, dip-, and drop cast-coated over any substrate to reform the thin films of these mesophases. [46] These systems are ready for further reactions to form for instance mesoporous metal oxides, metal chalcogenides, metal phosphates, and metal sulphates.

Over the years, many studies showed that the LLC phases can be used as templates for mesoporous silica [47] [48], mesoporous metal sulfides [44] [49], mesoporous metals [42], metal oxides and mixed metal oxides [50] [51], catalytic Pd nanoparticles [52], and Pt, Pd, Ag nanotubes [53].

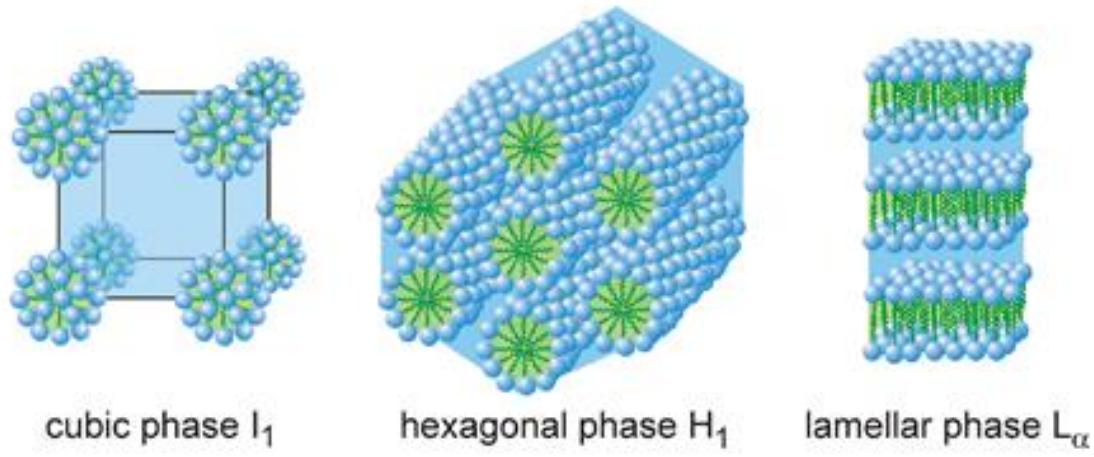

Figure 1.4.1.1. The schematic representations for LLC I_1, H_1i and L_α phases. [54][8]

In this thesis, the LLC templating is used for the synthesis of mesoporous silver phosphate. In this system, the only needs are solvents (water or ethanol), surfactant, phosphoric acid,

[8] Reprinted by permission from [RightsLink]: [Royal Society of Chemistry] [New Journal of Chemistry] Dirk Blunk, Patric Bierganns, Nils Bongartz, Renate Tessendorf and Cosima Stubenrauch New speciality surfactants with natural structural motifs [Copyright] (2006).

and silver salt. The LLC templating can be used to obtain mesoporous powder with high surface area. Introducing mesoporosity may enhance photocatalytic properties of Ag_3PO_4. Expectation from such structure is a better activity and high stability that may be achieved by *in-situ* incorporating surfactant as carbon species. The aim of using LLC templating for silver phosphate is to increase the surface area with mesoporosity as a transparent film to enhance photocatalytic activity and to improve stability by introducing carbon more effectively.

1.4.2 Soft Mesocrytals

Mesocrystals are oriented superstructure of nanocrystals by the process of mesoscale transformation, which are special type of colloidal crystals. [55] A fabrication of bottom up process for mesocrsytal is based on self-assembly of nanocrystal building blocks, colloids. [56] Cölfen reported that mesocrystals' formation process is the same as single crystals, the difference is mesoscale intermediate self-assembly. [55] In this decade, mesocrystals are known and studied systematically, but the first definition of mesocrystals was reported in 1986 for calcium carbonates in silica gel. [57] These mesocrystals have interesting shapes; called as sheaf of wheat.

To distinguish our mesocrystals from the above definition, our mesocrystals were named as soft mesocrystals. Other examples of soft mesocrystals are observed among biomaterials and biomimetic materials. It has been reported that many different structure types, by nanocrystal building blocks with mutual alignment exist in the literature. Nevertheless, a mechanism of mesocrystal process is not yet well understood. [58]

In 2013, ionic mesocrystals and lyotropic plastic crystals with unit-cell parameter in mesoscales were identified from LLC mesophases of several salt-surfactant at RT and called soft mesocrystals by Dag's group. [59] The shape of soft mesocrystals are dictated by the LLC mesophase. Therefore, magnificent images are observed under POM and SEM like sheaf of wheat. The soft mesocrystals are very stable. Another characteristic property is noticed at ATR-IR spectrum, when soft mesocrystal forms, all broad peaks become sharper, and they behave as gel and solid at the same time, called intermediate crystal types.

1.5. Cation exchange synthesis

Ion exchange was discovered by Thomson, Way and Roy in soils [60]; then it was used for water softeners and zeolites [61]. In solid-state chemistry, ion exchange for inorganic compounds is called cation exchange by Son. [62] The fundamental idea is the same as ion exchange process. Son's work showed that cation exchange is useful method to synthesize new type of inorganic compounds. [63] They synthesized Ag_2Se nanocrystals from CdSe by cation exchange method. [62] Their synthesis is based on solution-phases processing of colloids. Cation exchange synthesis is based on the exchange of cation of the solids by the cation in the solution. [64] The cation exchange method has been used because it is a fast and versatile process and also to get nanostructure, mesostructured, and morphology of the solid to the exchanged product that may not be produced by known methods. [65] [66] [67] [68] In this thesis, based on this concept, silver-phosphate is synthesized by cation exchange method in solution phase from mesoporous $LiMPO_4$s. The advantage is that the starting materials are mesoporous phosphate compounds and

exchanging metal ions by silver ion to get mesoporous silver phosphate may produce mesoporous silver phosphate.

1.6. The aim of this thesis

Since 2010 by Yi's work, the synthesis and photocatalytic properties of silver phosphate has been very widely studied. The reason is that silver phosphate has an excellent photocatalytic activity under visible light, as mentioned in previous sections. The synthesis procedure is the same as bulk silver phosphate. Therefore, many researchers obtained similar silver phosphate particles with similar disadvantages, like stability. Stability is a problem because silver ion transforms to silver as a scarifying agent during a photocatalytic processing. This needs a proper solution to use Ag_3PO_4 as an efficient photo-catalyst. Nevertheless, the solution is not easy and also not easy to understand whole process of silver phosphate behavior as a photocatalyst. If the problem is completely overcome, silver phosphate might be the future bench mark of photocatalyst.

In Tunkara's thesis [32], mesoporous calcium hydroxyapatite thin films have been synthesized using our approach. Addition of a small amount of silver nitrate to the initial synthesis media produce anti-bacterial thin films. Moreover, increasing silver nitrate amount produces yellow colored thin films, indicating the formation of Ag_3PO_4 embedded into mesoporous calcium hydroxyapatite. Therefore, we have employed the same method to produce pure Ag_3PO_4 using LLC mesophases by replacing calcium salt with silver salt. Thus, the LLCM templating may produce mesoporous silver phosphate as a transparent thin film.

The expectation under this concept is higher surface area with mesoporosity, high photocatalytic activity, nanostructured silver phosphate and introducing carbon more effective way to decrease silver formation in photodegradation experiment. Introducing carbon is important to reduce or eliminate the decomposition process. Therefore, we have prepared Ag_3PO_4 under various conditions and tested their photocatalytic properties under visible light.

The synthesis has been carried by using cation exchange, LLCM templating, and soft mesocrystal templating approaches. We also included the synthesis of bulk Ag_3PO_4 under our reaction conditions to test a large range of reaction condition for a more stable Ag_3PO_4.

CHAPTER 2

2.Experimental

2.1. Materials

In this work, silver nitrate, phosphoric acid, nitric acid, and 10-lauryl ether ($C_{12}E_{10}$, $C_{12}H_{25}(OCH_2CH_2)_{10}OH$, molecular weight 626 g/mol) and P123 ($EO_{20}PO_{70}EO_{20}$ (EO = ethylene oxide, PO = propylene oxide, molecular weight 5800 g/mol) as surfactants are used as purchased. All chemicals are bought from Sigma Aldrich and used without been stored for a long time. The concentrations of phosphoric acid, silver nitrate, and nitric acid are 85-88%, ≥99.5%, and 65%, respectively. Deionized water is obtained from Millipore synergy185 water purifier used in the preparation of all samples.

2.2. Sample Preparation

2.2.1. Preparation of Silver Nitrate-Phosphoric Acid (SNPA) Lyotropic Liquid Crystalline Mesophases

The LLC mesophases (LLCM) of these materials are prepared depending on characterization technique to be used. Generally, a mixture of 5 ml of deionized water and 1 g of 10-lauryl ether in closed glass vail is prepared by magnetic stirring for about 1 hour. After obtained well homogenized mixture, certain amount of phosphoric acid, nitric acid, and silver nitrate are added to the above mixture. The amount of silver nitrate and phosphoric acid are determined based on 1 g of surfactant and varied in a broad range. Thus, generally, 3 to 1 mole ratio of Ag/PO_4 is used. Table 2.2.1.1 and Table 2.2.1.2 show solution compositions from $C_{12}E_{10}$ and P123, respectively.

In a typical solution, the order of addition of the ingredients is as following; Dissolve 1 g of surfactant in 5 ml of water by stirring for 1 h, then add 0.365 g of phosphoric acid followed by stirring 30 min, finally add 0.3 ml of concentrated nitric acid followed by 1.621 g of silver nitrate and stir the mixture for another 30 min. After obtained well homogenized solution, the spin coating (2000-500 rpm) and drop casting (6 drops used to spread glass slide) method are used to produce thin films. Then the films are calcined in an oven as soon as possible. The films are calcined between 300 and 500˚C and the calcination time duration is 3 hours for spin coated samples and 5 hours for the thicker drop casted samples.

Table 2.2.1.1 Solution compositions for thin films from 10-lauryl ether.

Surfactant ($C_{12}E_{10}$)	*HNO_3*	*$AgNO_3$*	*H_3PO_4*	*$C_{12}E_{10}$:Ag:PO_4 Mole Ratio*
1 g	0.3 ml	0.810 g	0.183 g	1:3:1
1 g	0.3 ml	1.080 g	0.243 g	1:4:1.33
1 g	0.3 ml	1.621 g	0.365 g	1:6:2
1 g	0.3 ml	2.431g	0.548 g	1:9:3
1 g	0.3 ml	3.241 g	0.730 g	1:12:4
1 g	0.5 ml	4.321 g	0.973 g	1:16:5.33
1 g	0.5 ml	6.482 g	1.46 g	1:24:8

Table 2.2.1.2 Solution compositions for preparation of thin films from P123 solutions.

Surfactant (P123)	*HNO_3*	*$AgNO_3$*	*H_3PO_4*	*P123:Ag^+:PO_4^{3-} Mole Ratio*
1 g	0.3 ml	1.75 g	0.397 g	1:60:20
1 g	0.3 ml	3.51 g	0.793 g	1:120:40

2.2.2. Preparation of Bulk Ag_3PO_4 from Silver Nitrate-Phosphoric Acid (SNPA) solutions

The bulk silver phosphate is easily prepared without any special effort. In 2.2.1 section, it is mentioned how to prepare SNPA solutions. In here, the only difference is nitric acid. The ingredients are surfactant, water or ethanol, phosphoric acid and silver nitrate. The mole ratios of these are tabulated in **Table 2.2.2.1**.

The same steps in section 2.2.1 are followed up to addition of nitric acid. After adding certain amount of phosphoric acid, it is mixed to obtain a homogenous solution. These solutions, in a very short time, produce yellow fine precipitates upon adding certain amount of aqueous silver nitrate. After waiting all particles stalled down, products filter and wash first with water then with ethanol. Upon washing the samples, the precipitates are collected by either suction filtration or centrifugation than dried in a dark place. The dried samples are calcined at 300˚C for N_2 adsorption-desorption measurements. Also, all yellow particles are characterized using XRD, ATR-FTIR, SEM, and N_2 adsorption-desorption techniques.

Table 2.2.2.1 Solution composition for bulk Ag_3PO_4 samples.

Surfactant ($C_{12}E_{10}$)	*$AgNO_3$*	*H_3PO_4*	*$C_{12}E_{10}$:Ag:PO_4 Mole Ratio*
1 g	1.080 g	0.243 g	1:4:1.33
1 g	1.621 g	0.365 g	1:6:2
1 g	3.241 g	0.730 g	1:12:4
Surfactant (P123)	$AgNO_3$	H_3PO_4	P123:Ag:PO_4 Mole Ratio
1 g	1.75 g	0.397 g	1:60:20

2.2.3. Preparation of Soft Mesocrystals from Silver Nitrate-Phosphoric Acid (SNPA)

The preparation procedure is the same with 2.2.1 section SNPA system at room temperature. The aging time and temperature are varied from 1 min to 10 days and 70-100˚C, respectively with drop casted samples (6 drops on glass slide). The mole ratios and, aging times and calcined temperatures are tabulated at **Table 2.2.3.1 & 2**. All the samples are kept in a closed box and characterized using XRD, POM and ATR-IR techniques.

Table 2.2.3.1 Soft Mesocrystal Sample Preparation

Surfactant ($C_{12}E_{10}$)	*$AgNO_3$*	*H_3PO_4*	*$C_{12}E_{10}$:Ag:PO_4 Mole Ratio*
1 g	1.080 g	0.243 g	1:4:1.33
1 g	1.621 g	0.365 g	1:6:2
1 g	3.241 g	0.730 g	1:12:4
Surfactant (i.e. P123)	$AgNO_3$	H_3PO_4	P123:Ag:PO_4 Mole Ratio
1 g	1.75 g	0.397 g	1:60:20
1 g	3.50 g	0.794 g	1:120:40

Table 2.2.3.2 Soft Mesocrystal Sample Observation

Aging time	*Temperature*
0 min, 5 min, 10 min, 30 min, 1 h, 1-10 days	RT
0 min, 5 min, 10 min, 30 min, 1 h, 1-5 days	70˚C
After evaporation of water	90-100˚C
100˚C calcined film	Under SEM
Melting Point determination	25˚C-210˚C

2.2.4. Preparation of SNPA Using High Amount of Phosphoric Acid

The SNPA solutions are all stoichiometric (i.e. $Ag_3(PO_4)_1$ and its derivatives). The first procedure is the same as section 2.2.1, the only difference is phosphoric acid amount, see **Table 2.2.4.1**. ATR-IR, POM and XRD, SEM techniques are used for characterization part.

The second procedure is that 1 g of surfactant and certain amount of phosphoric acid like 3.65 g are mixed at 70˚C in oven to obtain a gel phase in 2-3 days. After obtaining homogenous gel phase, add aqueous solution of 0.810 g silver phosphate in hot gel. A whitish monolithic is formed. Washing with water yields yellow fine tiny particles.

In the third procedure no water is added to the media, however this procedure results a small explosion. Thus, it needs caution. 1 g of surfactant and high amount of phosphoric acid (18.25 g) are mixed, then solid silver nitrate is added to above mixture. After a while, an explosion occurred if the lid of vial is closed, therefore keep the vial open to atmosphere.

Table 2.2.4.1. Sample Preparation of Increasing Phosphoric Acid Amount

Surfactant ($C_{12}E_{10}$)	*$AgNO_3$*	*H_3PO_4*	*$C_{12}E_{10}$:Ag:PO_4 Mole Ratio*
1 g	1.080 g	0.243 g	1:4:1.33
		0.365 g	1:4:2
		0.730 g	1:4:4
		1.095 g	1:4:6
		1.46 g	1:4:8
		1.825 g	1:4:10
1 g	0.810 g	3.65 g	1:3:20
1 g	0.810 g	18.25 g	1:3:100

2.2.6. Preparation of SNPA by Introducing Carbon

The preparation procedure and steps are the same as all above sections. The only differences are in the calcination step. To introduce carbon, the samples are heated in a vacuum oven. The time duration was 6-8 hours. The calcination started as soft mesocrystal.

The bulk yellow precipitates (look Section 2.2.2) are used without washing step. The precipitate and remaining solution is placed in cuvette and then calcined for 6 hours at certain temperatures.

2.2.7. Preparation of Silver Triflate-Phosphoric Acid (STPA) Lyotropic Liquid Crystalline

The STPA preparation is the same as SNPA preparation procedure. The only difference is Ag^+ ion source, $AgCF_3SO_3$ is used in place of $AgNO_3$. The observation and results will be discussed in Chapter 3

Table 2.2.7.1. Sample Preparation of STPA

Surfactant ($C_{12}E_{10}$)	*HNO_3*	*$AgCF_3SO_3$*	*H_3PO_4*	*$C_{12}E_{10}$:Ag:PO_4 Mole Ratio*
1 g	0.3 ml	4.902 g	0.730 g	1:12:4
1 g	0.3 ml	4.902 g	1.46 g	1:12:8
1 g	0.3 ml	4.902 g	2.19 g	1:12:12
1 g	0.5 ml	4.902 g	2.92 g	1:12:16
1 g	0.5 ml	4.902 g	3.65 g	1:12:20
1 g	0.5 ml	4.902 g	4.38 g	1:12:24
1 g	0.5 ml	4.902 g	6.57 g	1:12:36
Surfactant (P123)	HNO_3	$AgCF_3SO_3$	H_3PO_4	P123:Ag:PO_4 Mole Ratio
1 g	0.5 ml	0.265 g	0.039 g	1:6:2
1 g	0.5 ml	2.652 g	0.397 g	1:60:20
1 g	0.5 ml	5.304 g	0.794 g	1:120:40
1 g	0.5 ml	5.304 g	0	1:120:0

2.2.8. Preparation of Ag_3PO_4 by Cation Exchange

Prepare a silver nitrate solution at a certain molarity (7 times higher than starting mesoporous compound) in 1:9 methanol:water (volume ratio), and then add the precursor compound that is $LiMPO_4$ (M= Ni, Co, Mn). After covering the solution with aluminum foil, stir the mixture for certain time, see Table 2.2.8.1 for details.

In general, 0.1M silver nitrate solution is prepared in 1ml of methanol and 9 ml of deionized water. Then, add 25 mg of $LiMPO_4$ into 0.1M silver nitrate solution. Put a magnetic stirrer, cover the vial with aluminum foil, and stir for 15 min. Then, centrifuge the solution to gather yellow powder, and wash with water, then dry in dark place.

The synthesis of $LiMPO_4$ has been carried in Işıl Uzunok's thesis study and the details of the synthesis will not be given here since thesis is not published yet. P123 is used as the surfactant. Overall procedure is similar to our synthesis, metal salts ($LiNO_3$ and $[M(OH_2)_6](NO_3)_2$) and phosphoric acid are used as precursors.

Table 2.2.8.1. Cation exchange with silver nitrate

$LiMPO_4$	*Water*	*Methanol*	*$AgNO_3$*	*Duration Time*
3 mg	10 ml	0 ml	17 mg	1 week
3 mg	9 ml	1 ml	17 mg	3 hours
25 mg	0 ml	10 ml	169 mg	5 days
25 mg	1 ml	9 ml	169 mg	1 day
25 mg	9 ml	1 ml	169 mg	15 min

2.3. Isotropization Measurement

SNPA thin films are prepared as in section 2.2.1. Then the films are placed on a controlled, Linkam LTS350 temperature controlling stage attached to a polarized optical microscope and a LinkamT95-LinkPad temperature programmer is used to control the temperature to determine the isotropization temperature. Heating and cooling procedures are varied between 1 and 5 ˚C/ min and the images of the thin films are captured by an inbuilt camera, attached at the top of the microscope.

2.4. Dye Degradation Experiment

Photocatalytic behavior of silver phosphate in aqueous solution are investigated under visible light using RhB dye. The measurement set up of Ozensoy research group is used for this purpose. The set up consist of fans, magnetic stirrer, visible light source in a metal box. For the tests, 25 mg of sample is dispersed in 30 ml of water by sonication for 5 min. Then, 6 ml of dye (from 60 mg/L concentrated solution)) is added to above solution in dark. Before exposing to visible light (the mixture was kept 30 min for adsorption of dye to the catalyst surface), 3 ml of sample is taken from the above vial to record a UV-vis spectrum as time zero. After turning lights on, a 3 ml of sample is taken from the solution to centrifuge tube after every certain time. After complete degradation experiment, all 3 ml of samples are centrifuged for 10 min. The spectra of these samples are recorded using a UV-Vis spectroscopy. From these data, C/C_0 vs time graph is obtained. After that, the reaming solution is reused for repeating the dye degradation experiment by first adding the centrifuged solids and then adding a fresh dye solution.

To observe the catalytic process, a similar experiment is carried under ambient room light conditions by immersing film samples over the glass slides to the dye solutions. 4 spin-coated glass slides are placed in a beaker with 100 ml of water and 2 drops of RhB dye.

2.5. ATR-IR Temperature Dependence

ATR-IR plate temperature range is 5-120˚C. Place 1 drop of SNPA solution on ATR-IR plate (diamond), and then increasing the temperature gradually. At each temperature, the ATR-IR spectrum is recorded

2.6. Instrumentation

2.6.1. X-Ray Diffraction (XRD)

Rigaku Miniflex diffractometer, generated with a Miniflex goniometer and an X-ray source with a Cu-Kα radiation, at 1.5405 Å wavelength, and 30 kV/15 mA is used to characterize all thin films and powder samples. Fresh samples of thin films' XRD pattern are measured between 1˚ and 5˚ with 0.5˚/min and Cu plate as a block sometimes inserts in front of detector to protect detector by reducing intensity of diffraction pattern (by a factor of 10). Calcined thin films and powders' XRD pattern are collected between 10˚ and 80˚ with 5˚/min. After that, the diffraction patterns are indexed by using Joint Committee on Powder Diffraction Standards (JCPDS) cards.

2.6.2. Polarized Optical Microscope (POM)

The phase transitions in all samples (fresh films coated by spin coating/drop casting) are monitored in transmittance mode by using a ZEISS Axio Scope.A1 polarized optical microscope. Top of the microscope has a camera to capture POM images.

2.6.3. UltraViolet-Visible Absorption Spectroscopy

A Varian Cary 5 double beam spectrophotometer is used to collect UV-Vis absorption spectra. The spectra measures with 100 nm/min scan rate and a resolution of 2 nm over a wavelength range from 200 to 800 nm in absorption mode. Quartz cuvette are used for solutions and quartz slide for the thin films.

2.6.4. Fourier Transform Infrared Spectroscopy (FTIR)

A Bruker Tensor 27 model FTIR spectrometer is used by attaching a Digi Tect TM DLATGS detector. The FTIR spectra are collected with a resolution of 4 cm^{-1} and 64 scans in 400-4000 cm^{-1} wavenumber range. The samples are prepared by making KBr pellets using 1% w/w samples.

2.6.5. Attenuated Total Reflectance Infrared Spectroscopy (ATR-IR)

A Bruker Alpha Platinum ATR-IR spectrometer with a Digi Tect TM DLATGS detector is used. The ATR-IR spectra are obtained at a resolution of 4 cm^{-1} in 400-4000 cm^{-1} wavenumber range using 32, 64, 128 scans. One drop of liquid samples places on ATR-IR diamond crystal stage and less amount of solid samples placed on the same stage with pressure part.

2.6.6. Scanning Electron Microscope (SEM) and Energy Dispersive X-Ry Spectroscopy (EDS)

A Zeiss EVO-40 SEM microscope is used for The SEM images operating with 15 kV. A Bruker AXS XFlash EDS detector 4010 attaches to microscope and it is used for elemental analysis. The samples prepare by spin coated on glass slide calcine at various temperature. Then scratch on glass slide. Another preparation is by coated on silicon wafers or on aluminum and calcine at certain temperature. Then these attach to sample holders with carbon adhesive tabs.

2.6.7. Transmission Electron Microscope (TEM)

A FEI Technai G2 F30 is used for TEM images operating with 200 kV. The sample preparation part is the same as above sections. Obtaining yellow calcined powders disperses in 10 ml of ethanol or water solution using a sonicator for 10 minutes. The dispersed solution is put on copper grids for TEM measurement after evaporating ethanol or water.

CHAPTER 3

3.Results and Discussion

In this chapter, general observation during the synthesis and role of various synthesis parameters will be discussed. In other words, this section aimed to show clear patterns on the SNPA system. Therefore, the sections of results and discussion part were planned according to elucidate the roles of; high (thin films) and low (soft mesocrystals) temperature, nitric acid, type of silver salt type (i.e. silver triflate versus silver nitrate), and cation exchange reactions using preformed $LiMPO_4$ particles. Then, all of these effects will be combined for the photo-catalytic activity.

3.1. SNPA: Lyotropic Liquid Crystalline Mesophases

The salt-acid-surfactant lyotropic liquid system [69] has been used to achieve high surface area by controlling the Ag_3PO_4 growth in confined space of hydrophilic domains of the mesophase, high activity due to high surface area, high stability by converting surfactants to carbon on the Ag_3PO_4 surface. Therefore, the first step is to establish the LLC mesophase of the AgX-H_3PO_4-S (S stands for surfactant) to obtain expectedly a mesoporous thin film of silver phosphate. First problem appears during the clear solution preparation step, where bulk Ag_3PO_4 particles form upon bringing $AgNO_3$ in contact with the phosphate source in the solution phase. Immediately, some yellow particles precipitate upon mixing these two precursors. The amount of Ag_3PO_4 precipitation is much more in ethanol solutions and less in water. Moreover, this precipitation can be completely eliminated upon addition of some nitric acid to the aqueous media. Acidification reduces

the PO_4^{3-} ion concentration below solubility limits of Ag_3PO_4 in the presence of some nitric acid (this will be discussed under the effect of nitric acid).

The clear solutions can be obtained upon either filtering out of the bulk Ag_3PO_4 crystals or by adding nitric acid to the media. Then these solutions can be either spin coated or drop cast-coated over a substrate. However, we found that the LLC phase is only stable for a short period of time upon coating the SNPA solution over a substrate and the coated gel-like mesophase undergoes slowly to form mesocrystals. These processes and the resulting Ag_3PO_4 upon various treatments will be discussed in the following chapters using various analytical techniques.

3.1.1. The Role of Nitric Acid and Other Synthesis Parameters in SNPA System

In preparation part of SNPA solution, a small amount of nitric acid, i.e. 0.3 ml, is added to the solution before adding $AgNO_3$ to the media. This eliminates the bulk Ag_3PO_4 formation and resulted clear solutions that are stable for certain time. Nevertheless, without nitric acid, the clear solution can be obtained upon separating the precipitates. Simply, high acidity of the media (can be achieved by adding nitric acid or decreasing pH by precipitating some of the silver ion as bulk silver phosphate) eliminates the bulk Ag_3PO_4 formation. Therefore, no further investigation has been carried on the role of nitric acid.

In this subsection, the effects of solvent, surfactant, amount of phosphoric acid, and temperature, on the bulk silver phosphate formation and decomposition of Ag_3PO_4 under light will be discussed by using SEM, EDS, XRD, ATR-IR data and photographic images.

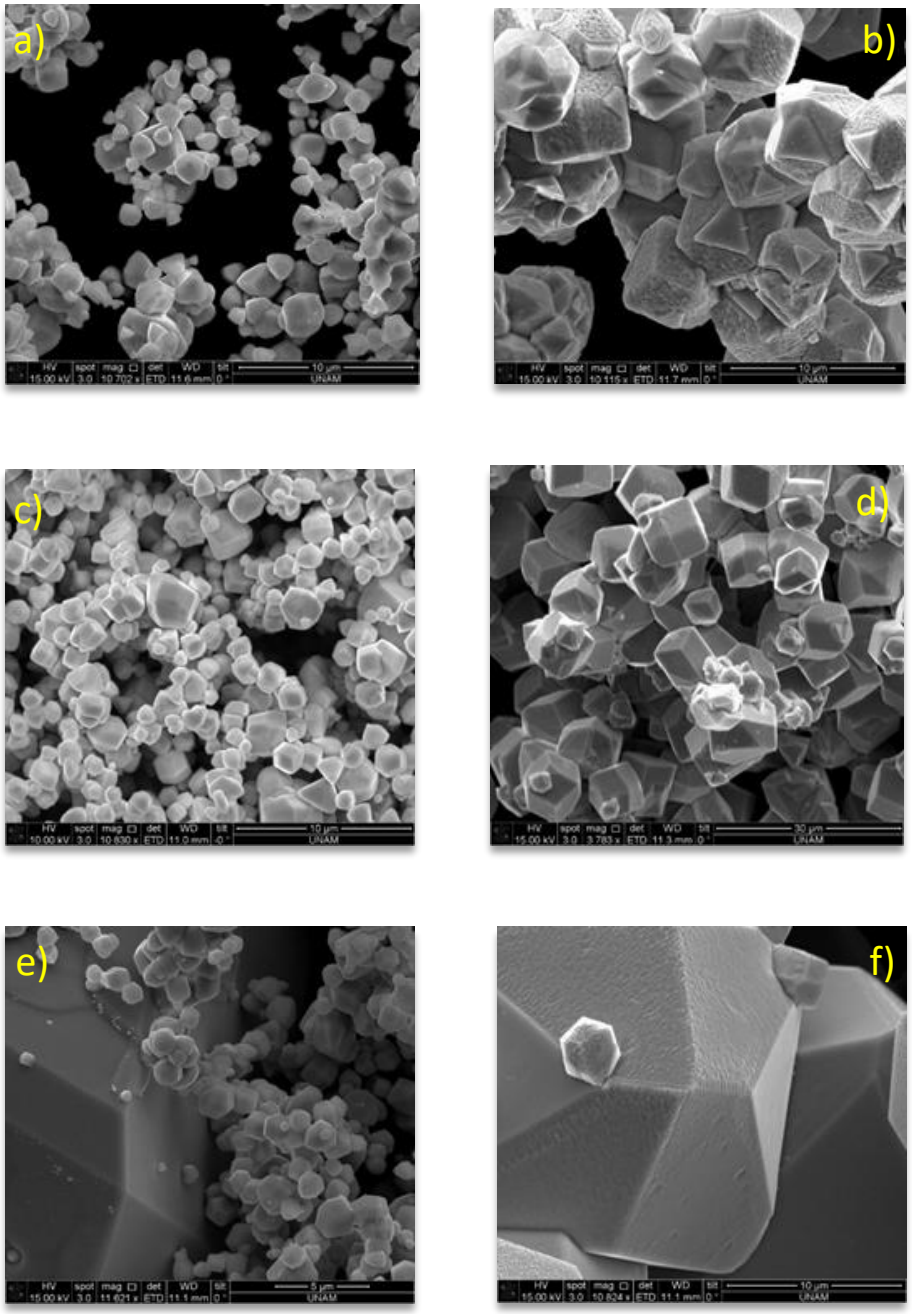

Figure 3.1.1. The SEM images of yellow precipitates in a) 1:6:2 ($C_{12}E_{10}$:$AgNO_3$:H_3PO_4) mole ratio of ethanol solution b)1:6:2 ($C_{12}E_{10}$:$AgNO_3$:H_3PO_4) mole ratio of water solution, c) 1:60:20 (P123: $AgNO_3$:H_3PO_4) mole ratio of ethanol solution ,d) 1:60:20 (P123: $AgNO_3$:H_3PO_4) mole ratio of water solution, e) 6:2 ($AgNO_3$:H_3PO_4) mole ratio of ethanol solution and f) 6:2 ($AgNO_3$:H_3PO_4) mole ratio of water solution.

It is noticed that yellow fine precipitates form much more in ethanol solutions rather than water solutions for both surfactants. Therefore, ethanol as a solvent is not preferred for thin film preparations. Nevertheless, in both water and ethanol, the color of precipitates is the same, but the rate and amounts are different. In other words, in ethanol case, the precipitation occurs immediately and yields around 300 mg of Ag_3PO_4, but, in water, the precipitation also occurs immediately with a lower yield of around 100 mg. This corresponds to 15 % and 5% of silver in each solution, respectively. Figure 3.1.1 shows the SEM images of the samples from these two solutions; the particles differ in morphology. In water, the cubic particles are uniform but with some deformation. In ethanol, the edges of the particles are smoother, thus, they look like spherical. However, there is no surfactant effect on morphology. Even though the morphology of the yellow precipitates is influenced by the solvent, rather than surfactant, choose of surfactant affects the size of crystals; an order of size of yellow precipitates is like;

$$P123 < C_{12}E_{10} < No\ surfactant.$$

Under these knowledge, Figure 3.1.2 shows the XRD patterns of these particles, the patterns display sharp diffraction lines, and all can be indexed to cubic Ag_3PO_4, indicating bulk formation and contains no crystalline impurities. Nevertheless, to prove that these particles are not porous, the N_2 adsorption-desorption branches are also recorded.

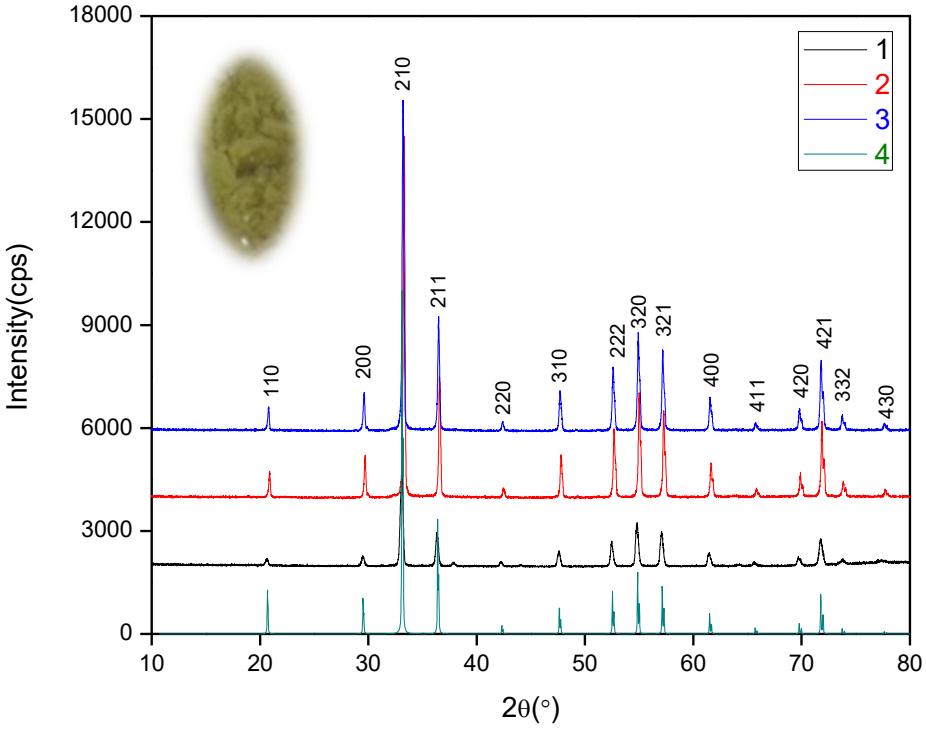

Figure 3.1.2. XRD pattern for yellow ppt. from 1:6:2 mole ratios of $C_{12}E_{10}$:$AgNO_3$:H_3PO_4 solution is in water (1), without any surfactant in ethanol (2), in ethanol (3), and JCPDS cards of Ag_3PO_4 (4) number 01-074-1876, by attaching yellow powder image.

The SEM images are blurry, see Figure 3.1.3. This blurry image may have two reasons; the one is that the particles could be mesoporous by surfactant effect, or the focusing problem. To be sure this, the N_2 adsorption-desorption measurements are carried using these samples.

a)

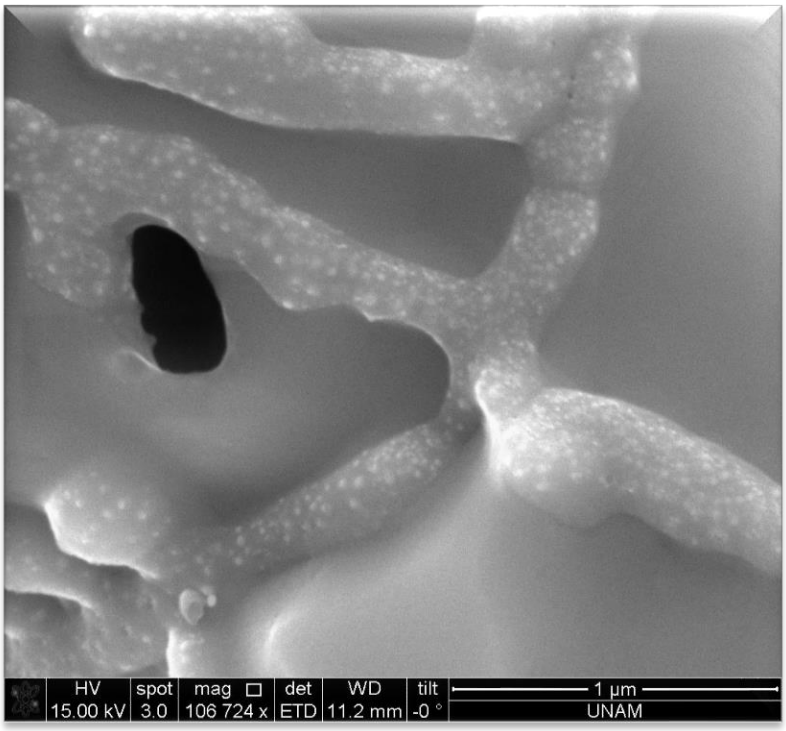

b)

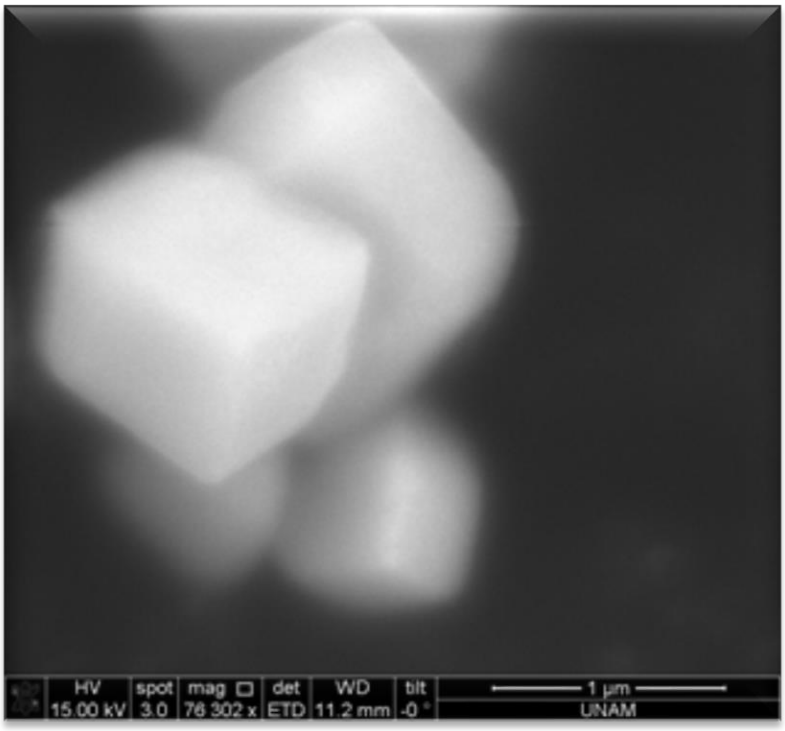

Figure 3.1.3. The upper SEM images is a) 6:2:1 $AgNO_3$:H_3PO_4:$C_{12}E_{10}$ precipitate in water calcined at 300˚C, and b) 60:20:1 $AgNO_3$:H_3PO_4: P123 precipitate both in ethanol.

According to SEM images and N_2 adsorption-desorption isotherms, the precipitates are bulk crystalline silver phosphate. Typical surface area of the precipitates is 2.5 m^2/g from the $C_{12}E_{10}$ system and 3.5 m^2/g from the P123 system. Shape of the samples, calcined at 300˚C, does not change in the precipitates from ethanol solutions, but in water, the shape also changes, and in both precipitates, particles has big holes, see Figure 3.1.3.

Color of the yellow silver phosphate crystals changes to brown under visible light and in solution after a while. Additionally, it is noticed that in a homogenous solution, after 1 day, some black tiny particles are formed. This process enhances in the absence of nitric acid. These experiments show the importance of fresh solutions. For further investigations and to investigate the LLC and mesocrystal formation in later stages, every time a new fresh solution is prepared.

XRD pattern of the yellow particles can be indexed to cubic structure of silver phosphate, see Figure 3.1.4. The XRD pattern of the brown sample also displays characteristic diffraction lines of silver phosphate with additional lines due to $HAg_2(PO_4)$ and Ag. This explains the color change. It is also clear from the patterns that HAg_2PO_4 is more than Ag metal in the samples. The formation of HAg_2PO_4 and Ag is triggered by light in aqueous solution. It is likely that Ag^+ ion is reduced to Ag metal by the photo-generated electrons in the conduction band of Ag_3PO_4 and HAg_2PO_4 is formed in a Ag^+ deficient and acid rich media due to reduction of silver ion. These processes will be discussed later in the photocatalysis section.

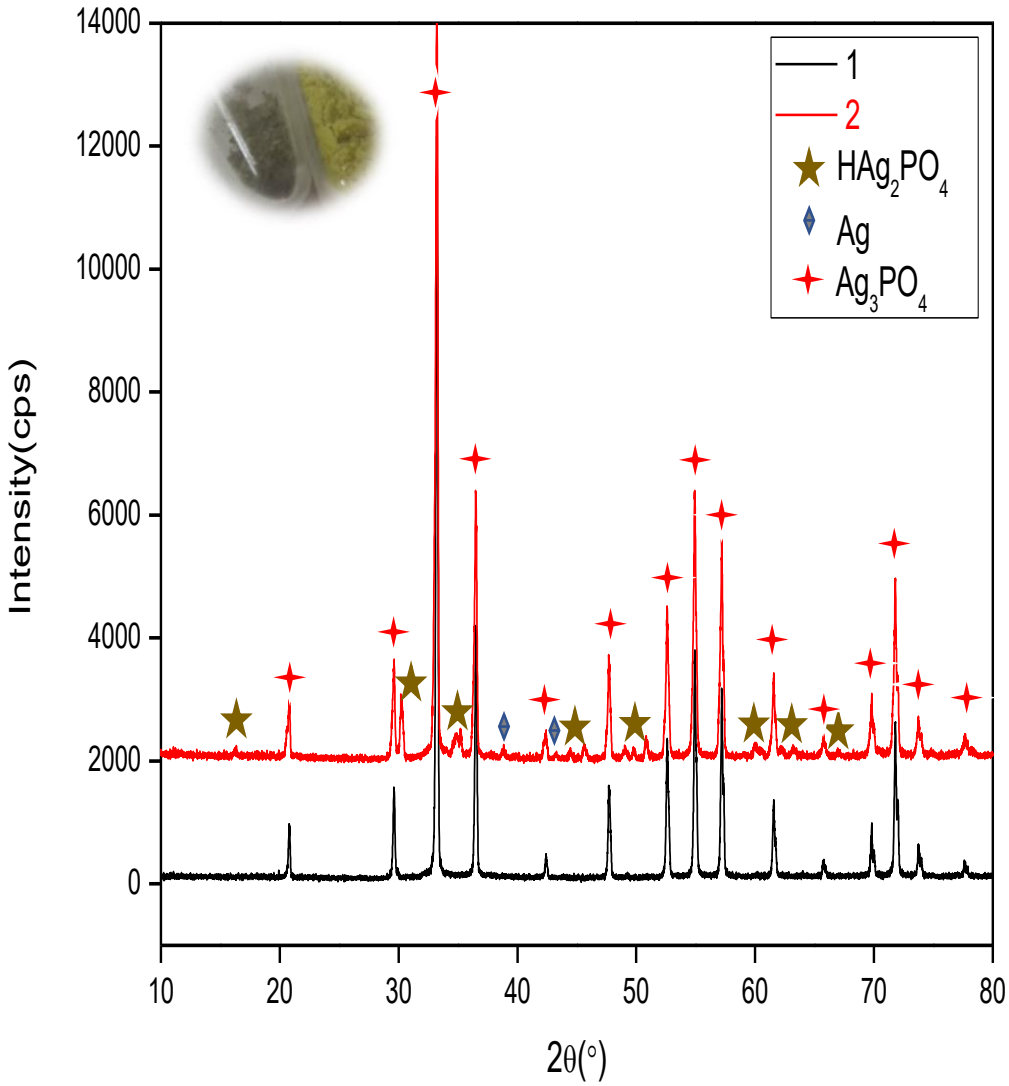

Figure 3.1.4. XRD pattern of the precipitate from 1:6:2 mole ratios of $C_{12}E_{10}$:$AgNO_3$:H_3PO_4 solution in water immediately after washing (1) and without surfactant in water in solution after a while (2).

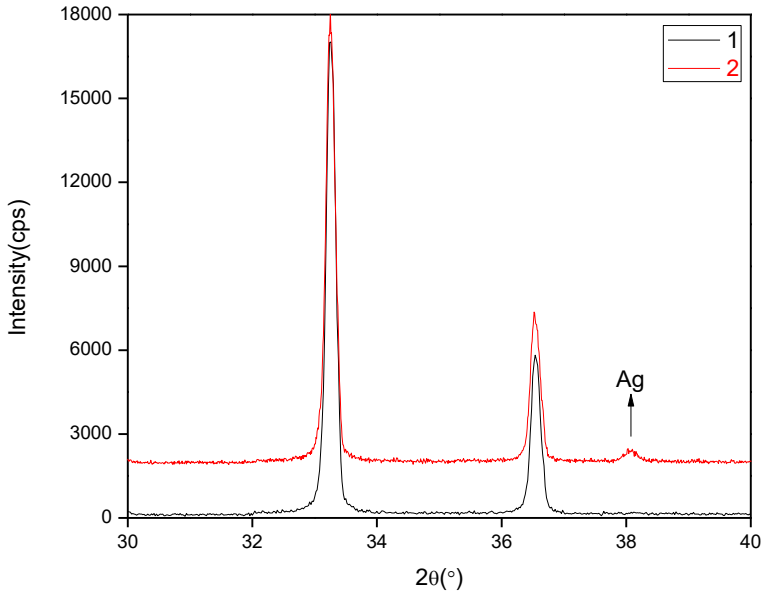

Figure 3.1.5. XRD pattern of the powder precipitate from 1:6:2 mole ratios of $C_{12}E_{10}$:$AgNO_3$:H_3PO_4 solution in ethanol before light irradiation (1) and under light irradiation after 11 days (2).

Figure 3.1.5 shows the XRD patterns of yellow precipitates, obtained from 1:6:2 mole ratios of $C_{12}E_{10}$:$AgNO_3$:H_3PO_4 solution in ethanol, after washing and drying process placed under light. After 11 days, exposed to light, it is clearly shown that the silver metal is the only side product, no silver hydrogen phosphate or unexpected impurities of silver oxide. However, the deformation and color change are much faster in aqueous solution. Thus, light and water accelerate the deformation of silver phosphate. The impurities provide insights on mechanism in photodegradation process. This will be discussed later.

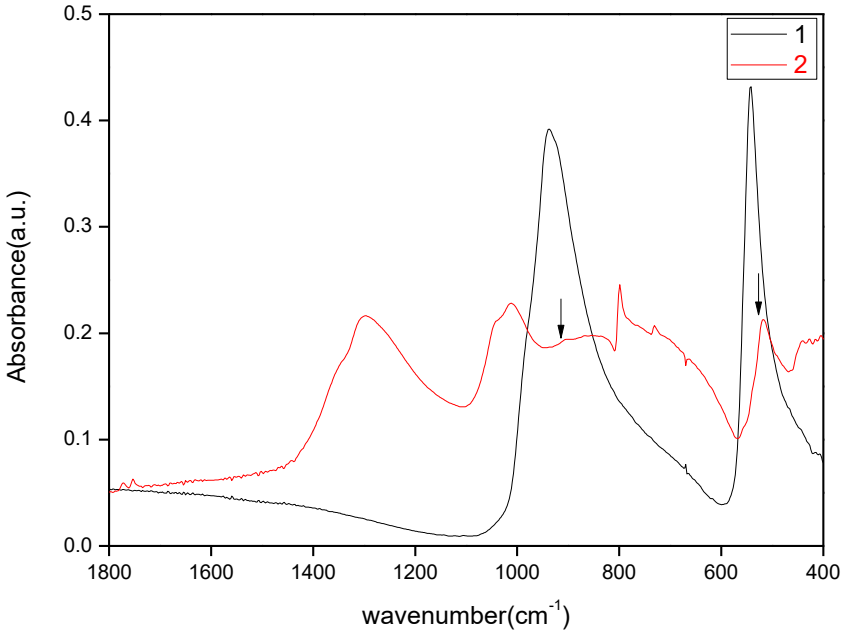

Figure 3.1.6. ATR-IR spectra of the yellow ppt. from 1:6:2 mole ratios of $C_{12}E_{10}$:$AgNO_3$:H_3PO_4 solution with $C_{12}E_{10}$ in water immediately after washing (1), and without surfactant in water after a while (2).

To understand what happens in the solution, ATR-IR spectroscopic technique has also been employed. The yellow precipitate (Y) has two sharp peaks due to stretching and bending modes of PO_4^{3-} moieties of Ag_3PO_4. [41] Ag_3PO_4 display peaks at 909 and 955-997 cm^{-1} due to symmetric and asymmetric stretching vibrational modes, respectively and at 406 (407-458) and 551 cm^{-1} due to the symmetric and asymmetric bending modes, respectively. [70] The brown precipitates (B) also display phosphate related peaks with additional peaks. Figure 3.1.6 shows the ATR-IR spectra of both Y and B. Previous XRD pattern indicates that Y is silver phosphate and B has silver phosphate, silver metal and silver hydrogen phosphate fingerprints of XRD patterns. Therefore, B has additional

peaks of HPO_4^{2-} units. An asymmetric stretching vibrational mode of P-OH (and P=O) is seen at 1298 cm^{-1}. [71] [72] Symmetric and asymmetric stretching vibration modes of P-O is observed at 1040 and 1012 cm^{-1} [73], and its bending modes at 665 and 520 cm^{-1}. [71] Therefore, light increases the silver formation, which is enhanced in water, silver ion deposits as silver particles on the surface of silver phosphate. Increasing acidity of the media stabilizes silver hydrogen phosphate. Therefore, without water, there is no significant change in powder silver phosphate.

The phosphate peaks are sharper in the IR spectra, obtained from ethanol solution compared to water, see Figure 3.1.7, 8, & 9. Also notice that all precipitates, obtained from water change color faster than the ethanol precipitates.

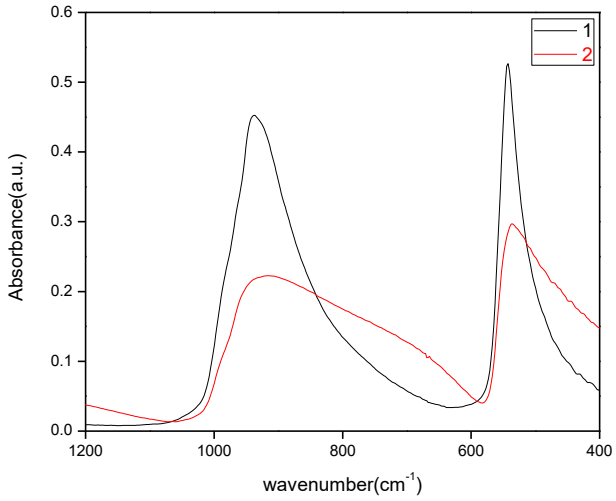

Figure 3.1.7. ATR-IR spectra of yellow precipitates from 6:2 mole ratios of $AgNO_3$:H_3PO_4 solution without surfactant in ethanol (1) and water (2).

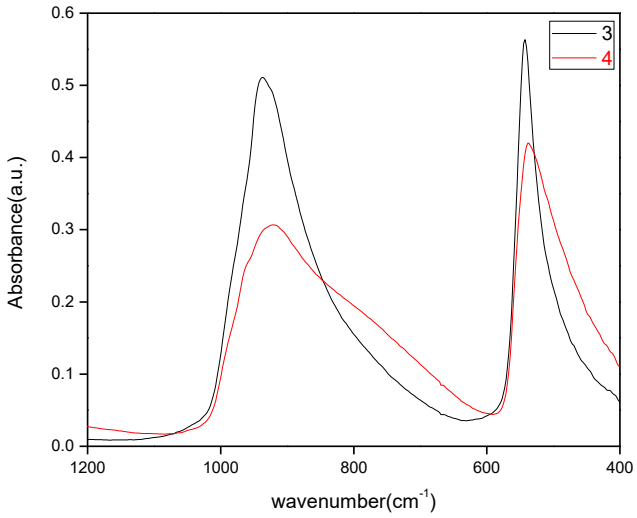

Figure 3.1.8. ATR-IR spectra of yellow precipitates from 1:6:2 mole ratios of $C_{12}E_{10}$:$AgNO_3$:H_3PO_4 solution in ethanol (3) and water (4)

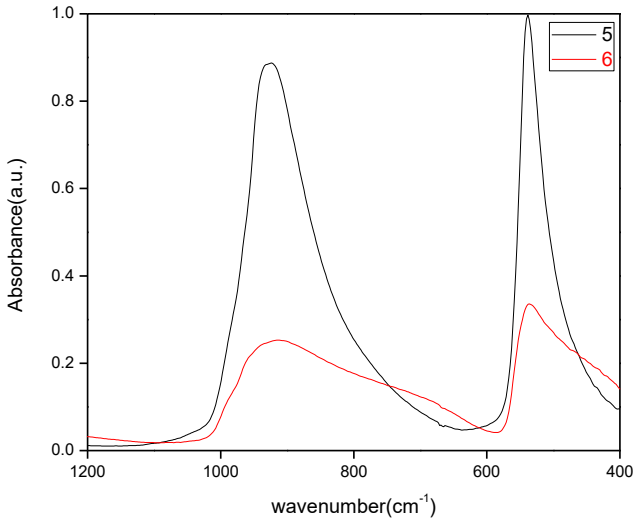

Figure 3.1.9. ATR-IR spectra of yellow precipitates from 1:6:2 mole ratios of P123:$AgNO_3$:H_3PO_4 solution in ethanol (5) and water (6).

Yellow precipitates obtained from water solution was calcined at 300˚C in order to see the effect of temperature on these crystals. Particles are much larger with better defined shape and worm like futures on their surface, see Figure 3.1.10. Some of these particles also have small holes (around 30-1000 nm). These worm-like species could be silver hydrogen phosphate, as predicted from the ATR-IR and XRD data. The EDS data also verifies this prediction, see Figure 3.1.10. This showed the changing morphology of silver phosphate on surface by temperature effect.

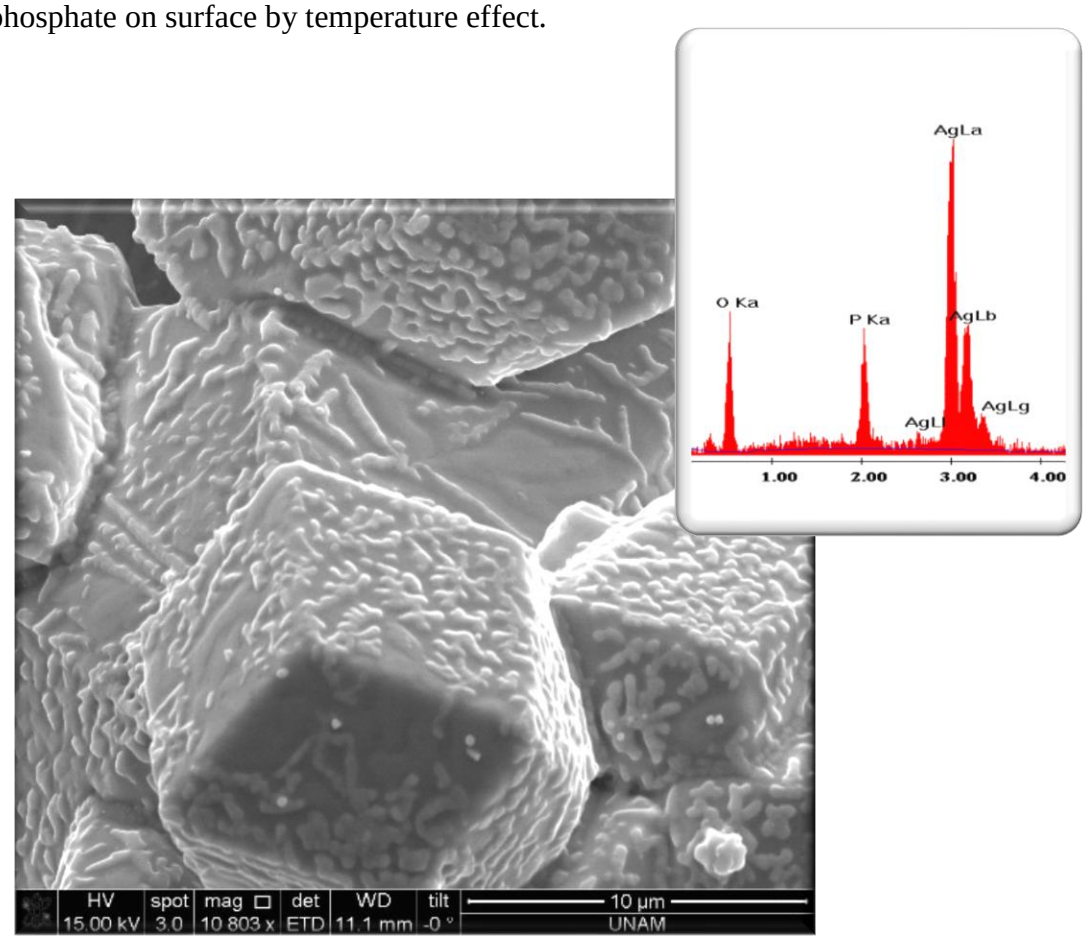

Figure 3.1.10. The SEM image of the precipitates in water solution calcined at 300˚C attachment with EDS spectrum for selected area.

The precipitates, obtained from ethanol solution has a smooth surface with an almost spherical morphology, see Figure 3.1.11, even after calcination. The trend of EDS is the same for both precipitates in all compositions, thus, the only particles of 60:20 ethanol and water solution are shown in Figure 3.1.10 & 11. The oxygen intensity of the ethanol precipitate is less than water precipitates. This may refer to the formation of HAg_2PO_4 in water and the high intensity of silver in both case, clearly higher than 3 times of phosphate peak, indicates the formation of metallic silver. This explains the observation of some brownish-blackish color of the samples. The tiny particles on surface are likely metallic silver in ethanol and water, also observed after a while in solution. HAg_2PO_4 formation is more in water than in ethanol case. Therefore, it is not noticed any worm like structure on ethanol precipitates. This is also proof of ATR-IR differences of water and ethanol with increasing changes of morphology by temperature.

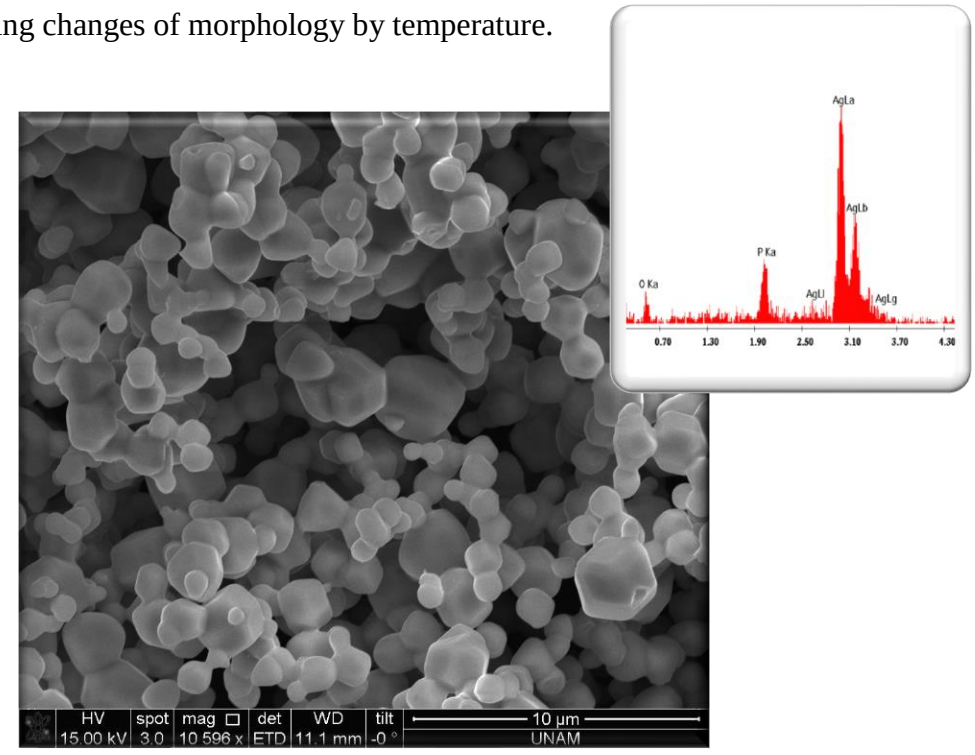

Figure 3.1.11. SEM image of the precipitates in ethanol solution and calcined at 300˚C, attachment with EDS spectrum.

The second investigation of deformation is carried under a visible light. The samples expose to visible light was investigated using SEM imaging to clarify the changes. The bright tiny small particles amount, and size are increased upon exposure to light, see Figure 3.1.12. EDS data also show enhanced Ag signal. By supporting the previous data, see Figure 3.1.5, light increased the silver formation, evidenced by observing small tiny shinny particles on surface in both cases, even after calcination process.

To eliminate the formation of bulk Ag_3PO_4, we introduce some nitric acid to the media. Since nitric acid is a strong acid, it reduces the concentration of phosphate ion as a result decreases the formation of Ag_3PO_4 in the solution phase. Therefore, nitric acid is used to decrease the formation of bulk Ag_3PO_4 crystals in the solution phase and also to keep the $C_{12}EO_{10}$:Ag(I):H_3PO_4 mole ratios in the solutions to compare the results of each experiments. It is difficult to propose the whole mechanism, but the data enables us to imply that in water case, the formation of HAg_2PO_4 is triggered in solution and forms as particles on the surface of the precipitates until all silver ions turn to silver metal. Silver formation is observed in every step and experiment, thus the final product after visible light irradiation and color change is due to silver metal.

a)

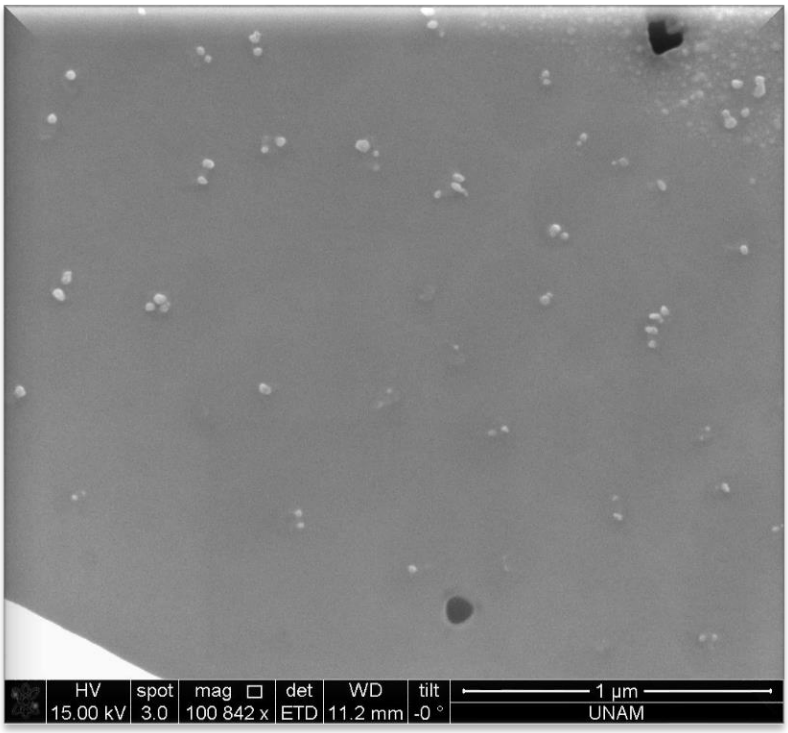

b)

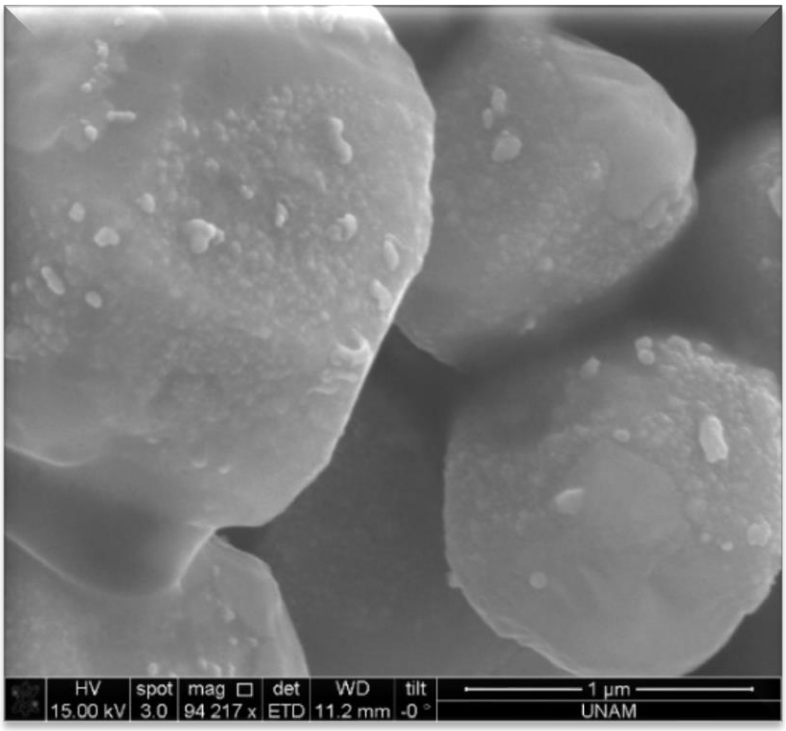

Figure 3.1.12. SEM images of calcined precipitates under visible-light after 2 weeks of the precipitates from a) water and b) ethanol.

3.1.2. The Thin Films from SNPA System

The SNPA-surfactant solutions can be spin or drop-cast coated over glass slides to form the LLC films upon fast evaporation of the excess solvent. These films can be used to produce mesoporous Ag_3PO_4 films upon calcination. Therefore, in this section, a general path will be followed for the synthesis mesoporous thin films. Notice that our group synthesized the first transparent mesoporous hydroxyapatite using a very similar system, $Ca(NO_3)_2$:H_3PO_4:$C_{12}EO_{10}$. [32]

Tunkara on his thesis used phosphoric acid surfactant system that produce LLC phase in a broad range of phosphoric acid concentrations. Then he employed this phase and add the calcium salt to the media to synthesize calcium hydroxyapatite (CaHAP) mesoporous thin films. [32] The only difference between Tunkara's system and our system is the metal ion, Ca^{2+} versus Ag^{+}. However, the Ca^{2+} system was stable in the solution phase (no precipitates) and stable in the gel phase for long enough for further heat treatments. As a senior project, CaHAP with silver was performed to show antibacterial activity keeping the transparency of the films. Before discussion the SNPA system, demonstrating some observation about Ag^{+} incorporated CaHAP could be useful for further discussion.

After preparing calcium hydroxyapatite solution, different mole percentage of $AgNO_3$ was added to the solution but most of data was obtained from Ag/Ca mole ratio of 10. Firstly, if a very small amount of silver nitrate was added, there was no color change in the solution. However, when the $AgNO_3$ amount reached to 30 mole percent, some crystalline particles formed over the freshly prepared film upon spin coating above solution. Furthermore, a color change was observed upon calcining the films at 400°C. As soon as introducing the thin film in 200 °C preheated oven, the color of the film turned

brown, but the temperature rose to 400 °C, the film became colorless and transparent, but at the edge of the glass slides white particles were observed, and the powder of the sample was also white, see Figure 3.1.2.1. To clarify what happen around 200˚, the samples were first calcined at 150-180 °C region. The films were coated over a quartz substrate and monitored using UV-Vis spectrophotometer. The Ag plasmon mode was observed upon heating the samples at 150-180°C see at Figure 3.1.2.1, then it was deduced that the silver nanoparticles oxidize to form silver phosphate or incorporate into HAP. This experiment is important for our further investigations.

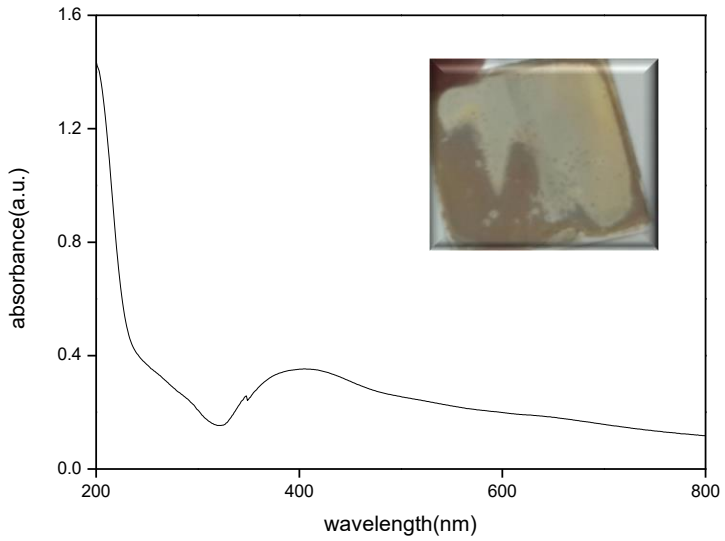

Figure 3.1.2.1. The UV-Vis spectrum of the sample with 10 mole percent Ag in CaHAP at 150-180°C with a photograph of the sample after annealing.

Figure 3.1.2.2 showed transparent films of CaHAP with silver amount. Two pictures were very similar due to high transparency. An edge of slide had different color and also when scratching these to collect powder, the color of the powder sample of 40 mole ratio of silver was light yellowish and 10 is white. Therefore, it was considered there is no

difference between two pictures from a first impression. However, edges of slides belonging to 40 mole ratios of silver had slightly light-yellow color than 10. Honestly, 40 mole ratios were not an extreme silver amount, but changing color was demonstrated that this transparent thin film of CaHAP with Ag (40) property was changed by introducing impurity because of silver phosphate formation.

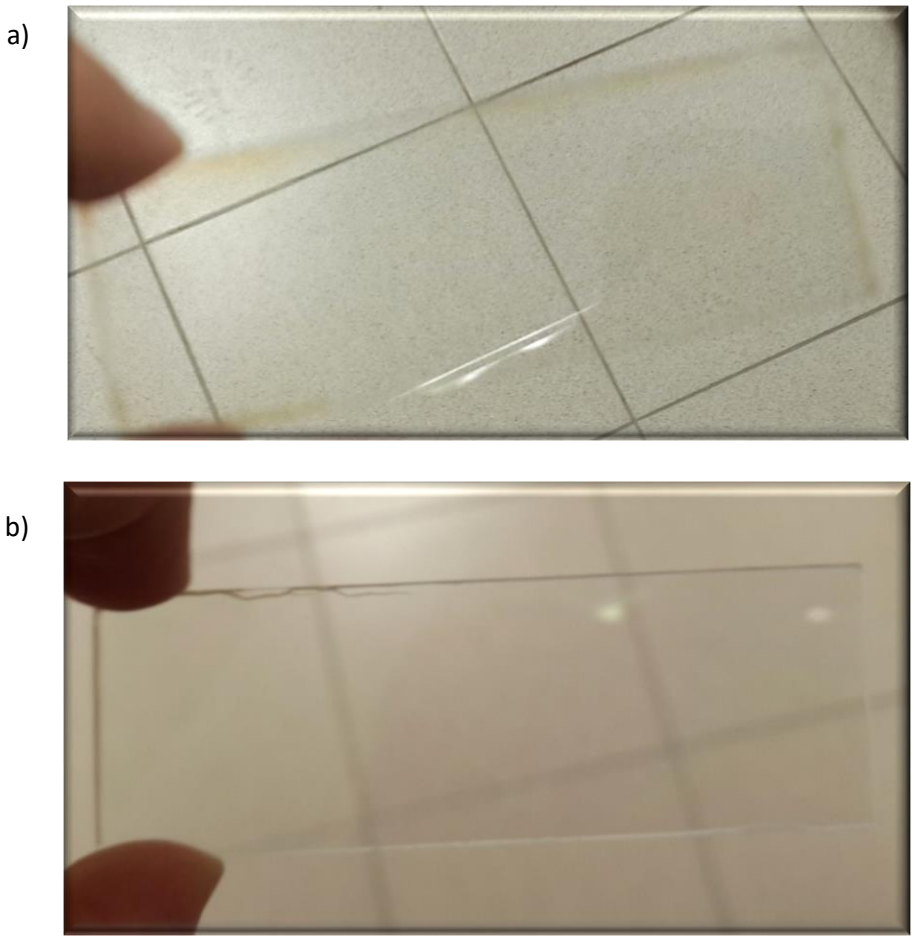

Figure 3.1.2.2. The photographs of the films of silver-calcium hydroxyapatite calcined at 400°C, the mole percentage of silver is a) 40 and b) 10.

The CaHAP with high amount of silver such as more than 40 mole percentage with respect to Ca provides an idea for the synthesis of Ag_3PO_4 from lyotropic liquid crystalline mesophase templating method. The beginning of this work, it is tested that the nitric acid prevents yellow bulk silver phosphate formation. First experiments are carried in water. Figure 3.1.2.3 shows two XRD patterns of a fresh film obtained from water solution of acid-surfactant with HNO_3 before and after adding $AgNO_3$ to clarify a procedure step. Both samples diffract at small angles, showing that the mesophase form in both cases. Therefore, it is decided to use HNO_3 before adding silver source.

As a solvent, both ethanol and water are tested. However, in ethanol, a homogenous solution is not stable as in water. The reason is the lower K_{sp} of silver phosphate in ethanol than in water. Therefore, for further steps, only water is used as the solvent. The preparation of samples followed the following steps; 1 g of surfactant is fully dissolved in water, then certain amount of phosphoric acid is added to the media by stirring, followed by adding 0.3 ml of nitric acid (this is the amount that stops precipitation of bulk Ag_3PO_4 in aqueous media), and last certain amount of silver nitrate. The mole ratios were chosen using Tunkara's thesis [32] on phosphoric acid part. According to his thesis, the phosphoric acid-surfactant system forms mesophase from 1 to 20 acid/surfactant mole ratio. Behind this knowledge, the stoichiometric ratio of silver per phosphoric acid is chosen as 3 to 1. The solutions of 3:1, 6:2, and 9:3 Ag^+:H_3PO_4 per surfactant are prepared.

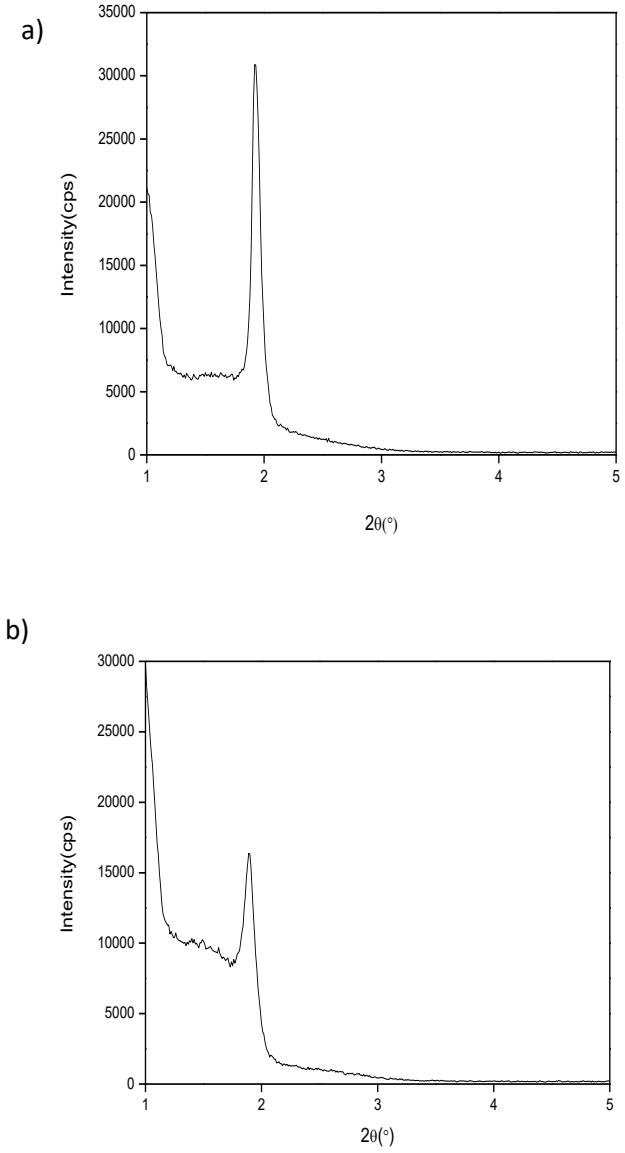

Figure 3.1.2 3. Small angle XRD patterns of the fresh films at RT a) with 0.5 ml HNO_3 before adding silver nitrate, b) with 0.5 ml HNO_3 after adding silver nitrate.

After optimizing the synthesis procedure in terms of nitric acid amount, surfactant mole, and solvent as a water, the amount of salt (also acid, stoichiometric) and surfactant and

also the calcined temperature for SNPA-LLM system is optimized by varying the ingredient concentrations and calcination temperature, respectively.

The first synthesis temperature was taken from the CaHAP system. Thus, the spin coated sample is first put into a preheated oven at 200˚C for 30 min and then calcined at 400˚C for 3 hours. The SEM images of the 3:1, 6:2, 9:3 and 12:4 mole ratio of $AgNO_3$:H_3PO_4 solution are shown in Figure 3.1.2.4. The images showed that increasing the mole ratio of silver and phosphate, a film formation is observed. The crystal formations are noticed at low mole ratios.

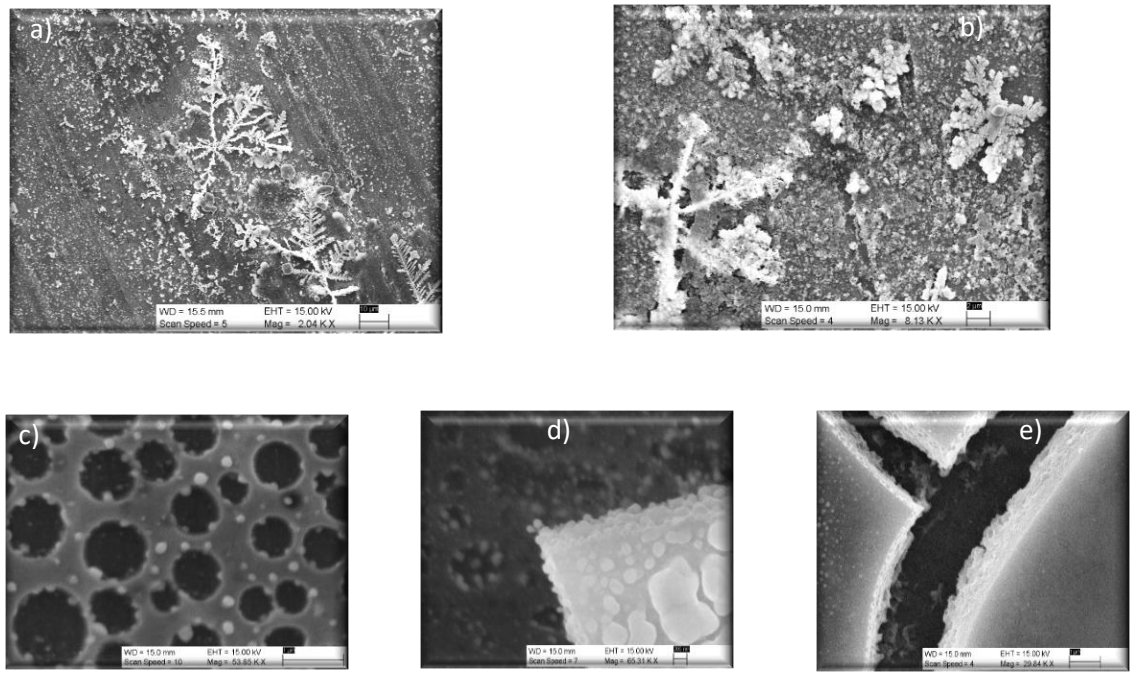

Figure 3.1.2.4. SEM images of the samples over steel upon calcination at 400°C: Ag/PO_4 mole ratio of a) 3:1 b) 6:2 c) 9:3 d) and e) 12:4.

Raman spectra of the samples display peaks related to PO_4^{3-} bending mode at around 500 cm^{-1} and stretching mode at 1000 cm^{-1}, Figure 3.1.2.5. The vibrational bands at 429 and 450 cm^{-1} are attributed to the O-P-O bending modes, and the bands at 1046 and 1074 cm^{-1} to asymmetric (P-O) stretching. [42] The peaks at 589 and 608 cm^{-1} have also been assigned to the O-P-O bending modes. [74] Our results are also consistent with those assignments; thus the 400-1100 cm^{-1} region of the spectrum shows the phosphate peaks. The spectra show difference with aging the samples. The intensity of the high energy peaks above 1000 cm^{-1} goes up while the most intense peak below 1000 cm^{-1} goes down with aging. To elucidate the origin of these changes, we exposes one of the sample to green laser for 5 minutes and recorded the spectrum of the same sample once more, see Figure 3.1.2.5b. Similar to aging the spectral changes follow the same trend and found that samples are very sensitive to light.

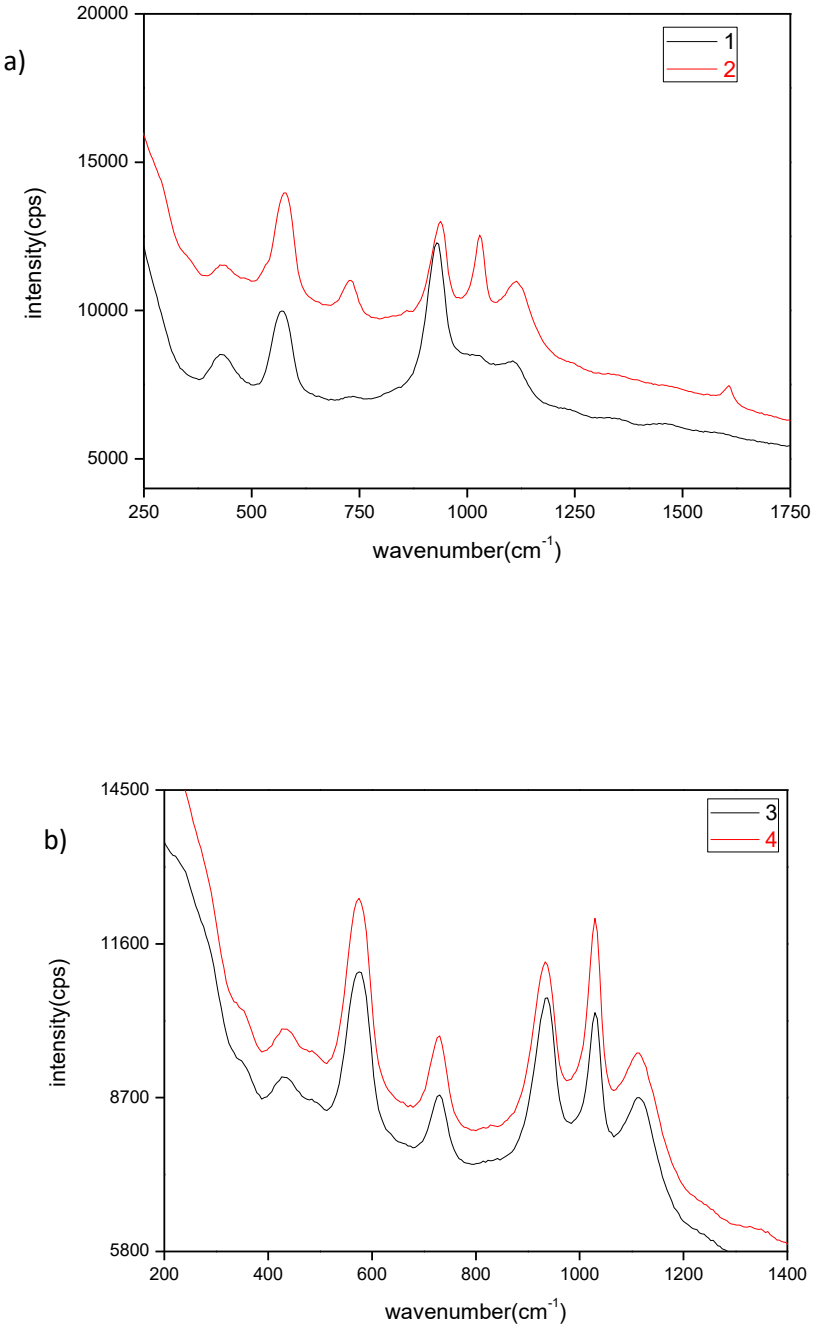

Figure 3.1.2.5. Raman spectra of 1:12:4 $C_{12}E_{10}$:Ag:PO_4 thin film a) fresh (1) and 1day old film (2), and b) old film before (3) and after green laser exposure for 5 min (4).

With aging (likely due to room light) and exposure to laser beam, a new peak emerges at around 730 cm^{-1} and its intensity follows the same trend as the asymmetric stretching bands (peaks above 1000 cm^{-1}) of phosphate. Also, these spectral changes to support the photo-degradation of Ag_3PO_4 to Ag and other silver oxide types by additional peaks and increasing intensity of some certain peaks 250-1600 cm^{-1}. [75] Therefore, the new peaks originate likely from the light induced decomposition products.

The XRD patterns of the thin films, calcined at 300˚C, on a glass slide shows diffraction pattern identical to crystalline Ag_3PO_4 (PDF 01-075-6002), see Figure 3.1.2.6. Two XRD patterns are recorded directly from glass slide (from the films) from two different compositions (Figure 3.1.2.6a); namely from 1:12:4, and 1:9:3 $C_{12}E_{10}$:Ag:PO_4 solution mole ratios. The pattern in Figure 3.1.2.6b is collected from a powder sample. In the patterns, in addition to Ag_3PO_4 lines, some Ag lines are also observed. This shows that either silver is forming during calcination and it is deficient in the LLC phase to produce stoichiometric Ag_3PO_4 or Ag metal forms upon exposure to sun light. It is a product of aging. This might be explained from the silver plasmon mode, started appearing at 150˚-180˚C. However, the fresh samples do not display diffraction lines due to metallic Ag that enhances under certain conditions and exposure to light and reducing agent, indicating that the initial product is Ag_3PO_4 and Ag is forming as a degradation product. Nevertheless, the characterization also continues to understand the system by collecting more experimental data.

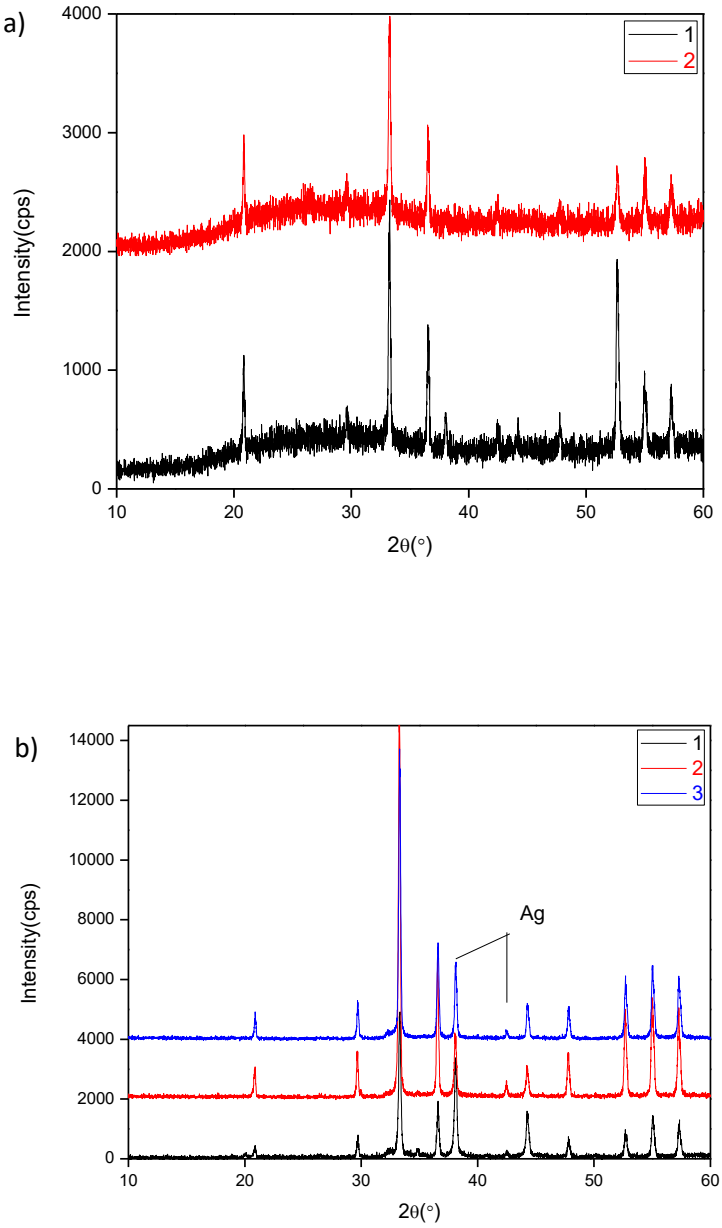

Figure 3.1.2.6. The XRD patterns of $C_{12}E_{10}$:Ag:PO_4 mole ratios (a) 1:12:4 (1) and 1:9:3 (2) thin films on glass slides, calcined at 300˚C and (b) 1:12:4 powder sample with different calcination steps, spin coating films (1), aged film with drop cast (2) and preheated oven before calcination process (3).

To understand the role of inorganic ingredients, we also prepare samples by increasing the silver nitrate and phosphoric acid from 4:1.33 to 24:8 per surfactant in the solutions. The SEM images of the films, obtained from 1:4:1.33, 1:12:4, 1:16:5.33, and 1:24:8 mole ratios of $C_{12}E_{10}$:Ag:PO_4, calcined at 300˚C on silicon, show that the bulk formation is enhanced, see Figure 3.2.1.2.7 The shape of Ag_3PO_4 domains changes with increasing mole ratios, rod or worm like shape forms. This shows us the surfactant effect on the shapes. Therefore, increasing mole ratios increases the formation of mesophase and thin film. Nevertheless, it is not enough to achieve desired product, films.

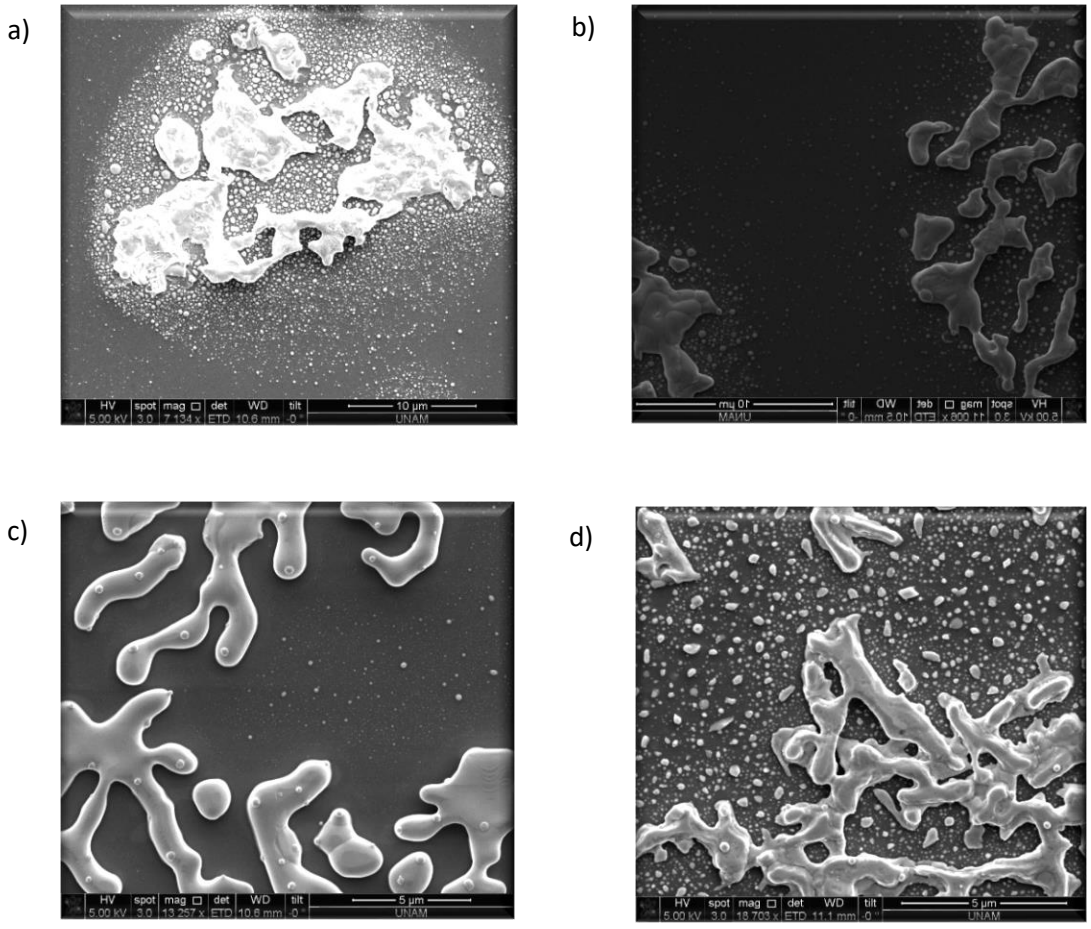

Figure 3.1.2.7. The SEM images of thin films from mole ratios of 4:1.33 (a), 12:4 (b), 16:5.33 (c), & 24:8 (d), respectively on silicon.

Particles have tiny shiny smaller particles over the large ones, Figure 3.1.2.8. The size of the particles changes from tens of nanometer to micron. The particles are beam sensitive, upon focus on the sample by electron beam in SEM, the shapes start to change, see Figure 3.1.2.8. It is difficult to focus and image the details of the structure, such as mesoporosity or nanostructures over the large crystals.

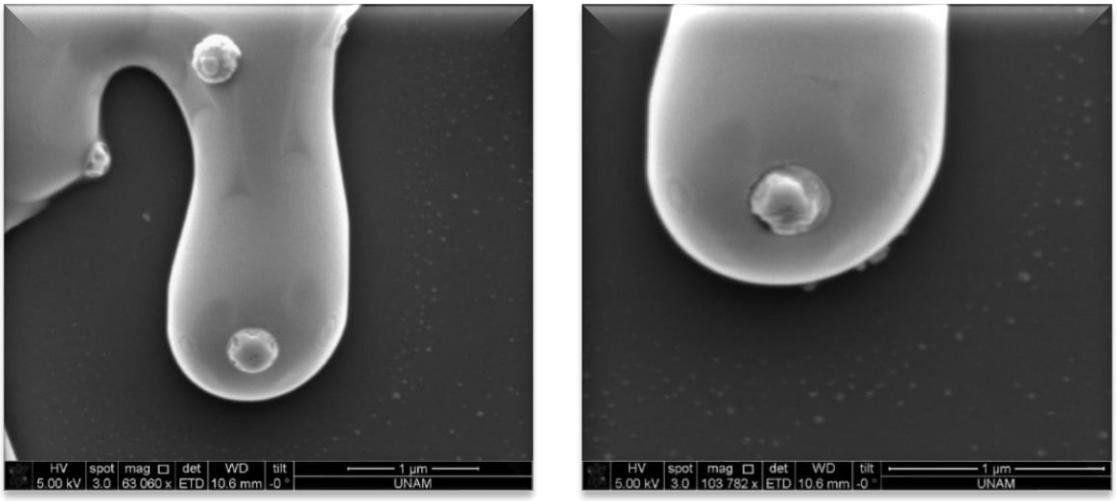

Figure 3.1.2.8. The SEM images of 1:16:5.33 $C_{12}E_{10}$:Ag:PO_4 mole ratio of thin film on silicon by focusing sample.

Increasing calcination temperature to 500˚C results a new undefined product. Figure 3.1.2.9 shows the XRD pattern of this product; diffraction lines do not match with neither Ag_3PO_4 nor Ag, but also with other silver oxide and phosphate types, which are the typical side products of heat treatment. Thus, the maximum calcination temperature for these thin films is determined to be below 500˚C. Increasing temperature facilities the silver metal formation as evidence from the silver plasmon mode and XRD pattern. Increasing temperature gradually from 200˚C to 500˚C, the silver metal formation increased, see Figure 3.1.2.9.

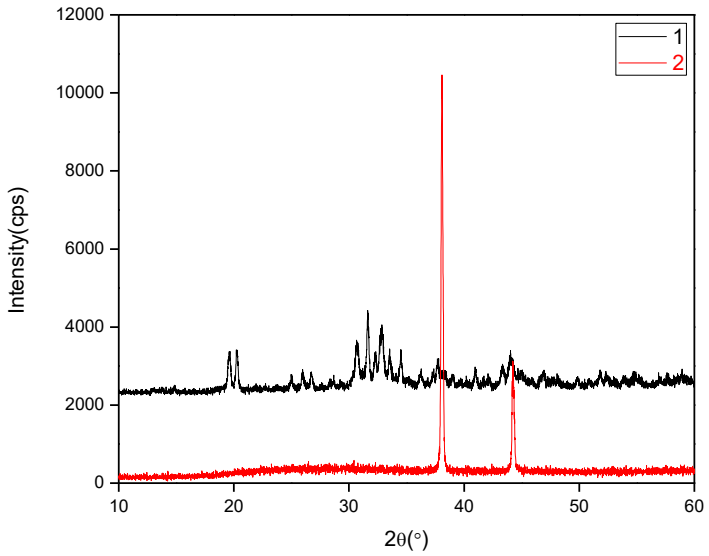

Figure 3.1.2.9. The XRD pattern of the thin film, obtained from 1:12:4 $C_{12}E_{10}$:Ag:PO_4 and calcination at 500˚C (1), and Silver metal XRD pattern (2).

These thin films are more light sensitive than precipitates (section 3.1.1), and the shape is not cubic under SEM but XRD pattern belongs to cubic silver phosphate. Therefore, the salt surfactant LLM system changed the morphology of the samples.

3.1.3. The Soft Mesocrystals

In this section, the behavior of the fresh coated samples of SNPA thin films will be investigated by aging under different conditions and a new synthesis method will be introduced. The previous section is on a general synthesis method of the salt-surfactant LLM system to generate mesoporous transparent thin films. However, as shown in the

previous section, the calcination product is always bulk Ag_3PO_4 with some Ag metal. Also, in the previous section, we used thicker films obtained from drop cast coating method to obtain starting LLC mesophase. However, drop casting is more useful than spin coating to evaluate the behaviors of the fresh samples. Furthermore, this section will include low temperature and phosphoric acid effect on formation of a new type of crystals, namely soft mesocrsytal. POM, ATR-FTIR, XRD, SEM and melting point techniques were used to characterize the films.

In salt-surfactant LLC mesophase, the expected mesostructures are hexagonal, cubic, or lamellar and can be identified using POM imaging and XRD techniques. Interestingly, our observations shows that the mesophases are not stable to water evaporation. The $AgNO_3$-surfactant mixtures do not hold sufficient water to form stable mesophase, instead it crystallizes into mesocrystals. The spin coated films crystallize so fast like around 50 sec, but the drop films' crystal form duration time was long enough, around 10 min.

Figure 3.1.3.1 shows a POM image and largescale photograph of those crystals. The crystal growth imitates a typical defect patterns of LLC phases, thus they appear like flower, growing out from the defect centers, observed in a typical fan-texture of LLC 2D-hexagonal phase. To figure out the crystal form, small and high angle XRD patterns are recorded. The diffraction pattern shows both small and high angle lines that cannot be indexed to neither $AgNO_3$ (starting salt) nor Ag_3PO_4 (likely product).

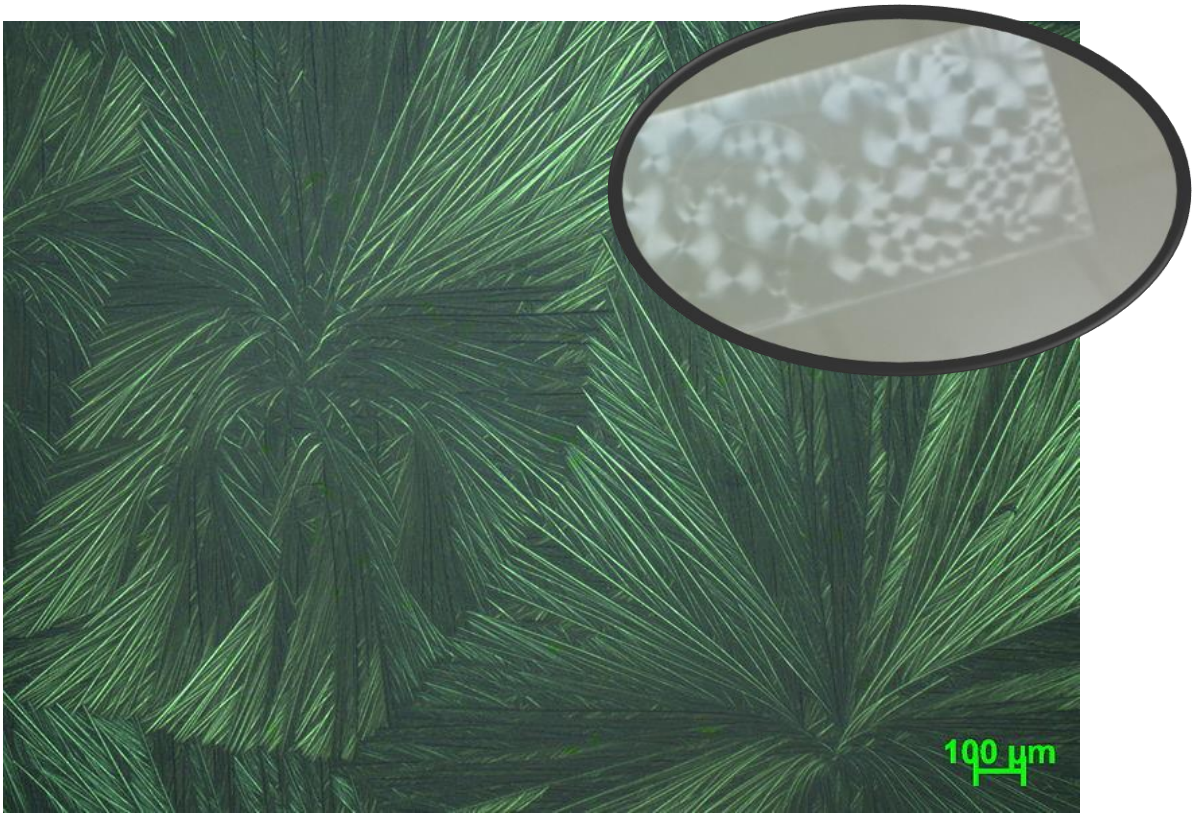

Figure 3.1.3.1. The POM image [76] and the photograph of the drop casted films from 6:2 solution.[9]

The XRD pattern shows formation of a crystal but the diffraction lines cannot be indexed to any known possible crystals in the data base, see Figure 3.1.3.2. In 2013, Dag' group found similar type of crystals from surfactant and LiI, $CaCl_2$ and $MgCl_2$ systems and named the crystals, soft mesocrystals. They noted that "hydrated $CaCl_2$, LiI, and $MgCl_2$ salts induce self-assembly in nonionic surfactants (such as $C_{12}H_{25}$-$(OCH_2CH_2)_{10}OH$) to form lyotropic liquid-crystalline (LLC) mesophases that undergo a phase transition to a new type of soft mesocrystal (SMC) under ambient conditions" [59]. The POM images of

[9] https://commons.wikimedia.org/wiki/File:Nuve6.jpg

our samples and mesocrystal are very similar. [59] ATR-IR spectra also display sharp surfactant peaks similar to soft mesocrystals of other salts, indicating crystalline nature of the surfactant domains. The XRD pattern display lines at small and high angles, characteristic for the mesocrystals. However, it is very difficult to evaluate the crystal details of mesocrystals from this data.

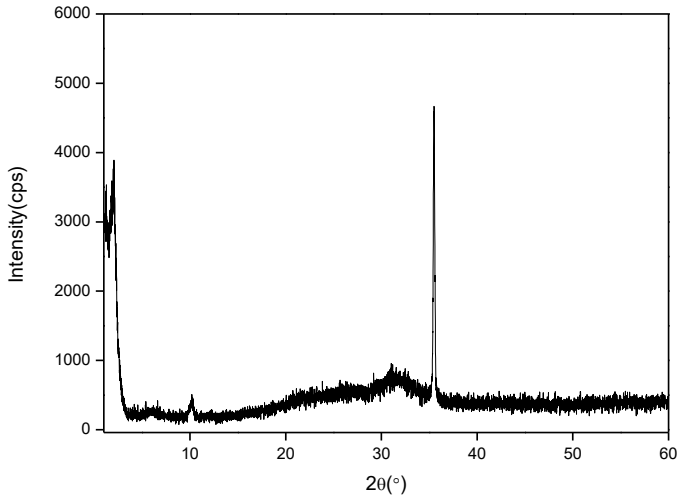

Figure 3.1.3.2. The XRD pattern for 12:4 solution after 30 min in RT aging as a film.

The ATR-IR spectra show that the phosphate (around 1000 cm^{-1}) and nitrate (around 1400 cm^{-1}) stretching regions become sharper after complete water evaporation. This system is different form the LiI, $CaCl_2$, or $MgCl_2$ systems in term of water region. The water peak almost completely disappears upon aging the SNPA LLC phase. The soft mesocrystal of SNPA system are stable even after months in a closed container. However, under ambient conditions, silver ion slowly turns to silver metal. Soft mesocrystals looks like soft solids.

Figure 3.1.3.3 shows time dependent ATR-IR spectral changes of 4:1.33 Ag/PO_4 system. The sharp and intense peaks originate from nitrate, phosphate, and surfactant species and assigned to soft mesocrystals. As shown in the spectra, mesocrystal formation is complete in a short time and no more changes were observed even after 10 days, see Figure 3.1.3.3.

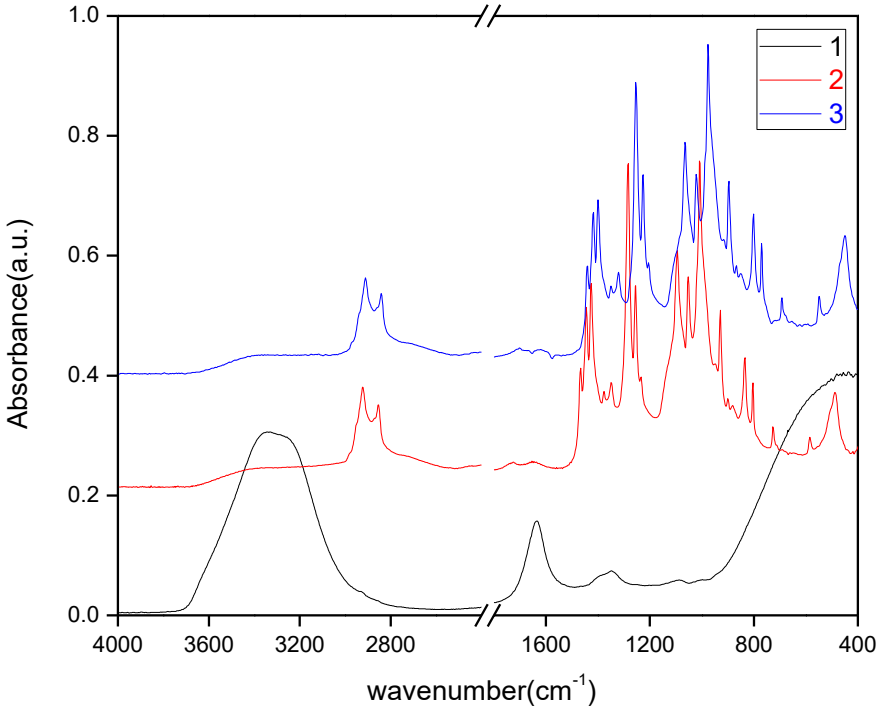

Figure 3.1.3.3. The ATR-IR spectral changes over time in the 4:1.33 coated films at RT, fresh drop (1), after 30 minutes (2) and after 10 days (3).

Formation and stability of mesocrystals are also checked by increasing the phosphoric acid amount in the samples using ATR-IR spectroscopy. The silver/surfactant mole ratio is kept 4 and the phosphoric acid/silver ratio has been changed from 0 to 10. Two control samples are also prepared, one without phosphoric acid (4:0, 4 silver nitrate/surfactant) and the other without silver nitrate (0:10, 10 phosphoric acid/surfactant). Then the small angle XRD patterns of the samples are collected upon coating over glass slides. Figure 3.1.3.4 shows a series of small angle XRD patterns, collected from those samples. The XRD pattern demonstrates the low amount of phosphoric acids' pattern resembles only silver nitrate-surfactant LLC phase and diffraction line is quite broad. The origin of this line could be either LLC phase or mesocrystals. The high amount of phosphoric acids' LLC phase display pattern like phosphoric acid-surfactant LLC phase. The 4:6 sample showed two characteristic XRD lines, meaning separation started, soft mesocrystal (lower angle broad line) and hexagonal phase of phosphoric acid rich LLC phase (higher angle sharper line). The POM images of this set also have a trend when increasing phosphoric acid from zero to ten, the firework shaped crystal morphology turns to rod like shapes. The phosphoric acid influences the structure of soft mesocrystals. According to the diffraction pattern, it is concluded that the soft mesocrsytal and hexagonal phase are separated in the films at high phosphoric acid concentrations.

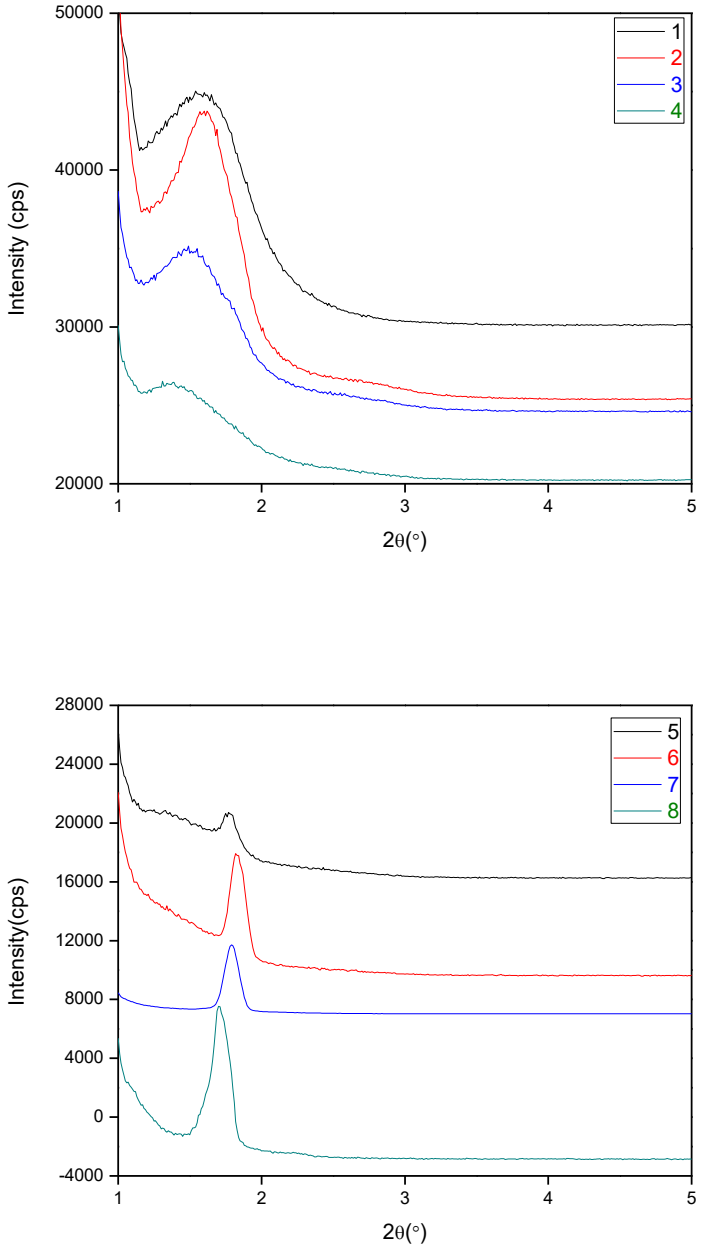

Figure 3.1.3.4. The XRD patterns of 1:4:0 (1), 1:4:2 (2), 1:4:4 (3), 1:4:4 (4), 1:4:6 (5), 1:4:8 (6), 1:4:10 (7) and 1:0:10 (8) $C_{12}E_{10}$:$AgNO_3$:H_3PO_4 fresh films.

a) b)

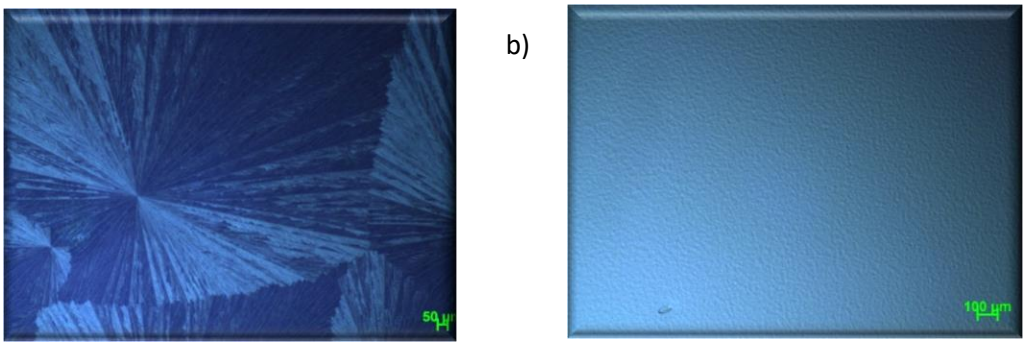

Figure 3.1.3.5. POM images of the a) 4:0 and b) 0:10 films of Ag:H_3PO_4 upon coating.

To check the stability of mesocrystal, the 4:0 samples is heated under POM using a Linkam heating-cooling stage with a temperature controller. The POM images of the sample up to 158^{o}C are identical and display images of typical mesocrystals, see Figure 3.1.3.6. At 158˚C, some white tiny spots appear; changes begin. At 160-180˚C, soft mesocrystals start to disappear and at 215˚C, black spots formed. It is likely that mesocrystals separate into $AgNO_3$ crystals and surfactant around 160^{o}C and higher temperature Ag metal forms. Cooling the sample, heated to 215^{o}C, to room temperature does not recover the soft mesocrystals. The XRD pattern shows that mesocrystals are converted to crystalline silver and silver nitrate, see Figure 3.1.3.7. Note also that silver nitrate melts around 212˚C. The same experiment is performed for SNPA-surfactant system to elucidate the role of phosphoric acid.

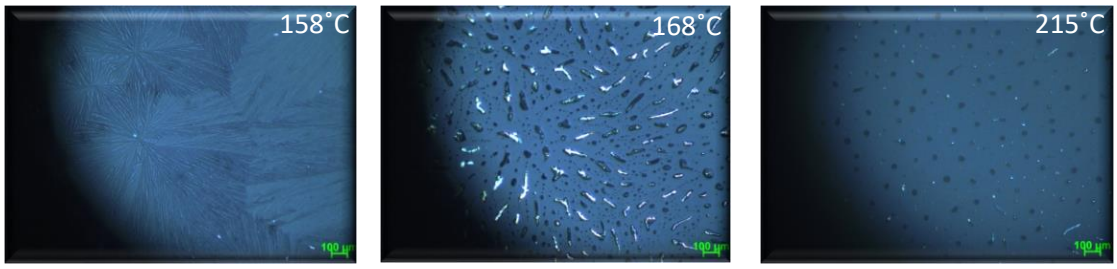

Figure 3.1.3.6. The POM images with different temperature and XRD pattern for 4:0 solution

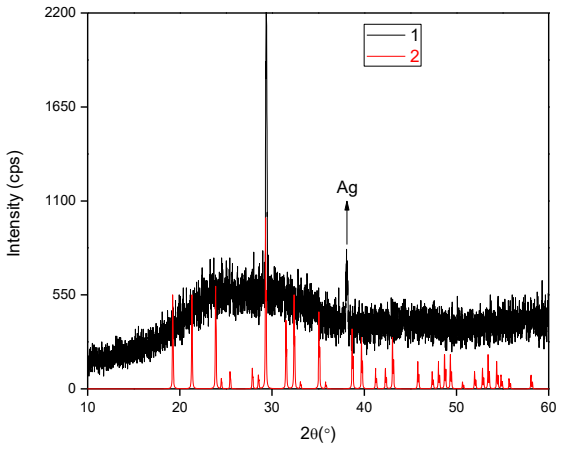

Figure 3.1.3.7. The XRD pattern for 4:0 solution after Linkam heating-cooling experiment (1), and JCPDS cards of $AgNO_3$.

In this experiment, the 6:2 mole ratio was used instead of 4:1.33, because of image quality. Up to 50˚C, it is not noticed any changes, compare images record at RT and 50˚C. Nevertheless, the images begin to become blurry, showing some changes started at 50^{o}C. Increasing temperature makes the soft mesocrystals blurrier and at 100˚C soft mesocrystals completely disappear. Similar, mesocrystals cannot be recovered upon cooling the sample to RT. In the presence of phosphoric acid, the decomposition temperature has been reduced to around 50˚C. The reaction is complete at 100˚C. The

XRD pattern of the sample, heated at 50˚C, shows the formation of silver phosphate, and at 80˚C, the other lines of silver phosphate emerge in the XRD pattern, see Figure 3.1.3.8.

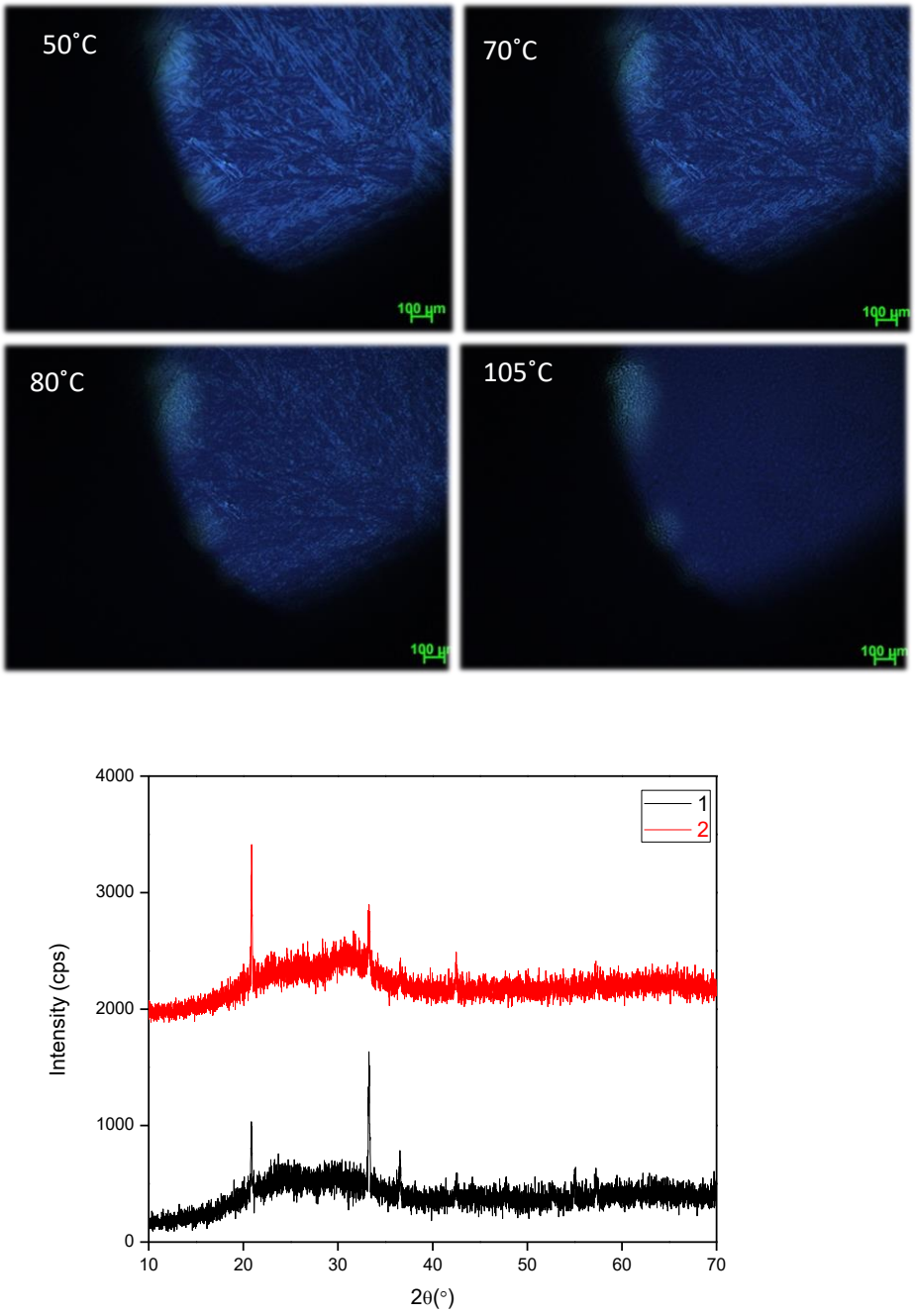

Figure 3.1.3.8. The POM images of 6:2 film at indicated temperatures and XRD patterns at 50(2) and 80°C (1).

A similar experiment is performed over ATR-IR by heating the samples from 40 to 100˚C. The spectral changes are shown in Figure 3.1.3.9. The sharp peaks in the 1300-1500cm^{-1} region originates from nitrate, likely a counter ion of a Ag^{+}-surfactant complex ion, building block of the mesocrystals. The surfactant C-O stretching peaks are also sharp and red shifted in the mesocrystals, and consistent with silver ion-surfactant complexation. The spectra start changing at around 50^{o}C, but the major changes occur above 70^{o}C. A relatively broad peak at 1000 cm^{-1} appears over 80^{o}C. The peaks around 945 and 545 cm^{-1} are due to phosphate group of Ag_3PO_4.Therefore, Ag_3PO_4 starts forming at around 80^{o}C and almost all silver ions are converted to Ag_3PO_4 at around 100^{o}C, see Figure 3.1.3.8. The surfactant peaks remain at all temperatures because surfactant burns above 200^{o}C. Intensity of the nitrate peaks decrease with increasing temperature.

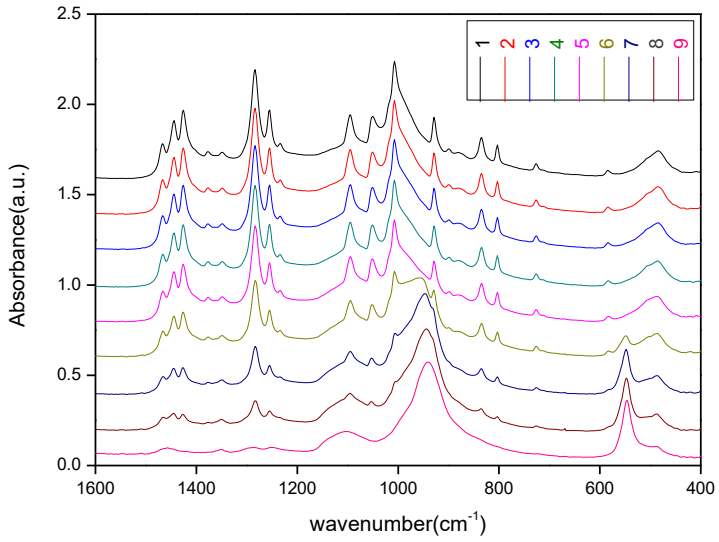

Figure 3.1.3.9. The ATR-IR spectra of 4:1.33 by heating gradually from 40˚C (1), 50˚C (2), 55˚C (3), 60˚C (4), 70˚C (5), 80˚C (6), 85˚C (7), 90˚C (8), and 100˚C (9).

Morphology of the Ag_3PO_4 particles are also checked using SEM imaging by considering the phosphoric acid amount, thickness of the film, and temperature. XRD shows the formation of cubic silver phosphate but the SEM clarifies the morphological changes. At 70˚C, the shape is like triangle with big holes in the 4:1.33 sample. Close inspection shows that these triangles are like smooth films with a few hundred nanometer pores and much larger holes (tens of micron), see Figure 3.1.3.10. The shape of the particles at 100˚C, prepared from the same solution, is tripodal with triangle holes.

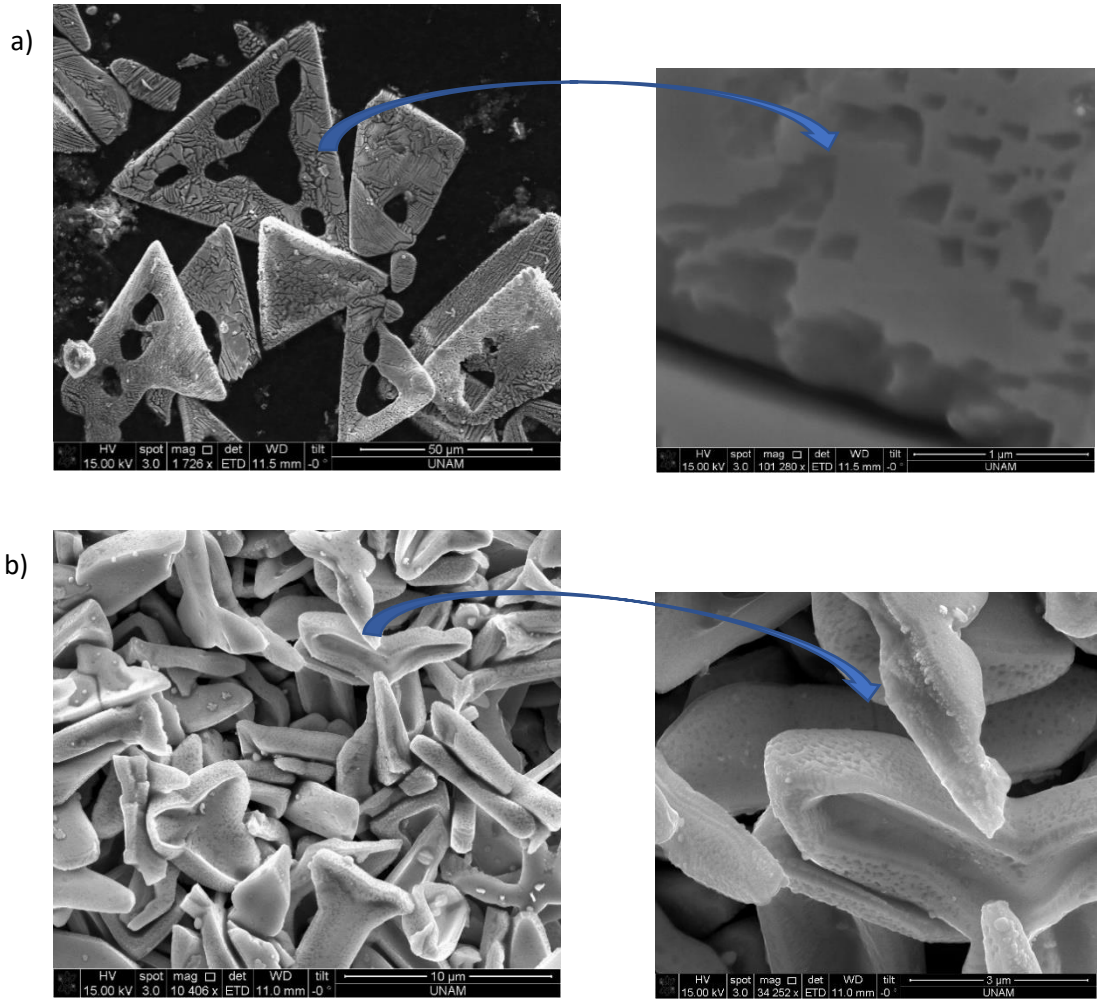

Figure 3.1.3.10. SEM images of the samples of 4:1.33 at a) 70˚C and b) 100ºC.

We also record the SEM images of the Ag_3PO_4 particles, prepared by increasing amount of phosphoric acid up to 4:10 Ag(I):H_3PO_4 in the initial solutions and heated at 100ºC, see Figure 3.1.3.10. The shapes are still tripodal but starts to deform with increasing phosphoric acid concentration, and the sample, prepared from 4:10 solution looks like a film. However, one of the problem of increasing phosphoric acid that it reacts with glass slide makes the Ag_3PO_4 stick on glass at higher temperature, like 300˚C. The spin coated (2000 rpm, 20 sec.) film is transparent, but even with a naked eye, some dusty particles are visible on glass slide. Still the quality of the thin film is poor, but this may not be an issue for some electrochemical applications. Another problem is the solubility of silver phosphate at higher phosphoric acid concentrations.

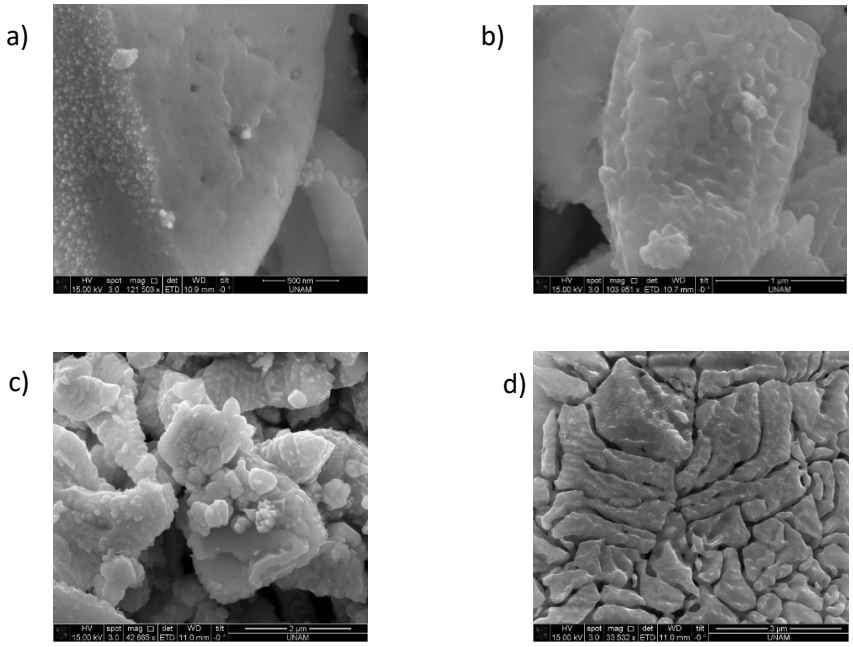

Figure 3.1.3.11. The SEM images at 100˚C the set of a) 4:1.33, b) 4:2, c) 4:8, and d) 4:10.

Figure 3.1.3.12 shows SEM image of the soft mesocrystals, exposed to high energy electron beam. The image show existence of porous regions, but it is difficult image for detail structural features. The beam sensitivity indicates the major difference between these samples and bulk silver phosphate (not sensitive in beam so much). The TEM images of 4:1.33 solution at 100˚C thin films showed the porosity, see Figure 3.1.3.13.

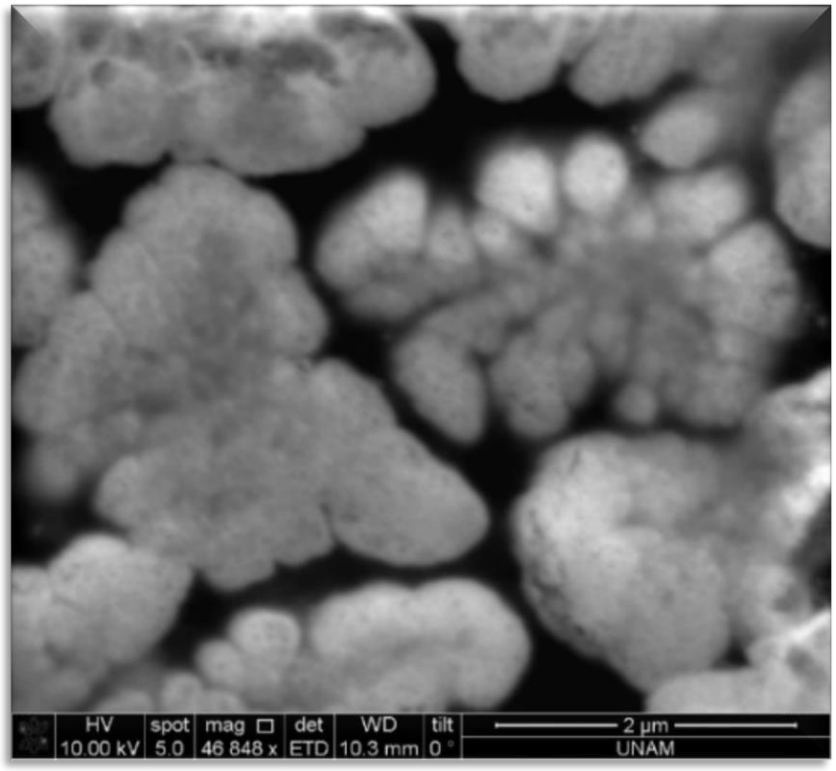

Figure 3.1.3.12. The SEM images of 4:1.33 mesocrystal at RT under beam.

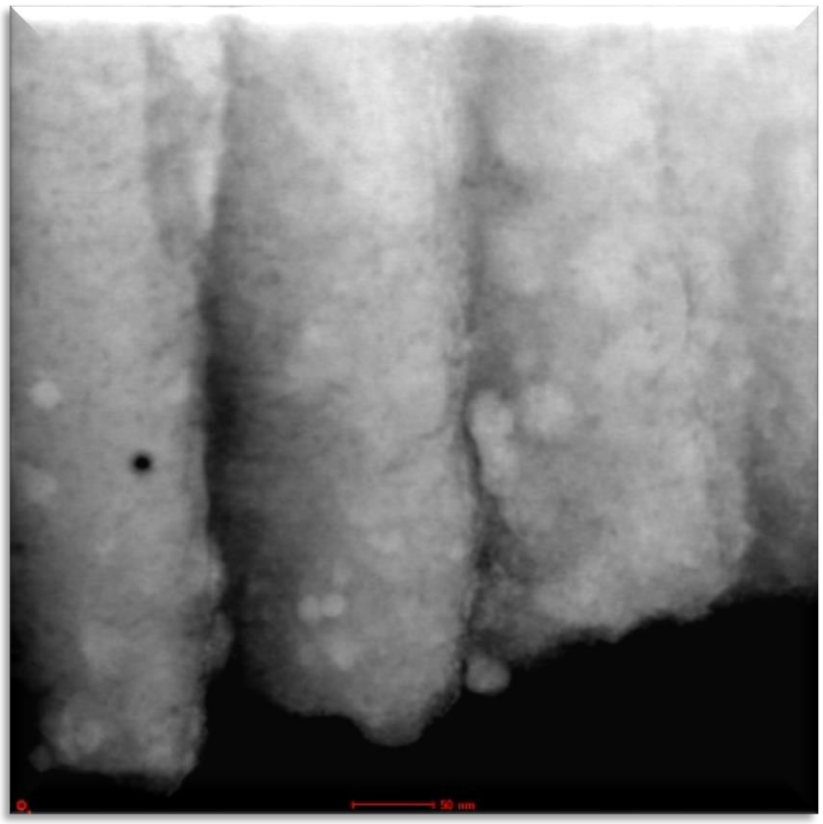

Figure 3.1.3.13. The TEM images of 4:1.33 calcined film at 100˚C.

In conclusion, the soft mesocrystals seems not the way to produce mesoporous silver phosphate using LLM system at high temperatures. The reaction started at low temperature. Soft mesocrystals are so sensitive, more active and mesostructured. Therefore, the temperature should be set to a range of 70-100˚C, and duration time should be longer for 70˚C and shorter at higher temperatures. 3-5 hours reaction time, at 100˚C. is sufficient. The washing procedure is also important, because when the sample is washed with water under light, the impurities related to Ag starts to form.

3.2. Decant Solution in the SNPA System

In Section 3.1, the SNPA system discussed by only considering the precipitates and homogenous solution by adding nitric acid. The nitric acid is important to control of the salt/surfactant mole ratios. Nevertheless, after removing the yellow precipitates, the homogenous solution are also coated, calcined, and characterized by using XRD, SEM, ATR-IR techniques.

It has been shown that the soft mesocrystal phase is so stable, even after 3 weeks. Without nitric acid in solution, the yellow bulk silver phosphate crystals from and precipitate that is, after a while, centrifuged to separate the precipitate. The remaining solution is homogenous and still contains stoichiometric $AgNO_3$ and H_3PO_4, except the salt/surfactant ratio is different than initial solution. After centrifugation, the remaining solution is coated on glass slide to observe the mesophase. Figure 3.2.1 shows the small angle and high angle XRD patterns of the freshly coated samples, obtained from the solutions with and without nitric acid. The small angle XRD patterns are the same, the difference is only on the intensity. However, their high angle XRD pattern are quite different. The reason could be lower concentrations of silver and phosphate sources in the gel media or in the soft mesocrystal. Notice that the thickness of the films is also different because of changing ingredient/surfactant mole ratio. The XRD pattern of the aged films, after 3 weeks, still display the pattern of soft mesocrystal, indicating high stability. Preventing soft mesocrystal formation seems to be impossible. The mesocrystal formation has been investigated by changing $AgNO_3$ concentration in the media (starting from zero and gradually increasing up to 2 $AgNO_3$ per phosphoric acid). The experiment shows that above soft mesocrystal start immediately forms at 0.6:1 and 0.65:2 mole ratios of

$AgNO_3$:H_3PO_4. However, after two days of coating, the soft mesocrystal forms even at 0.35:2 mole ratio, observed under POM. At the lower ratios, such as 0.35:2 mole ratio, first a hexagonal LLC mesophase is observed but in two days, the firework shaped mesocrystals are realized.

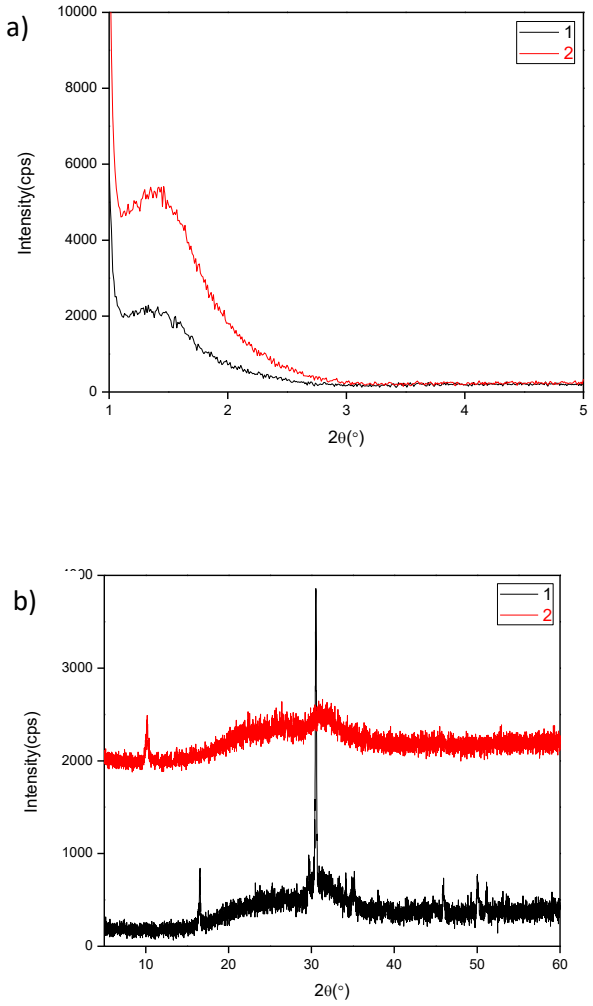

Figure 3.2.1. The XRD Patterns of 12:4 mole ratio of SNPA fresh films a) small angle and b) high angle with (1) and without (2) HNO_3 in water.

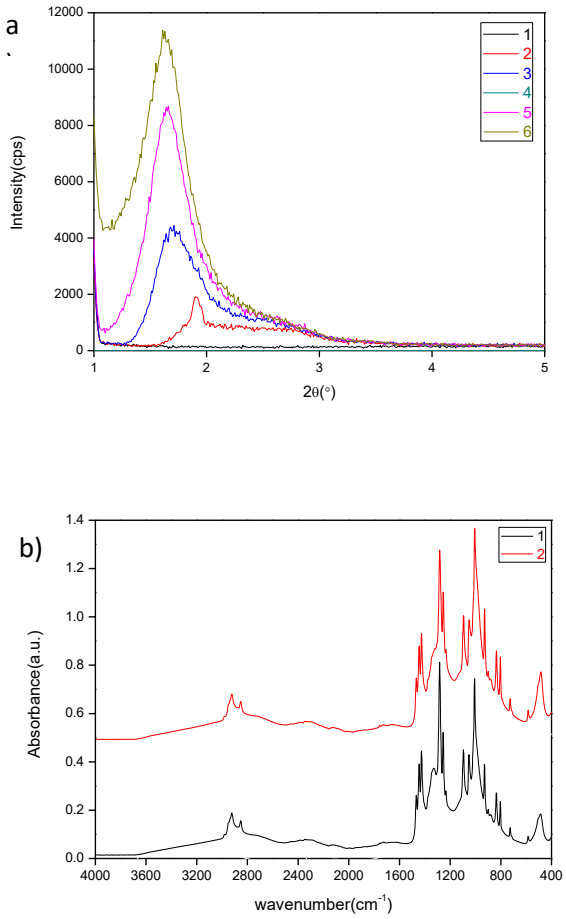

Figure 3.2.2. The XRD patterns of 12:4 SNPA decant aqueous solution after coating and aging the films; fresh (1), 5 min (2), 10 min (3), 15 min (4), 20 min (5), and 25 min (6) and b) ATR-IR spectra of the same samples after aging 5 min (1) and 12 min (2).

Aging of films are also monitored over time by collecting XRD patterns, see Figure 3.2.2. As shown in the small angle region, the diffraction line gradually shifts to lower angles by aging, this is indicating the formation of mesocrystals. However, the same trend is not observed in the 12:4 silver/phosphoric acid sample, after milliseconds the mesocrystal form so rigid. This investigation also shows that the amount of silver ion in the media is very important, mesocrystal formation is enhanced at higher silver concentrations. The

ATR-IR results also supports above proposal. The IR peaks becomes sharp upon mesocrystallization, see Figure 3.2.2b.

The films are calcined at various temperature to covert mesophase and mesocrystals to Ag_3PO_4. The SEM images of the 6:2 film (drop-cast coated), calcined at 300˚C shows a film, bulk silver, and silver phosphate formations. Spherical particles over the film, are likely bulk silver. This image shows that the silver phosphate thin films can be obtained from LLC mesophases, however either heat or light reduces the silver ion to silver metal, as evidenced from XRD and plasmon mode of Ag.

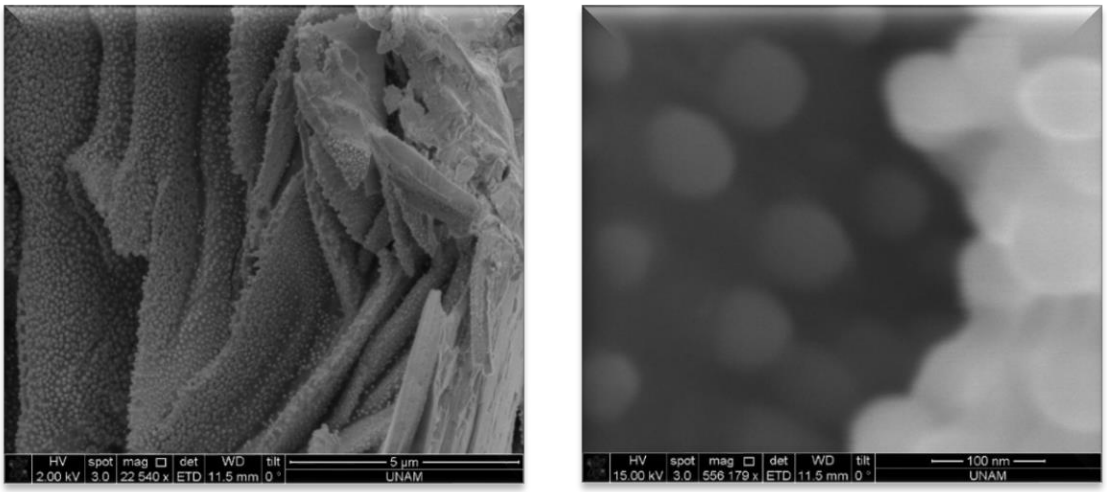

Figure 3.2.3. The SEM images of film, drop-cast coated using 6:2 $AgNO_3$:H_3PO_4 decant aqueous solution, at 300˚C.

As a result, preparation of SNPA solution from decanted solution shows that the thin film formation is feasible by slowing mesocrystal formation process. However, silver metal formation is clearly observed over film surfaces. Discarding precipitates decreased bulk

formation but still silver metal forms are noticed. The films need further investigations to elucidate their structure, porosity, surface area, etc.

3.3. Silver Triflate- Phosphoric Acid Lyotropic Liquid Crystalline Mesophase

The observation of the soft mesocrystal formation indicates that the behavior of silver nitrate in the salt-surfactant lyotropic liquid mesophases. To understand the unique behavior of silver salts in the system, another silver source is used, that is silver triflate ($AgCF_3SO_3$, denoted as AgOTf). Similar experiments are performed that is the nitric acid effect, phosphoric acid, surfactant, and temperature, and light sensitivity.

The importance of the surfactant effect has been tested using both a pluronic (P123) and 10 lauryl ether ($C_{12}EO_{10}$). For the phosphoric acid effect, 10-lauryl ether is used as the surfactant to compare the set of 4:1.33 to 4:10 Ag^+/H_3PO_4 solutions. The first stoichiometric mole ratio is chosen as 6:2:1 AgOTf: H_3PO_4:P123 solution in water. The ATR-IR spectra show sharp phosphate peaks and additional peaks related to triflate ion, see Figure 3.3.1. Clearly the sharp peaks observe at around 1300-1500 cm^{-1} region disappeared in the spectra of silver triflate samples, indicating that these peaks are due to coordinated nitrate ions and they are part of the mesocrystals. High angle XRD patterns display some sharp lines, also indicating a formation of the soft mesocrystal. The similar shapes are observed under POM. However, the some of the diffraction lines can be indexed to silver triflate, see Figure 3.3.1. The other undetermined diffraction patterns would be related to soft mesocrystal. This shows that the silver triflate leaches out from both the mesophase and/or mesocrystal.

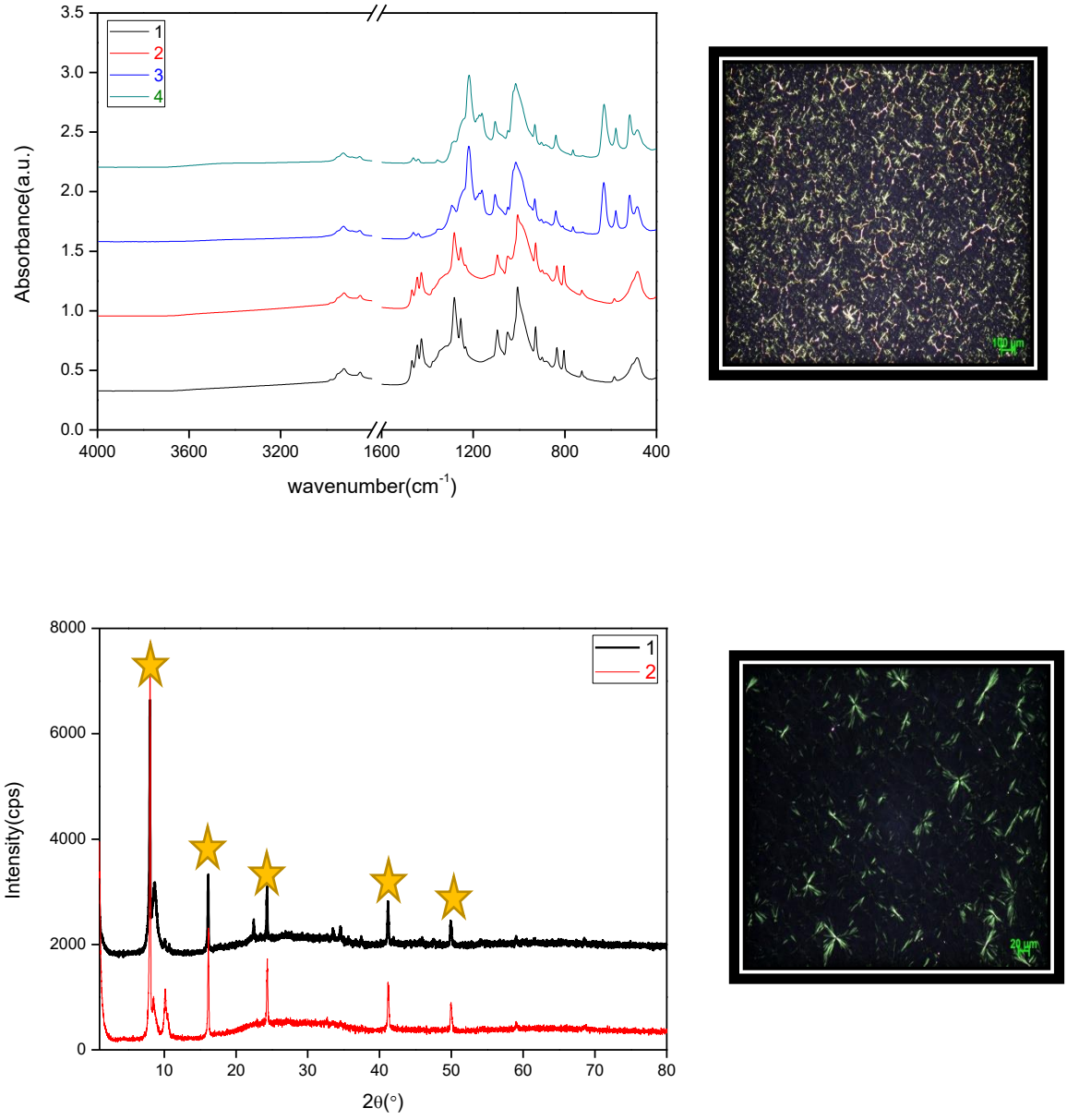

Figure 3.3.1. The ATR-IR spectra of 12:4 $AgNO_3$: H_3PO_4: $C_{12}E_{10}$ films without (1) & with (2) HNO_3 in water, and 6:2 AgOTf: H_3PO_4: P123, with (3) & without (4) HNO_3, XRD pattern of 120:40 (1) and 120:0 (2) AgOTf: H_3PO_4: P123 in water, and the POM images of 6:2 AgOTf: H_3PO_4: P123 in water and ★ is belong to AgOTF.

The SEM images of 6:2:1 AgOTf: H_3PO_4:P123 film, calcined at 400˚C show the differences of spin coating and drop casting films on silicon, see Figure 3.3.2. The drop film has big particles, and spin-coated sample is a more homogenous film with some shiny tiny particles. Nevertheless, still it has bulk silver formations and bulk silver phosphate with smaller size in films.

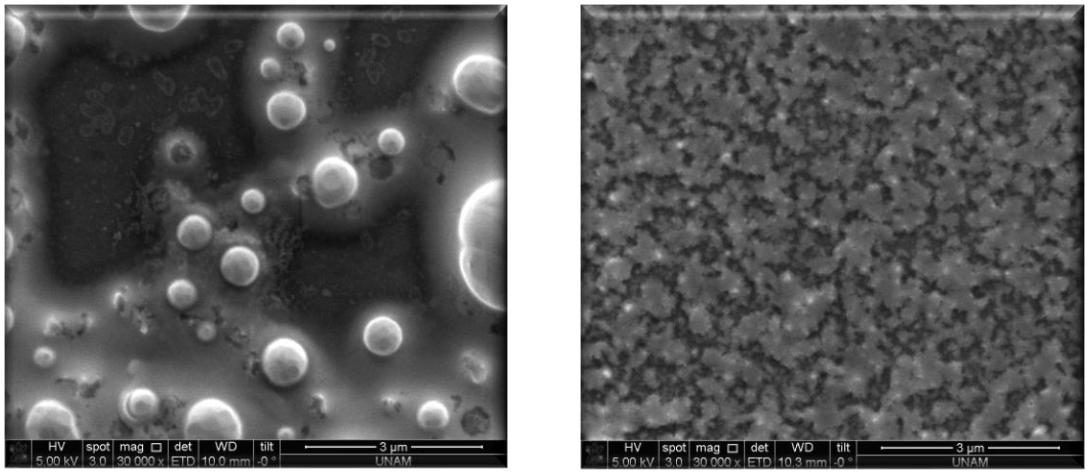

Figure 3.3.2. The of SEM images of sample calcined at 400˚C from of 6:2:1 AgOTf: H_3PO_4:P123 aqueous on silicon a) drop casting and b) spin coated.

Figure 3.3.3 shows the XRD pattern of calcined films, it displays sharp lines, indexed to Ag_3PO_4 crystals. JCPDS cards of its clarifies that Ag_3PO_4 is synthesized with some silver metal; observed around 38.13˚ 2θ. The probably tiny shiny particles observed in the SEM images is silver metal. The temperature, light, and beam sensitivity were also observed in this salt.

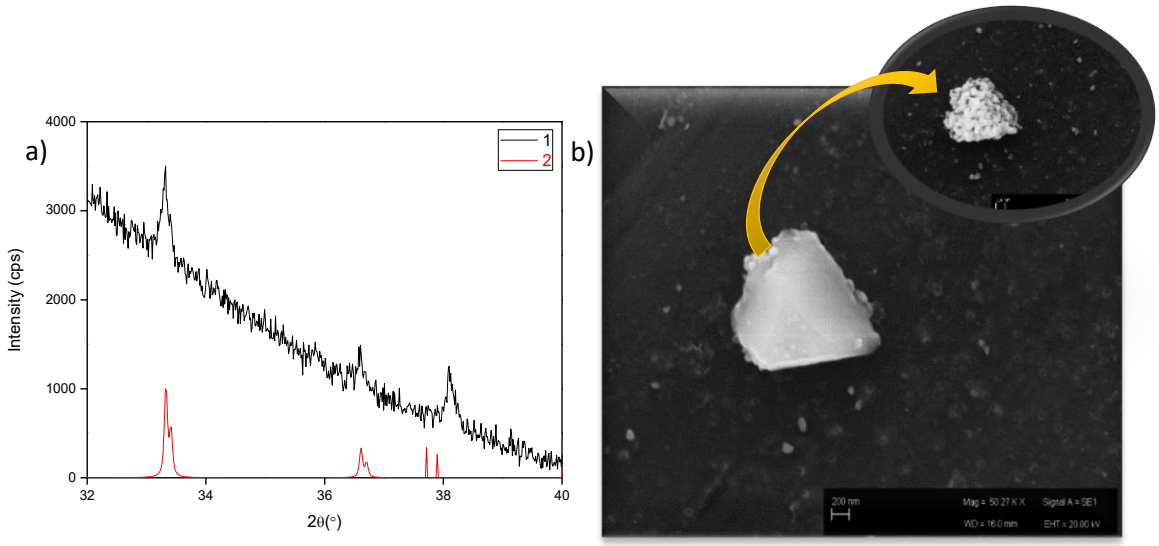

Figure 3.3.3. a) The XRD pattern the of samples calcined at 300˚C, from 60:20:1 AgOTf: H_3PO_4:P123 aqueous solution at 300˚C (1) and JCPDS card of Ag_3PO_4 (2), and b) SEM image of its on silicon.

The phosphoric acid effect has been investigated by increasing the phosphoric acid in the initial solutions of 12:1 mole ratios of AgOTf: $C_{12}E_{10}$ in water from 4 to 36 phosphoric acid mole ratios. In Figure 3.3.4, the XRD patterns display weak silver triflate lines, major lines originate from the soft mesocrystals. Mesoorder remains in all samples, inspect small angle region in the XRD patterns. The ATR-IR spectra and the POM image verify this fact. The effect of triflate decreases with increasing phosphoric acid amount. Therefore, this might be a solution to neglect AgOTf formation in RT. ATR-IR spectra shows that while increasing phosphate ion in solution, the pattern is similar to hexagonal phase like previous part. This is related to domination of phosphate and higher solubility of AgOTf in phosphoric acid in the mesophase. As a result, this section indicates that silver triflate can be used in this system, but the problem is that leaching of silver triflate and soft mesocrystal form are not easily distinguishable.

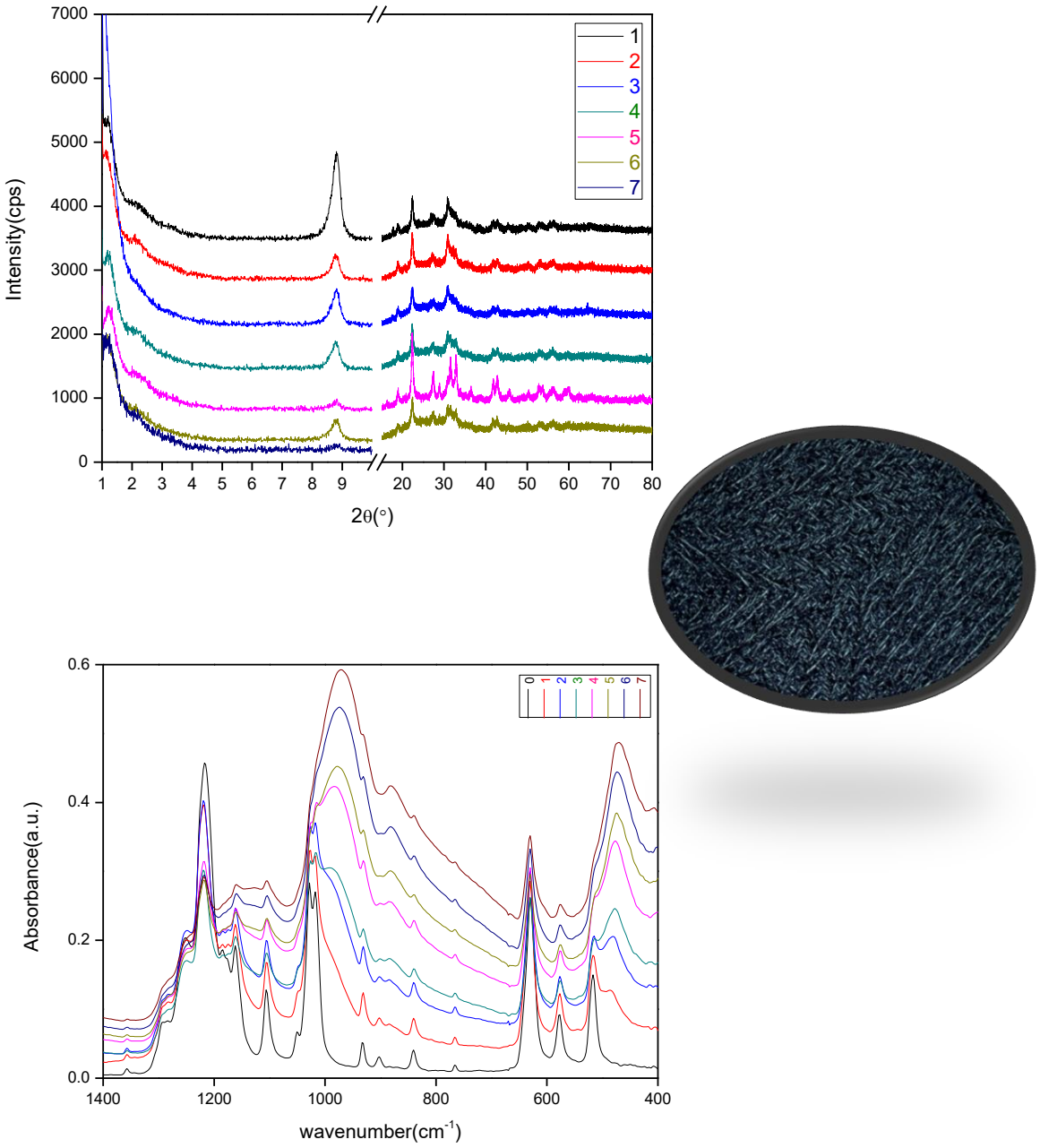

Figure 3.3.4. (Top) XRD patterns of different phosphoric acid mole ratios at 12 mole ratios of AgOTf in $C_{12}E_{10}$ and 5 ml water with various H_3PO_4 amount. (Bottom) ATR-IR spectra of the same samples and POM image of 12:36 Ag^+:H_3PO_4 mole ratios. The mole ratios of $C_{12}EO_{10}$:AgOTf:H_3PO_4 are 1:12:0 (0), 1:12:4 (1), 1:12:8 (2), 1:12:12 (3), 1:12:16 (4), 1:12:20 (5), 1:12:24 (6), 1:12:36 (7).

3.4. Cation Exchange of Mesoporous $LiMPO_4$ Powders

In this section, we will discuss a new type of synthesis of silver phosphate using cation exchange method. The targeted materials are $LiMnPO_4$, $LiCoPO_4$, and $LiNiPO_4$ that have been synthesized using similar approach in Işıl Uzunok's master thesis work, not published yet. Every step of cation exchange will be clarified by using XRD and SEM techniques and color observation.

Cation exchange method has been employed to obtain mesoporous silver phosphate using pre-formed mesoporous $LiMPO_4$ samples, synthesized by salt-acid-surfactant lyotropic liquid mesophases. Simply, similar solutions were prepared using lithium salt together with Mn(II), Co(II) or Ni(II) salts in place of silver salt and keeping the salt:H_3PO_4 ratio stoichiometric, then coating these solutions, and then calcination at around 300 or 400˚C yields the amorphous mesoporous $LiMPO_4$ powders. Details of the synthesis and characterization will be the thesis of Işıl Uzunok when it will be published, therefore those will not be discussed further in this thesis.

0.01 M of silver nitrate aqueous solution is prepared then 3-4 mg of $LiCoPO_4$ (prepared from 1:10:10:10 P123:Li(I):Co(II):H_3PO_4 solution and calcined at 400˚C, decoded as Co (10)) is added to the solution and stirred for several days. The blue powder of Co (10) turns black after 1 week. Since we knew the light sensitivity of silver phosphate, the same experiment is performed in dark condition, in a covered vial with an aluminum foil. After 1 week, a discoloration from blue to yellow is observed. Color is very important property to check whether the exchange proceeds or not.

Son's research group showed that cation exchange of CdSe with Ag^+ ion to obtain Ag_2Se nanoparticles. In their work, they used small amount of methanol to facilitate the cation exchange. [62] In the second round, we prepare 0.01M silver nitrate solution 1:9 volume ratio solution of methanol and water. After 3 hours of exchange, all blue powders turns to yellow, the amount of silver ion in the media is 5 to 6 times of $LiCoPO_4$. This observation encourages us to follow the pattern ambitiously. When looking at SEM images, it was seen some rod or fiber type and spherical particles, see Figure 3.4.1.

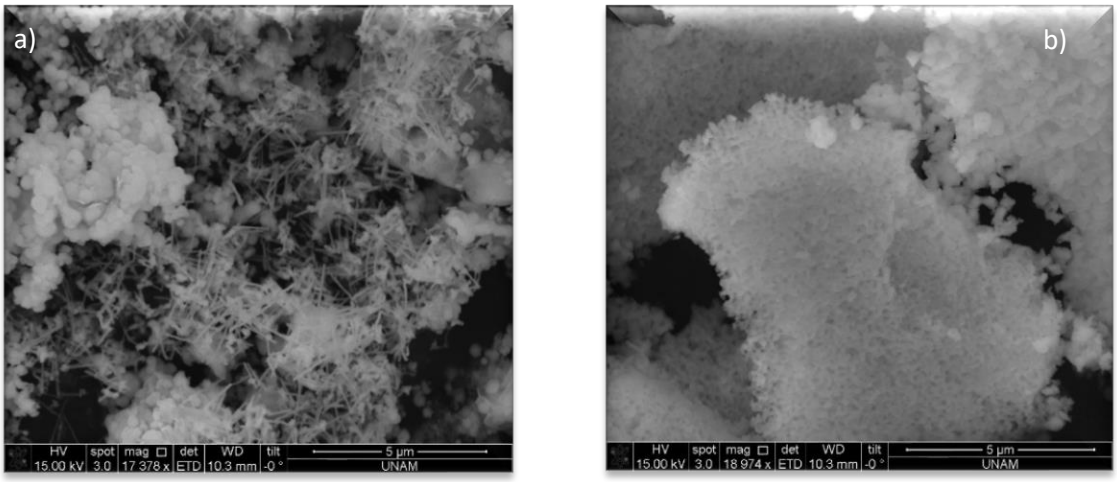

Figure 3.4.1. a) The SEM images of after cation exchange of $LiCoPO_4$ using 0.01 M $AgNO_3$ solution, and b) Co (10) before cation exchange.

Then, another $LiCoPO_4$ sample, prepared using1:90:90:90 (P123:Li(I):Co(II):H_3PO_4, decoded as Co(90) after calcination) solution, is used in the same procedure to obtain mesoporous Ag_3PO_4, but the calcination temperature of above sample is 300˚C. In this temperature and mole ratio, it is observed perfect mesoporous spherical particles in addition to rods and films, see Figure 3.4.2. Therefore, the final product of silver

phosphate has also rods and spherical particles, see Figure 3.4.2. Nevertheless, this demonstrates the success of this method in 1:9 mole ratios of CH_3OH:H_2O solution.

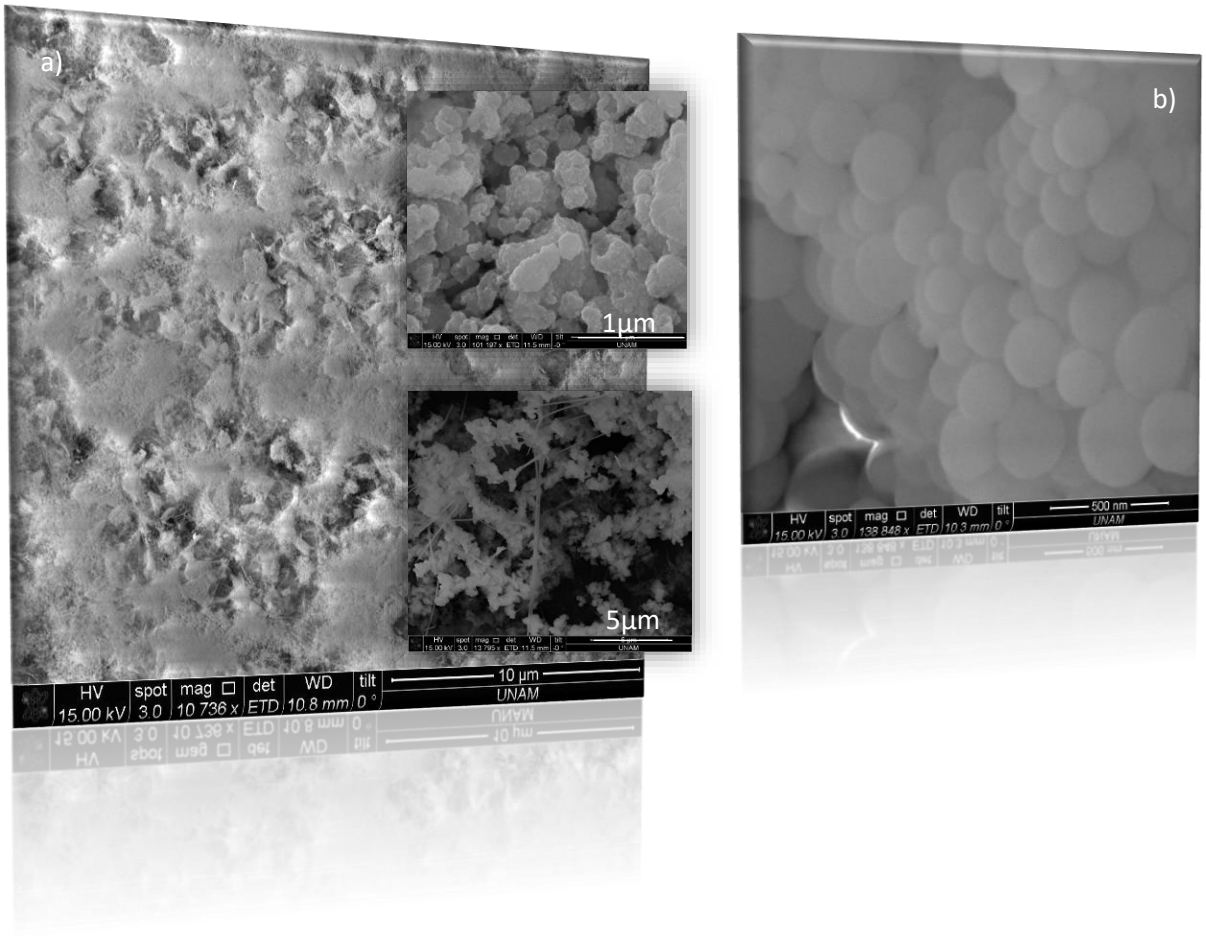

Figure 3.4.2. The SEM images of Co (90) a) after cation exchange, and b) before cation exchange.

TEM images shows contrast fluctuation, see Figure 3.4.3. The first implication of features is that there are two types of materials intact to each other. The first implication of bend structure silver is that shiny particles on grey particles are silver metal. The unknown grey

particles are probably phosphate or Co part. However, these are silver oxide or phosphate derivatives after deformation occurs.

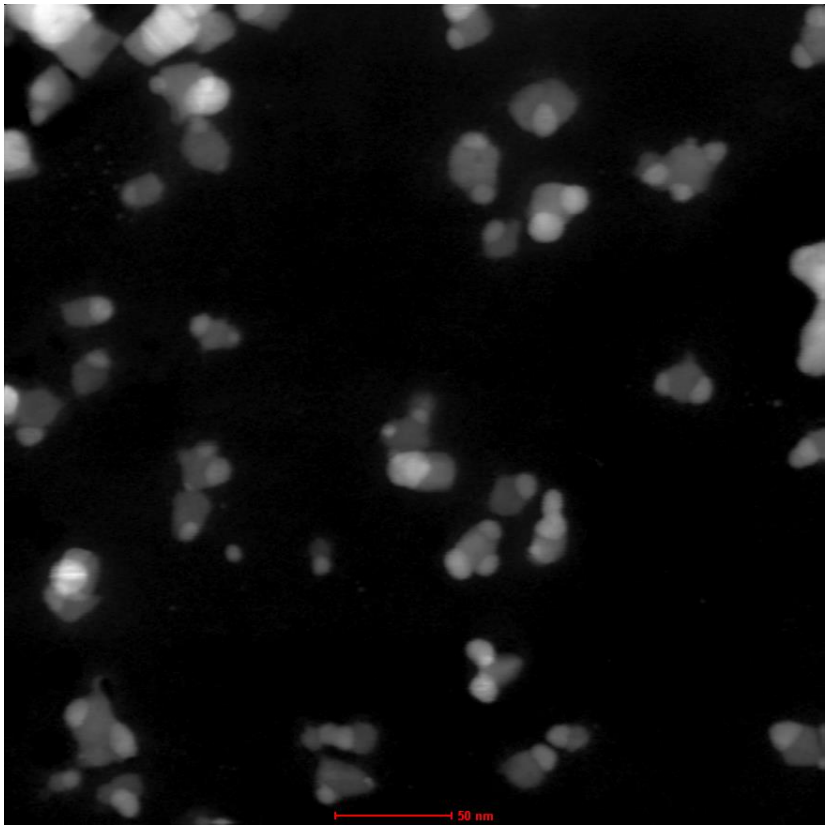

Figure 3.4.3. TEM image of Co (90) after 0.01M 1:9 volume ratio of CH_3OH:H_2O solution

EDS mapping of the TEM images, see Figure 3.4.4, indicates that the cation exchange began on the surface of the sample, then the middle part change, therefore small amount of Co exists between silver phosphate particles. In this exchange process, silver is not excess enough therefore remaining Co seems be large amount. Mesoporous silver phosphate is not observed but the mesoporosity of Co (90) makes the cation exchange easier and effective.

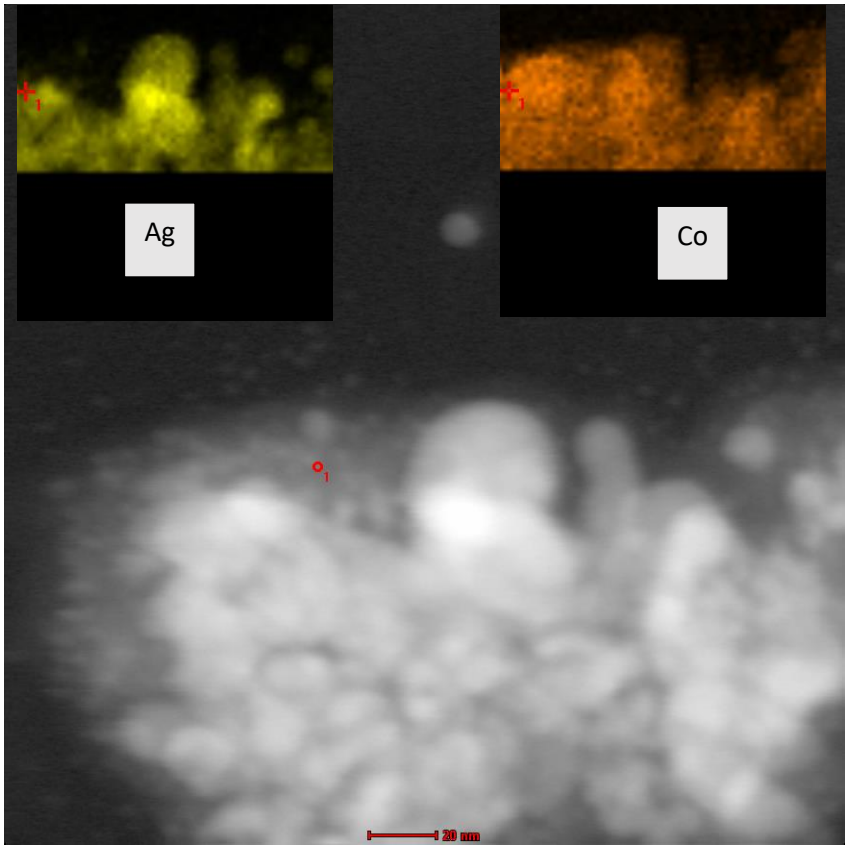

Figure 3.4.4. Ag and Co elemental EDS mapping of Co (90) after cation exchange and the TEM image of the same region.

To better analyze this process, the amount of $LiCoPO_4$ is increased to 25 mg in a 0.1 M silver nitrate solution to obtain large amount of sample, using the same exchange procedure. After 5 hours, it is observed that the color of powder and solution changed to yellow and pink, respectively, and reaction is almost complete. Therefore, it is kinetically controlled reaction. However, increased exchanged time also enhances the deformation of silver phosphate to silver metal and silver monophosphate. Interestingly, the order of the Ag_3PO_4 deformation is as $Co > Ni > Mn$. The cation exchange of $LiMnPO_4$ powder produces the most light-yellow powder and less light sensitive than the other powders.

The other samples ($LiCoPO_4$ and $LiNiPO_4$) produce darker (mixture of yellow and black) powders due to enhanced formation of silver-silver monophosphate as side products. The XRD pattern, see Figure 3.4.5, shows that all of precursors can be converted to silver phosphate, but Ni and Co samples have more silver and silver monophosphate crystals than Mn sample under the same conditions. The XRD pattern can be indexed to Ag_3PO_4 with a single line around 34°, 2θ, that is very low from the Mn sample. SEM images also shows the best cation exchange happens in Co (90) in terms of keeping the original morphology. However, the Mn sample seems to have cubic silver phosphate particle in regular pattern, see Figure 3.4.6.

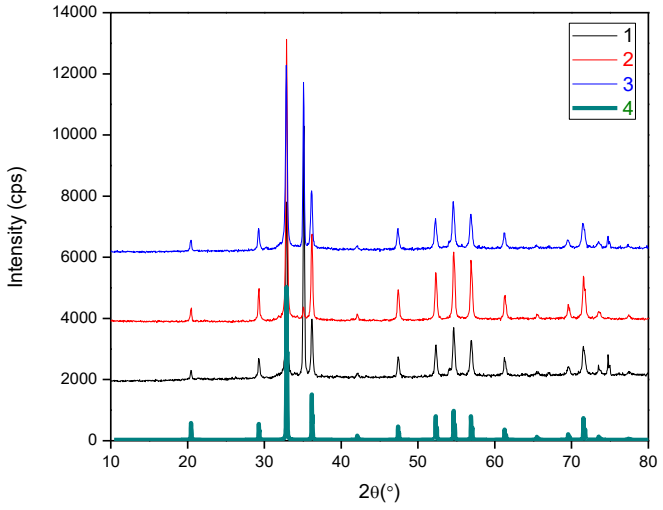

Figure 3.4.5. XRD patterns of Co (1), Mn (2), Ni (3) 90 mole ratios after cation exchange and with Ag_3PO_4 PDF card (4).

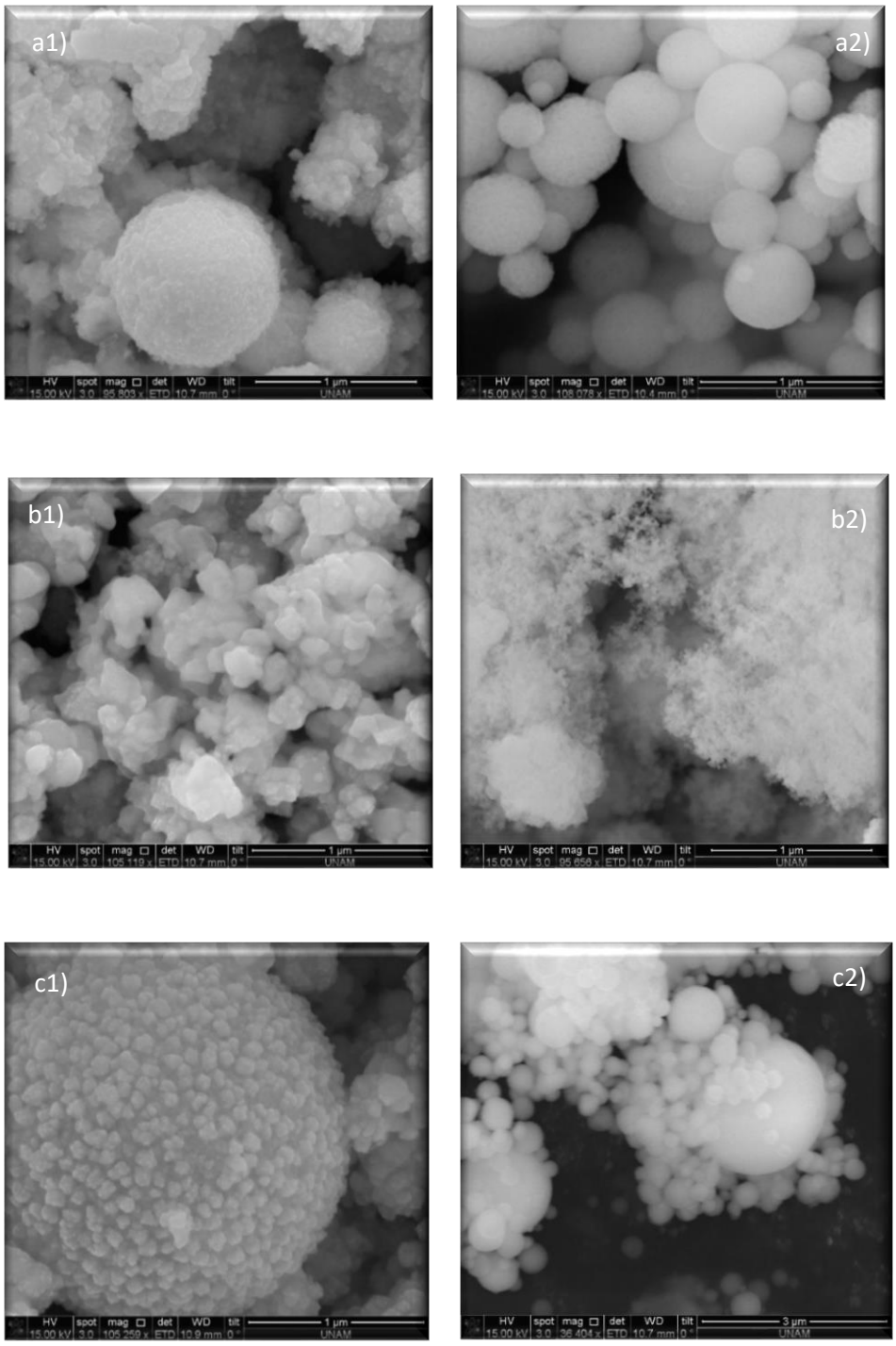

Figure 3.4.6. SEM images, before (right) and after (left) cation exchange of a1) and a2) Co (90) b1) and b2) Mn (90) and c1) and c2) Ni (90).

The exchange reactions are quite fast. Figure 3.4.7 and 3.4.8 show a set of photographs and SEM images recorded during the exchange reactions over time. The colorless solution turns pink in the Co (90) and green in the Ni (90) and no change in the Mn (90) samples after 15-30 minutes, indicating the exchange process is complete. SEM images of the samples, collects at different exchange time of the same samples show not much morphology change in the Mn sample, little change in the Ni sample (two different morphology, likely due to Ag_3PO_4 and silver-silver monophosphate side product) and more in the Co sample over time.

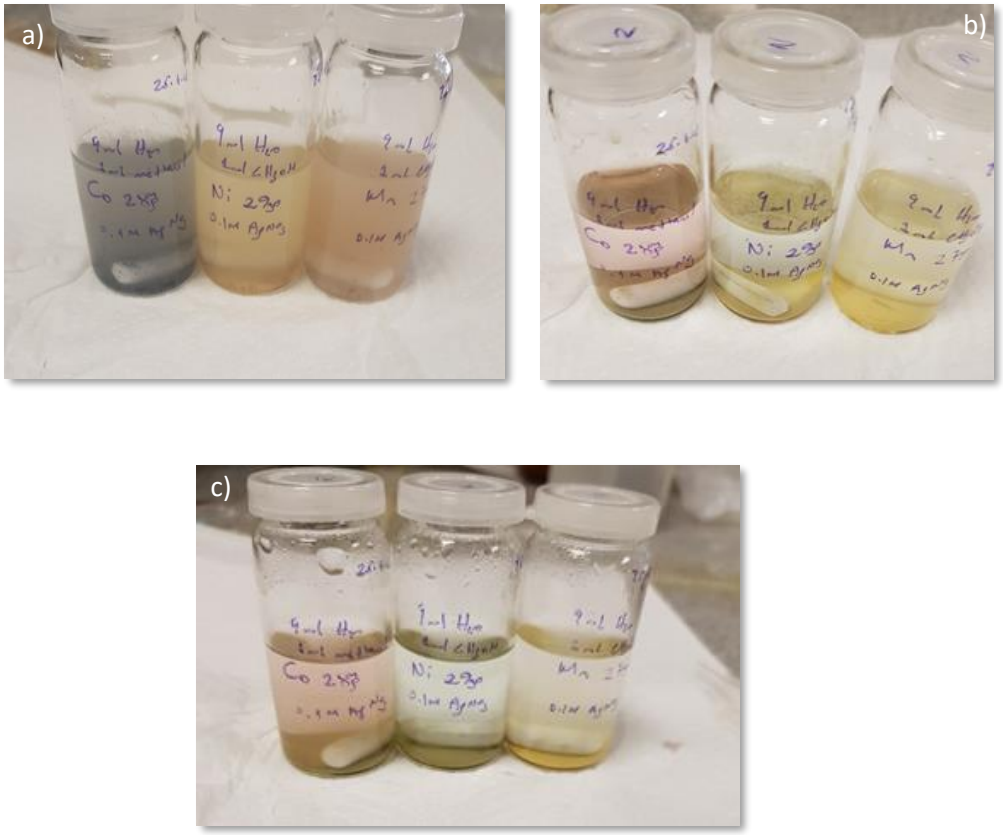

Figure 3.4.7. Photograph of the solutions of left to right Co (90), Ni (90), and Mn (90) over time a) starting point, b) after 15 min, and c) after 5 h.

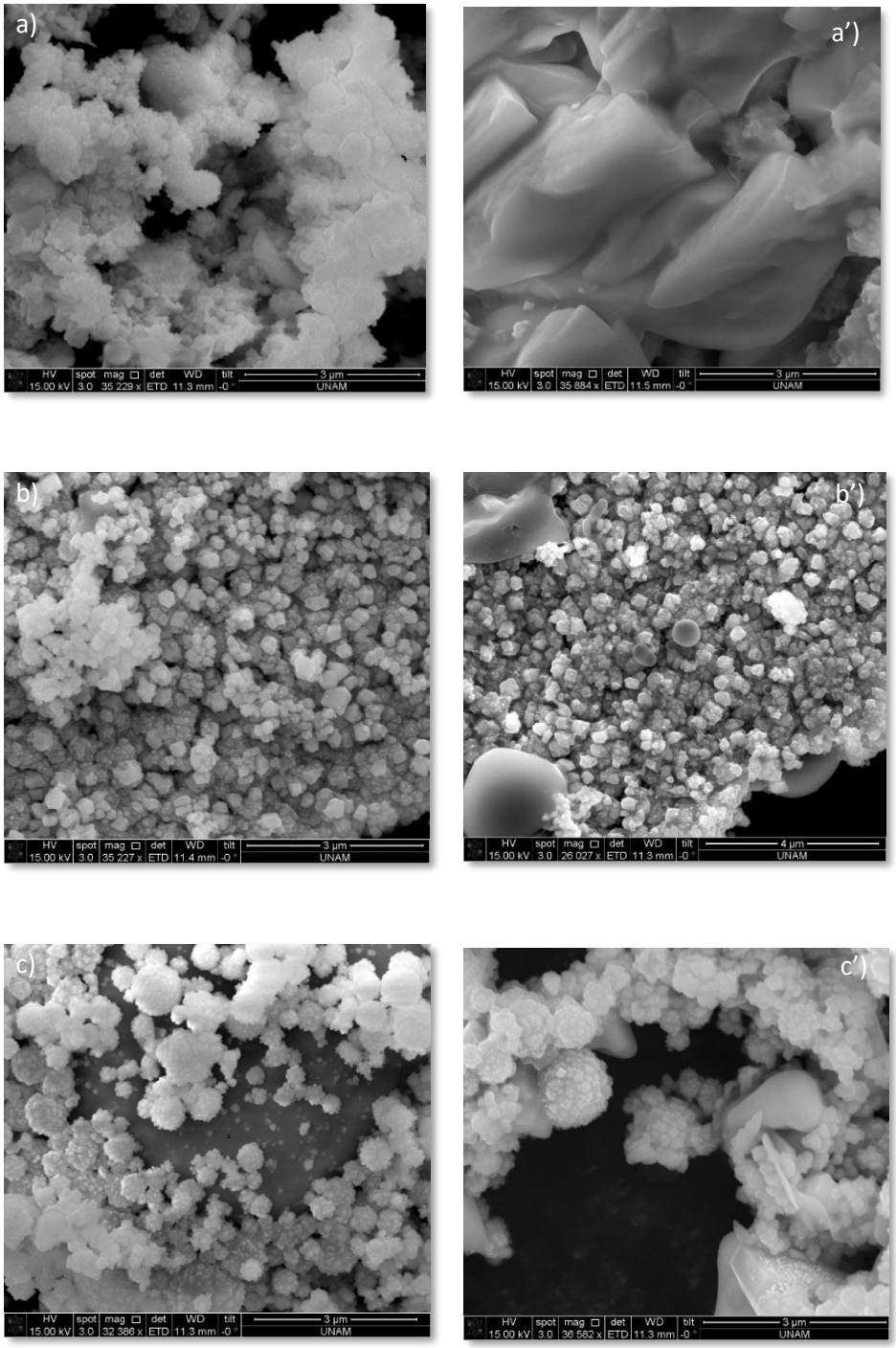

Figure 3.4.8. SEM images of powders, collected at indicated cation exchange time for a) Co (90) after 15 min, and a') after 30 min, a) Mn (90) after 15 min, and a') after 30 min, and a) Ni (90) after 15 min, and a') after 30 min.

As a result, the cation exchange is complete at around 15 minutes. UV-Vis spectra, see Figure 3.4.9, also show that after 15 minutes, cation exchange continues but in large part it is finished. Therefore, the cation exchange is almost complete in 15 min for 25 mg of $LiMPO_4$ (M=Co, Ni, Mn) of powder in 0.1M $AgNO_3$ 1:9 methanol:water solution. Note also that the silver and silver monophosphate bulk forms are increased because of stopping the reaction, taking picture, recording UV-Vis spectra and preparing SEM holders; during these processes, samples are exposed to ambient light. In every step, the dark condition was provided as much as possible; nevertheless, eliminating whole light is so limited because of human eye limitation. In the aqueous solution and presence of the catalyst (Ag_3PO_4) and Ag^+ in the media, the silver monophosphate (Ag_2HPO_4) form is inevitable.

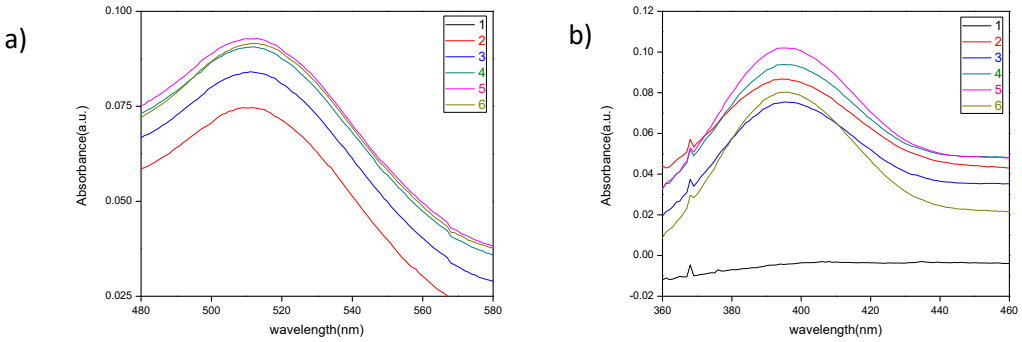

Figure 3.4.9. UV-Vis spectra of a) Co, b) Ni (90) over time during cation exchange of 0 min (1), 15 min (2), 30 min (3), 1 h (4), 3 hrs (5), and 5 hrs (6)

Xu *et.al* proposed a mechanism of photodegradation of CuS particles, where a photo-generated holes reacts with water and oxidize water and electron reduces Cu^{2+} to Cu(0) and reduces the photocatalytic activity. [77] This mechanism also fits to silver phosphate. Martin *et al.* proposed a mechanism for silver phosphate photodegradation in his review paper. [8] They assigned that when irradiation time increased, the formation of H_2O_2 is continued like in Xu's mechanism, referring to conduction band of silver phosphate reduction of oxygen to form H_2O_2, on the other hands, holes, generated in the valance band of silver phosphate produces hydroxide radicals. Therefore, silver phosphate catalyzes organic dye degradation by directly using photo-generated holes under visible light irradiation. [9] The accepted mechanism is;

$$Ag_3PO_4 + hv\ (visible\ light) \rightarrow h^+ + e^-$$

$$Ag^+ + e^- \rightarrow Ag_{(s)}$$

$$Organic(dye) + h^+ \rightarrow CO_2 + H_2O + OH^{\cdot}$$

This clarifies the meaning of photocatalyst for silver phosphate. Electrons and holes in photo-excited silver phosphate enforces the radical formations and these radicals are used to degrade organic dyes. However, silver phosphate decomposes in this process to form silver or silver monophosphate, as evidenced from XRD pattern, the extra sharp and intense line is assigned to Ag_2HPO_4 (silver monophosphate).

3.5. Dye Degradation Experiment

The last part of thesis is to compare the photoactivity of certain samples. It is known that silver phosphate is an excellent photocatalyst for dye degradation. We have produced Ag_3PO_4 in many different morphologies such as bulk cubic silver phosphate in water and ethanol by precipitation method, calcination of thin films and soft mesocrystals, and cation exchange methods.

In section 3.1.1, it was explained how to prepare yellow precipitates of bulk silver phosphate. Precipitates were obtained in water and ethanol solution. Their crystal structures are the same, but SEM images display morphological differences. The water precipitates have a cubic crystal with intended triangles. However, the ethanol precipitates have smoother surface and curvy cubic structure. Photo-degradation experiment also show some differences. Figure 3.5.1a shows time dependent changes of dye degradation using ethanol precipitates, first the catalyst solution is kept in dark for 30 min to make sure no reaction takes place without light. Then, dye degradation under visible light irradiation follows by recording the UV-vis spectrum of solution. The data shows that degradation is so fast and finishes in 5 min. Figure 3.5.1a and 1b show the surfactant effect. Time required for complete degradation seems dependent to the surfactant type. Even though the end times are very close, the best dye degradation performance is observed from the $C_{12}EO_{10}$ sample the second is P123, last is no surfactant. However, the difference is less than 1 minute for ethanol case. The same consideration is investigated using the precipitates from aqueous solutions. The same order is observed, degradation was completed first in the $C_{12}EO_{10}$ sample then P123, and finally no surfactant. In all experiments, 25 mg catalyst is dispersed in 30 ml water with 6 ml of Rh-B dye (from 60

mg/L). These observations show that the ethanol precipitates are more active than water precipitates. The reason is that water precipitates are easily deformed due to high solubility of Ag_3PO_4 in water. Even after 3 cycles (the catalyst has been used twice), the ethanol precipitate performs as good as the water precipitate. A similar precipitation is carried using LiH_2PO_4 as phosphate source, but the activity is not as good as the ones obtained from the phosphoric acid precipitates, see Figure 3.5.1d. The 1st cycle of these samples is similar to the ethanol 2nd cycle obtained from phosphoric acid. Again, the best results are obtained from the ethanol precipitates.

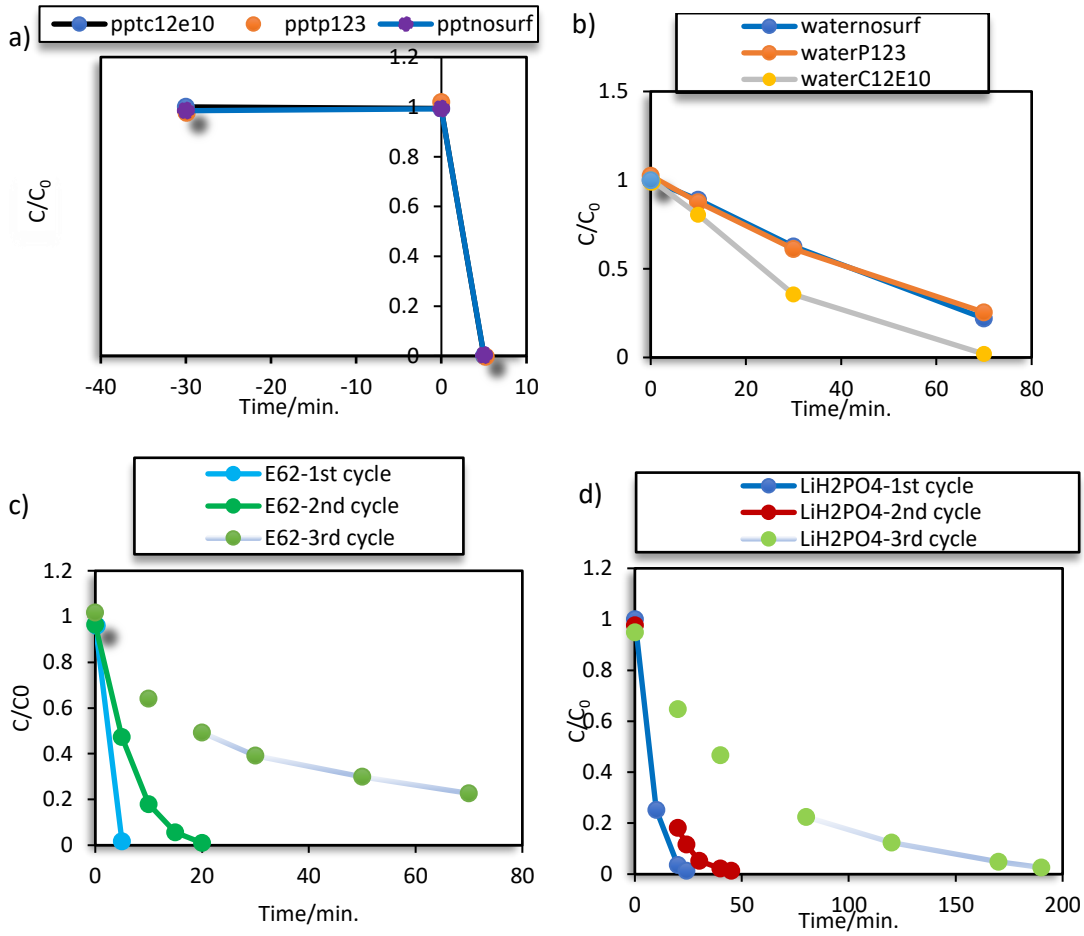

Figure 3.5.1. The graph of C/C_0 vs. time for precipitates a) in ethanol and b) in water c) in ethanol by 3 cycle and d) LiH_2PO_4 as a phosphoric acid source

In all cases stability of the catalyst is an issue. The degradation of dye takes longer time in consecutive runs, indicating decomposition or deactivation of the catalyst. One way to prevent the catalyst degradation is to incorporate some carbon to the surface of the catalyst. Surfactant could be a good source of carbon; therefore, samples without separating the precipitate can be calcined directly in a vacuum oven at 300°C. This ensures formation of black samples, however the black powder collected to test liquid photodegradation experiment using its 25 mg was a big disappointment; the dye degradation reaction is not finished even after 3hrs. The XRD pattern of the sample showed the presence of silver metal. Carbon probably reduces some of the silver ions to silver during carbonization before Ag_3PO_4 formation. Therefore, the calcination temperature is reduced to 150˚C. However, the activity of these samples is not as good as ethanol precipitates, but the stability is much better, see Figure 3.5.2. Introducing carbon improves the stability but enhances the problem of silver formation.

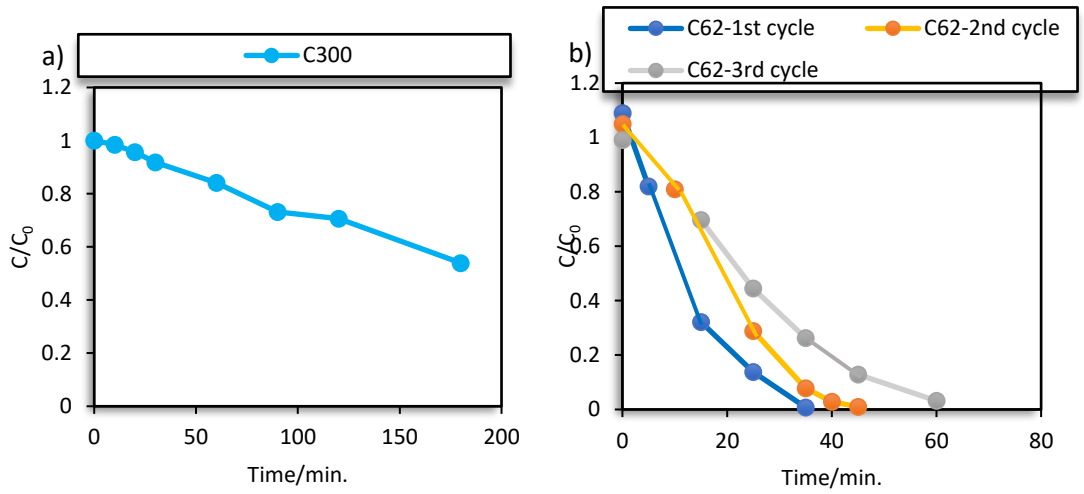

Figure 3.5.2. The graph of C/C_0 vs time for ppt in ethanol, the sample is calcined under vacuum without washing at a) 300˚C and b) 150˚C.

After understanding the precipitates and introducing carbon photodegradation activity, thin film SNPA is tested. The thin film, obtained from SNPA solution and calcined at 300˚C, shows a good; degradation of the same amount dye took 35 minutes, and no activity in dark, see Figure 3.5.3. The major reason is the silver metal formation, as shown in the XRD pattern. The amount of silver phosphate is less due to some silver metals. Therefore, we assigned above temperature at 400˚C.

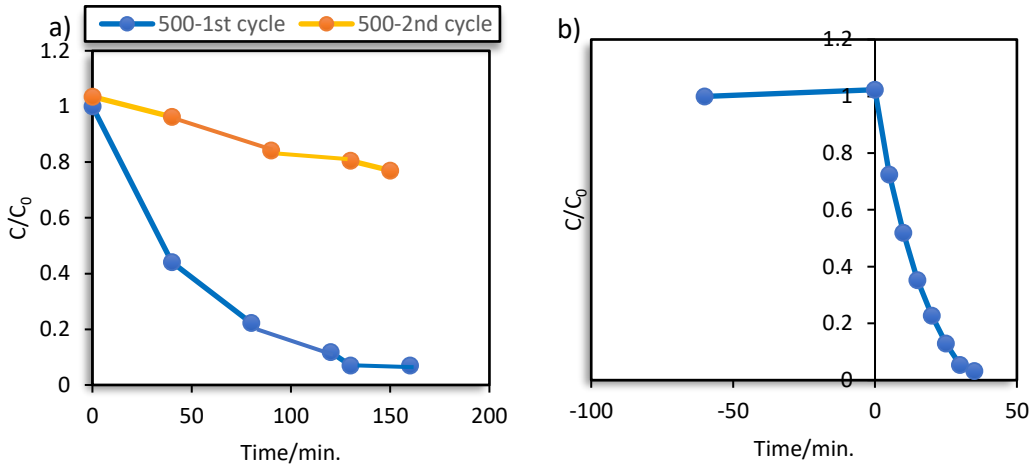

Figure 3.5.3. The graph of C/C_0 vs. time for SNPA thin films, obtained from two different solution and calcined at a) 500˚C, and b) 300˚C.

The 1:6:2 and 1:4:1.33 ($C_{12}EO_{10}$:$AgNO_3$:H_3PO_4) solutions are coated and calcined at 250˚C and 150˚C under vacuum and 15 mg of these samples are tested for dye degradation, see Figure 3.5.4. The time requires to complete the 1st cycle of 250˚C sample is higher than 150˚C sample; i.e. 110 minutes and 70 minutes, respectively. Surprisingly, their 2nd cycle finishes at the same time, 130 minutes later. The stability is improved at high temperature even though some silver metal formed, but at low temperature, it is likely that surfactants are not completely burned or carbonized. Therefore, this would increase the deformation of silver phosphate to silver metal.

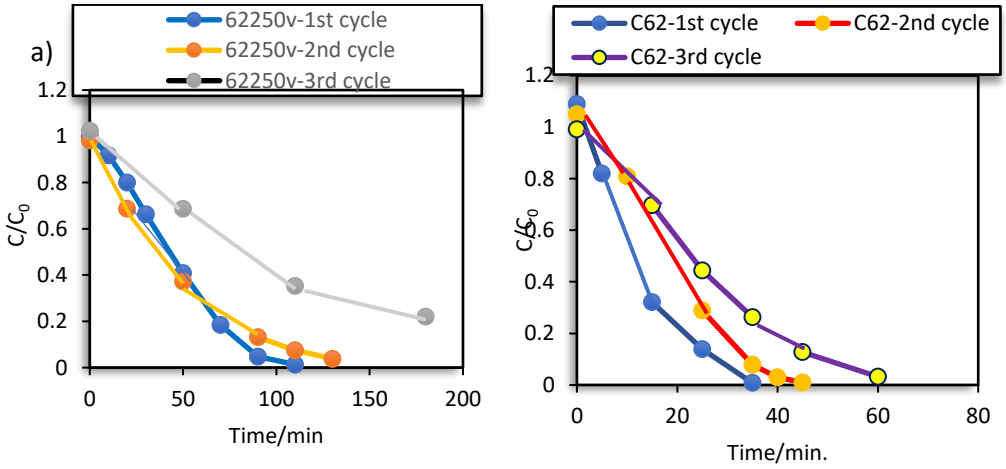

Figure 3.5.4. The graph of C/C_0 vs. time for thin film Ag_3PO_4 a) at 250˚C and b) at 150˚C under vacuum.

Then, soft mesocrystal, calcined at low temperatures are also used for the photodegradation experiment. Accordingly, 3 samples are obtained from ,1:4:1.33 solutions and heat treated under different conditions; conditions are 10 mg sample after heated at 100˚C, 25 mg of sample after 100˚C in vacuum, and 25 mg heat treated at 70˚C, and 10 mg of the last sample, obtained from 1:4:10 solution after heat treatment at 100˚C under vacuum. The gel-like sample is obtained from the 1:4:1.33 sample, heated at 100˚C under vacuum. Introducing carbon decreased activity little bit, but the stability problem was improved in the heat treated samples under vacuum. 1^{st} and 2^{nd} cycle photodegradation time are the same, even after 5^{th} cycle is better from the sample, heat treated at 100˚C under vacuum than the 2^{nd} cycle of just heat treated at 100˚C, compare plots in Figure 3.5.5. Figure 3.5.6 shows the activity behaviors of the samples obtained at 70˚C without washing, the cycle behavior is the same as above. 2^{nd} and 3^{rd} cycle have the same degradation time. However, 70˚C activity is better than 100˚C when looking at the C/C_0 vs time graph. Therefore, Ag_3PO_4 particles or films form at much lower temperatures and they have better activity, likely due to less silver metal formation. Therefore, it is better to avoid high temperature treatments as far as possible.

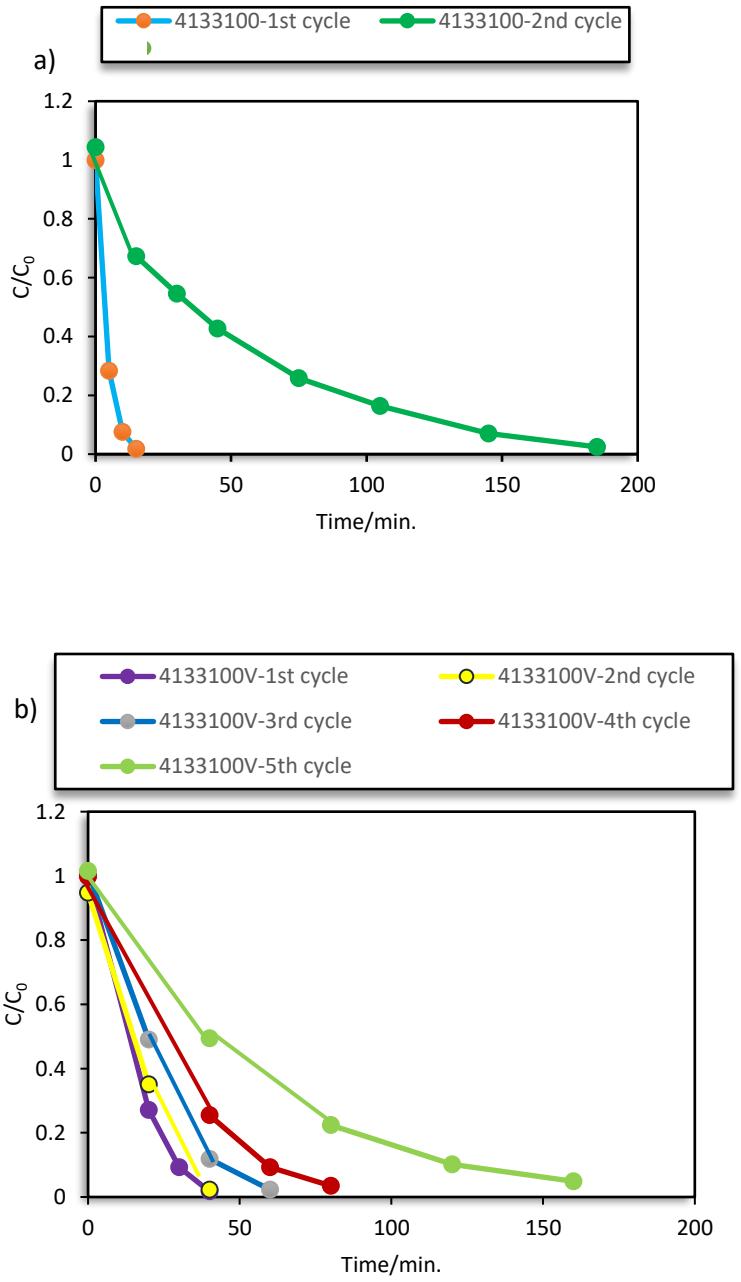

Figure 3.5.5. The graph of C/C_0 vs. time of Ag_3PO_4 obtained from soft mesocrystals at a) 100˚C and b) 100˚C under vacuum.

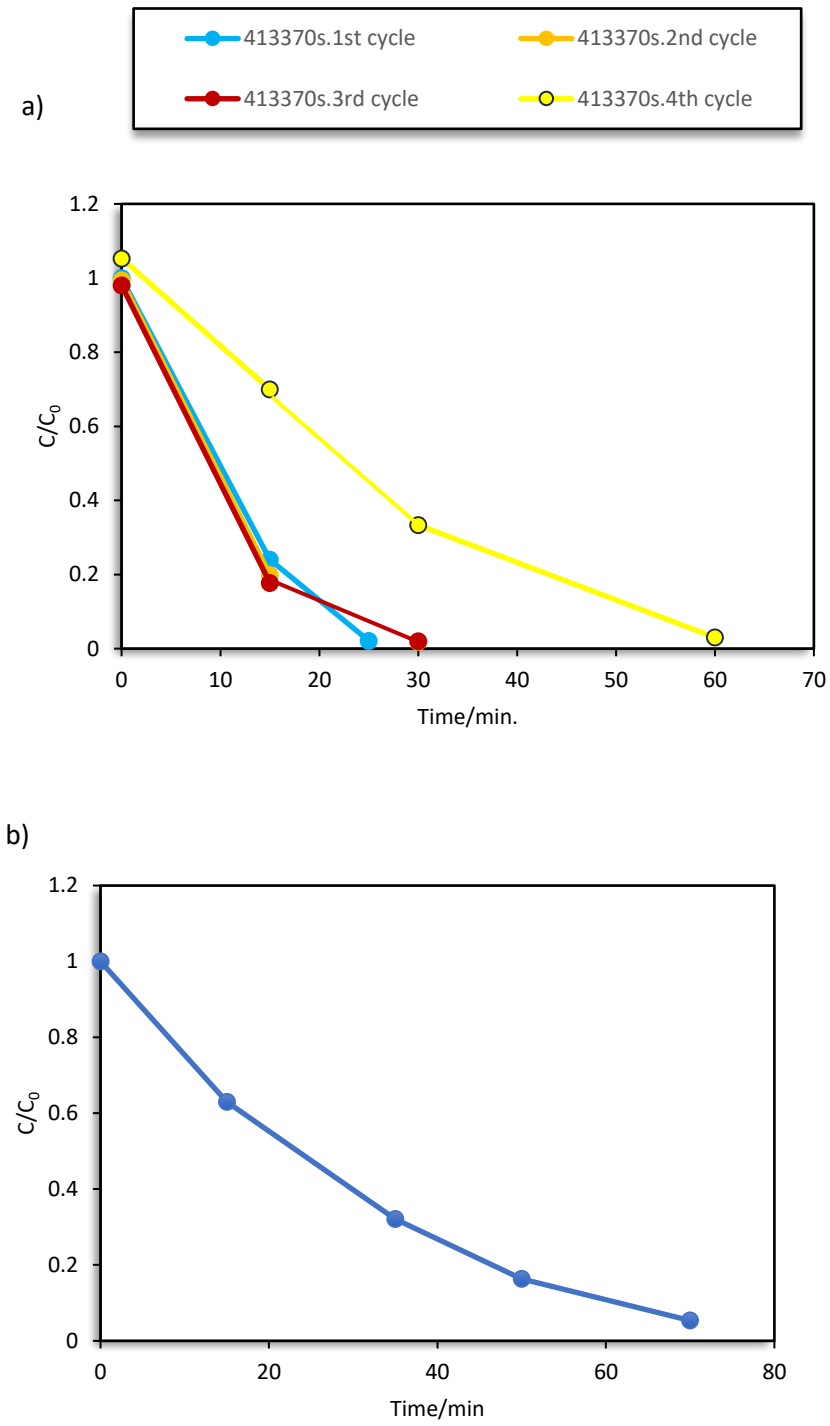

Figure 3.5.6. The graph of C/C_0 vs. time for a) 70˚C heat treated soft mesocrystal, and b) 1:4:10 ratios of silver phosphate at 100˚C vacuum.

The cation exchanged samples are also tested for their activity for the photodegradation of the same dye. Therefore, the same procedure is employed using 25 mg samples from each sample. In the cation exchange section, it is shown that the XRD pattern for each one display lines of crystalline Ag_3PO_4. In the Mn (90) case, there is weak silver and silver monophosphate lines in the XRD pattern; thus; the color is light yellow after cation exchange. It is expected that the samples obtained from Mn (90) will be more active. However, before this investigation, we expect that the higher activity will be observed from the sample with a higher surface area. The surface area follows the following trend; $Ni > Co > Mn$. According to this, the results Mn (90) will be the worst. Nevertheless, the obtained results do not fit both assumptions. Analysis of the XRD patterns and EDX spectra show that all metals of Co, Ni and Mn are in the solution; the cation exchange is complete. Another parameter could be the pore size of the starting precursors. Even though Ni (90) has the highest surface area, Co (90) pore size might be the best for cation exchange. SEM images show that the morphology of exchanged sample is best preserved in the Co (90) case. Therefore, the pore size could be more significant than surface area. The pores of Co (90) are clearly visible in their SEM images, but the pores of Ni (90) is only observed under TEM because the pores are much smaller and better ordered. The surface area Mn (90) is smaller but also the pore size and it is not as ordered as Co (90) and Ni (90). Therefore, the new order could be $Co > Ni > Mn$ in terms of porosity. Porosity could enhance the silver phosphate formation. However, enhancing silver phosphate formation may also enhance the silver and silver monophosphate formation. The samples of cation exchange reactions are also tested for photodegradation of organic dyes. Results show that the Co (90) products are the most active one but Mn (90) product

is almost inactive. Therefore, it is interesting and important to investigate what happens to the samples during cation exchange in the Mn (90). There is nothing in the literature showing this behavior.

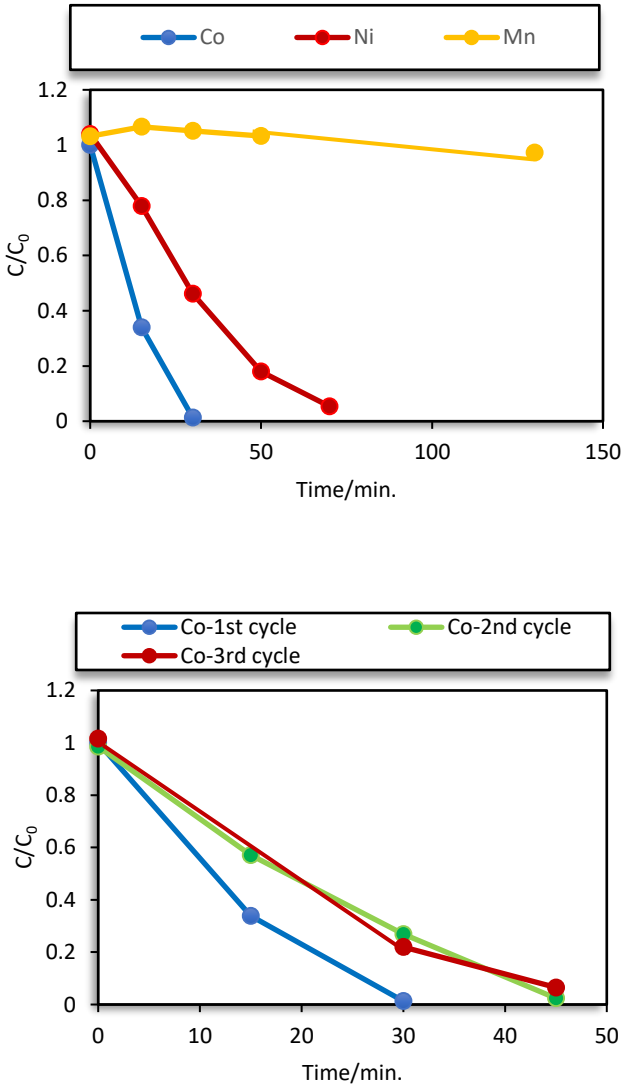

Figure 3.5.7. The graph of C/C_0 vs. time for cation exchange products of a) Co (90), Ni (90), Mn (90) and b) Co (90) three cycles.

3.6. The Future work on SNPA Lyotropic Liquid Crystalline Mesophases

In this section, we suggest new synthesis methods for the future research. In precipitate part, the different structure types were observed upon changing the amount of phosphoric acid in the initial solutions. Triangular silver phosphate particles are observed upon adding excess amount of phosphoric acid. Remember that to avoid soft mesocrystal formations, the mole ratio of phosphoric acid is added in excess. Phosphoric acid is also good solvent to dissolve surfactant. In other words, 1 g of $C_{12}E_{10}$ dissolves completely in 3.65 g of 85-88% phosphoric acid at 70˚C without stirring. 0.810 g silver nitrate can be dissolved in less than 1 ml water. Addition of above hot gel solution immediately produce a gel solution with a white monolithic, see Figure 3.6.1. This creature seems like a plastic; it is so soft and elastic. Washing this monolith with water, yellow particles are produced. The SEM images of this monolith without washing consist of small crystals, see Figure 3.6.2. But after washing process, observed under POM so fine and sharp crystals are obtained. This monolith needs to be further investigated that may initiate new directions.

Figure 3.6.1. Photographs of 1:3:20 $C_{12}E_{10}$:$AgNO_3$:H_3PO_4 solution after adding $AgNO_3$ solution.

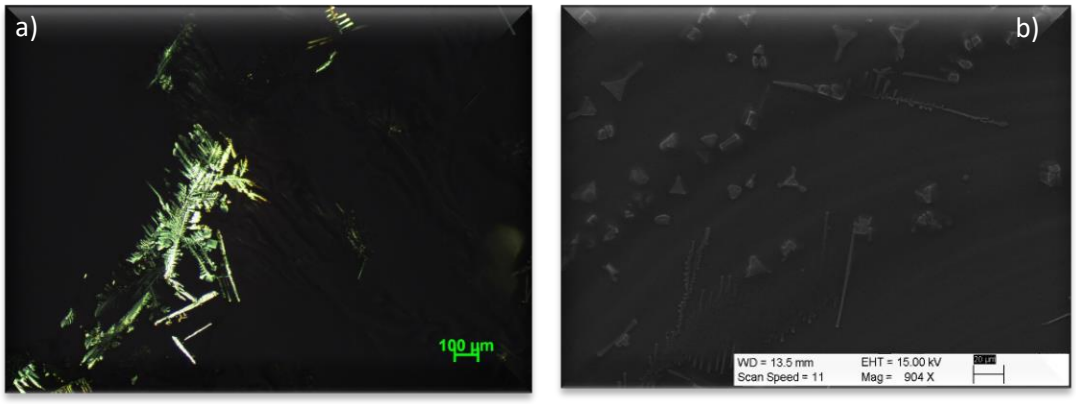

Figure 3.6.2. a) The POM image of 1:3:20 $C_{12}E_{10}$:$AgNO_3$:H_3PO_4 monolith after washing with water and b) the SEM image of 1:3:20 $C_{12}E_{10}$:$AgNO_3$:H_3PO_4 monolith before washing.

The silver phosphate films could also be tested as an electrode for solar cell, and water photo-oxidation processes. Soft mesocrystal covered glass after water evaporation might be used to make the electrodes. Increasing phosphoric acid to 10 mole ratios make sure sticking the films to the lass surface and this may improve the electrode quality on the glass slide or FTO surface.

4.CONCLUSION

In conclusion, a new SNPA thin film synthesis method has been investigated by considering the effects of temperature, amount of phosphoric acid, nitric acid, surfactant, using different silver salts. It is known that silver phosphate is an excellent photocatalyst and semiconductor electrode. Salt-surfactant lyotropic liquid mesophase creates a media to produce different structures, morphology, and porosity. The silver salt-phosphoric acid-surfactant also form LLC mesophases that gradually transforms to a soft mesocrystal. At 150˚C, mesostructured silver phosphate thin films transform to highly crystalline Ag_3PO_4 and silver metal. Freshly coated films slowly undergo mesocrystallization with an undefined structure that diffracts at both small and high angles. ATR-IR spectra and POM images display unique characteristic peaks and needle like features, respectively. ATR-IR data show that the mesocrystals do not keep water and display sharp nitrate and phosphate peaks, indicating crystallinity of some kind. Soft mesocrystals can be heat treated at low temperature (70-150˚C) to start the reaction to form mesostructured particles, but the films are obtained when phosphoric acid amount is increased in the media.

Clear water and ethanol solutions are not stable and produce precipitates as crystalline bulk Ag_3PO_4. These crystallites are highly active for photo-degradation organic dyes. However, during degradation process, Ag_3PO_4 slowly degrades to silver metal. To solve stability problem of silver phosphate, we employed two methods, in one we used surfactant as a carbon source to introduce carbon coating of Ag_3PO_4 particles and the other is the cation exchange method. Introducing carbon improves the stability. Specifically, the samples obtained from 1:4:1.33 ($C_{12}EO_{10}$:Ag(I):H_3PO_4) composition

produced stable Ag_3PO_4 towards dye degradation. Fast silver metal formation degrades the silver phosphate towards dye degradation (such as in the presence of high dye concentrations and exposing to intense light), but at low dye concentration and low beam intensity, the silver metal formation also helps to stabilize the silver phosphate, due to effective transfer of photo-generated electrons from Ag_3PO_4 to Ag metal. These electrons are not as reactive towards reduction of silver ion (due to solubility of Ag_3PO_4 in aqueous media) in the media. Therefore, silver-phosphate thin films could be effectively used for further applications.

Last but not least, cation exchange method opened a new window for the synthesis of porous silver phosphates. Pre-formed mesoporous $LiMPO_4$ (M = Mn, Co, and Ni) powder can be used effectively as a phosphate source and a template to produce mesoporous Ag_3PO_4 through simple cation exchange mechanism. Exchange reactions are very slow and sluggish in pure water and methanol, but their mixture (1:9 volume ratio of methanol:water solution) is an effective media for the cation exchange process. In water media, first of all the exchange process is too long and in such long time silver or silver monophosphate form as a side product. Another important effect seems like the pore size of the precursor/template rather than surface area. This needs to be further investigated to fully understand how pore size affects the exchange process. The material with the highest pore size acted as a best template with an increased stability. The material with the lowest pore size decreases the sensitivity towards visible light irradiation. Cation exchange process needs to be further investigated to determine the effects of various parameters.

Overall, mesocrystal formation limits the LLC templating process to produce mesoporous Ag_3PO_4 but it can be a new synthesis precursor for Ag_3PO_4 production in the form of powders and thin films. Further studies are required to fully characterize the powders and thin films. However, the LLC templating method works well for the synthesis of mesoporous $LiMPO_4$ that can be used as template to produce porous Ag_3PO_4 particles.

Bibliography

[1] W. D. Callister, and D. G. Rethwisch, Materials Science and Engineering An Introduction 7th ed., United States of America: John Wiley & Sons, 2007.

[2] M. Fischetti, and W. G. Vandenberghe, "The Electronic Structure of Crystals: Theoretical Framework," in *Advanced Physics of Electron Transport in Semiconductors and Nanostructures*, Switzerland, Springer Nature, 2016, pp. 57-69.

[3] S. Giménez, and J. Bisquert , "Semiconductor Electrochemistry," in *Photoelectrochemical Solar Fuel Production*, Switzerland , Springer Nature , 2016, pp. 3-40.

[4] W. H. Brattain, and C. G. B. Garrett, "Experiments on the Interface between Germanium and an Electrolyte," *Bell LabsTechnical Journal*, vol. 34, no. 1, pp. 129-176, 1955.

[5] R. W. G. Wyckoff, "Crystal Structure of Silver Phosphate and Silver Arsenate (Ag_3XO_4)," *Americal Journal of Society*, vol. 10, pp. 107, 1925.

[6] L. Helmholz, "The Crystal Structure of Silver Phosphate," *Journal of Chemical Physics* , vol. 4, pp. 316-322, 1936.

[7] H. N. Ng, C. Calvo, and R. Faggiani , "A New Investigation of the Structure of Silver Orthophosphate," *Acta Cryst.* , vol. B34, pp. 898-899 , 1978.

[8] Z. Yi, J. Ye, N. Kikugawa, T. Kako, S. Ouyang, H. Stuart-Williams, H. Yang, J. Cao, W. Luo, Z. Li, Y. Liu, and R. L. Withers, "Anorthophosphatesemiconductorwith photooxidationpropertiesunder visible-lightirradiation," *Nature Materials,* vol. 9, pp. 559-564, 2010.

[9] D. J. Martin, G. Liu, S. J. A. Moniz, Y. Bi, A. M. Beale, J. Ye and J. Tang, "Efficient visible driven photocatalyst, silver phosphate: performance, understanding and perspective," *Chem. Soc. Rev.*, vol. 44, pp. 7808-7828, 2015.

[10] J. O. Carneiro, A. P. Samantilleke, P. Parpot, F. Fernandes, M. Pastor, A. Correia, E. A. Luís, A. A. Chivanga Barros, and V. Teixeira, "Visible Light Induced Enhanced Photocatalytic Degradation of Industrial Effluents (Rhodamine B) in Aqueous Media Using TiO_2 Nanoparticles," *Journal of Nanomaterials,* vol. 2016, pp. 1-13, 2016.

[11] Y. Li, W. Xie, X. Hu, G. Shen, X. Zhou, Y. Xiang, X. Zhao, and P. Fang, "Comparison of Dye Photodegradation and its Coupling with Light-to-Electricity Conversion over TiO_2 and ZnO," *Langmuir,* vol. 26, no. 1, pp. 591–597, 2010.

[12] Y. Yu, T. He, L. Guo, Y. Yang, L. Guo, Y. Tang, and Y. Cao, "Efficient visible-light photocatalytic degradation system assisted by conventional Pd catalysis," *Scientific Reports*, vol. 5, 2015.

[13] L. Wang, J. Shang, W. Hao, S. Jiang, S. Huang, T. Wang, Z. Sun, Y. Du, S. Dou, T. Xie, D. Wang, and J. Wang, "A dye-sensitized Visible Light photocatalyst-$Bi_{24}O_{31}C_{110}$," *Scientific Reports,* vol. 4, 2014.

[14] M. Ge, N. Zhu, Y. Zhao, J. Li, and L. Liu, "Sunlight-Assisted Degradation of Dye Pollutants in Ag_3PO_4 Suspension," *Ind. Eng. Chem. Res*, vol. 51, pp. 5167−5173, 2012.

[15] Y. Xie, and C. Yuan, "Visible-light Responsive Cerium Ion Modified Titania sol and Nanocrystallites for X-3B Dye Photodegradation," *Applied Catalysis B: Environmental*, vol. 46, no. 2, pp. 251-259, 2003.

[16] T. Chai, Y. Liu, L. Wang, S. Zhang, Y. Zeng, J. Yuan, J. Ma, W. Dong, C. Liu, and S. Luo , "Silver Phosphate-based Z-Scheme Photocatalytic System with Superior Sunlight Photocatalytic Activities and Anti-photocorrosion Performance," *Applied Catalyst B: Environmental*, vol. 208, pp. 1-13, 2017.

[17] Q. Xiang, D. Lang, T. Shen, and F. Liu, "Graphene-Modified Nanosized Ag_3PO_4 Photocatalysts for Enhanced Visible-Light Photocatalytic Activity and Stability," *Applied Catalyst B: Environmental*, vol. 162, pp. 196-203, 2015.

[18] J. Ma, Q. Liu, L. Zhu, J. Zuo, K. Wang, and M. Yang, "Visible Light Photocatalyticactivity Enhancement of Ag_3PO_4 Dispersed on Exfoliated Bentonite for Degradation of Rhodamine B," *Applied Catalystis B: Environmental*, vol. 182, pp. 26-32, 2016.

[19] M. Niraula, S. Adhikari, D. Y. Lee, E. Kim, S. J. Yoon, S. K. Dhungel, W. Lee, N. K. Shresta, and S. Han, "Titania Nanotube-Silver Phosphate Hybrid Heterostructure for Improved Visible Light Induced Photocatalysis," *Chemical Physics Letters*, vol. 593, pp. 193-197, 2014.

[20] P. S. Suad, B. Pant, A. P. Twari, Z. K. Ghouri, M. Park, and H. Kim, "Effective Photocatalytic Efficacy of Hydrothermally Synthesized Silver Phosphate Decorated Titanium Dioxide Nanocomposite Fibers," *Journal of Colloid and Interface Science* , vol. 465, pp. 225-232, 2016.

[21] C. Dinh, T. Nguyen, F. Kleitz, and T. Do, "Large-Scale Synthesis of Uniform Silver Orthophosphate Colloidal Nanocrystals Exhibiting High Visible Light Photocatalytic Activity," *Chem. Commun.*, vol. 47, pp. 7797–7799 , 2011.

[22] Q. Liang, W. Ma, Y. Shi, Z. Li, and X. Yang, "Hierarchical Ag_3PO_4 Porous Microcubes with Enhanced Photocatalytic Properties Synthesized with The Assistance of Trisodium Citrate," *CrystEngComm,* vol. 14, pp. 2966–2973 , 2012.

[23] J. Liu, C. Luo, J. Wang, X. Yang, and X. Zhong, "Controlled Synthesis of Silver Phosphate Crystals with High Photocatalytic Activity and Bacteriostatic Activity," *CrystEngComm,* vol. 14, pp. 8714–8721 , 2012.

[24] Y. Bi, H. Hu, S. Ouyang, G. Lu, J. Cao, and J. Ye, "Photocatalytic and Photoelectric Properties of Cubic Ag_3PO_4 Sub-Microcrystals with Sharp Corners and Edges," *Chem. Commun.*, vol. 38, pp. 3748–3750 , 2012.

[25] Y. Bi, H. Hu, Z. Jiao, H. Yu, G. Lu, and J. Ye, "Two-Dimensional Dendritic Ag_3PO_4 Nanostructures and Their Photocatalytic Properties," *Phys. Chem. Chem. Phys.*, vol. 14, pp. 14486–14488 , 2012.

[26] S. Zhang, X. Gu, Y. Zhao, and Y. Qiang, "Effect on Annealing Temperature of Time on Structure, Morphology, and Visible-Light Photocatalytic Activities Ag_3PO_4 Microparticles," *Materials Science and Engineering B,* vol. 201, pp. 57-65, 2015.

[27] J. Yang, C. Zheng, Y. Wang, and M. Guo, "Phosphate-Assited One-Pot Synthesis of Silver Phosphate-Mesoporous Silica Composite From Sodium Silicate and Silver Nitrate," *Microporous and Mesoporous Materials,* vol. 204, pp. 58-61, 2015.

[28] L. Liu, Y. Qi, J. Lu, W. An, Y. Liang, and W. Cui, "A Stable Ag_3PO_4@g-C_3N_4 Hybrid Core@Shell Composite with Enhanced Visible Light Photocatalytic Degradation," *Applied Catalysis B: Environmental ,* vol. 183, pp. 133-141, 2016.

[29] T. Geelhaar, K. Griesar, and B. Reckmann, "125 Years of Liquid Crystals—A Scientific Revolution in the Home," *Angew. Chem. Int. Ed. ,* vol. 52, pp. 8798 – 8809, 2013.

[30] D. Andrienko, "Introduction to Liquid Crystals," *Journal of Molecular Liquids,* 2018.

[31] I. Tadwee, S. Shahi, V. Ramteke, and I. Syed, "Liquid Crystals Pharmaceutical Application: A Review," *Int. J. of Pharm. Res. & All. Sci,* vol. 1, no. 2, pp. 06-11, 2012.

[32] E. Tunkara, Lyotropic Liquid Crystalline (LLC) Phosphoric Acid 10-Lauryl Ether: Mesophases, Proton Conductivity and Synthesis of Transparent Mesoporous Hydroxyapatite Thin Films, Master of Science, Ankara: Bilkent University, 2014.

[33] B. Bahadur, Liquid Crsytals Applications and Uses, Singapore: World Scientific Publishing Co. Pte. Ltd., 1990.

[34] G. H. Brown, "Molecular Geometry and the Properties of Nonamphilic Liquid Crystals," in *Advances in Liquid Crystals*, London, Academic Press, Inc., 1976, pp. 2.

[35] R. Zana, M. Benrraou, and R. Rueff, "Alkanediyl-α,ω-bis(dimethylalkylammonium bromide) Surfactants. 1. Effect of the Spacer Chain Length on the Critical Micelle Concentration and Micelle Ionization Degree," *Langmuir*, vol. 7, pp. 1072-1075, 1991.

[36] P. Sakya, J. M. Seddon, R. H. Templer, R. J. Mirkin, and G. J. T. Tiddy, "Micellar Cubic Phases and Their Structural Relationships: The Nonionic Surfactant System $C_{12}EO_{10}$/Water," *Langmuir*, vol. 13, no. 14, pp. 3706-3714, 1997.

[37] J. S. Beck, J. C. Vartuli, W. J. Roth, M. E. Leonowicz, C. T. Kresge, K. D. Schmitt, C. T-W. Chu, D. H. Olson, E. W. Sheppard, S. B. McCullen, J. B. Higgins, and J. L. Schlenkert , "A New Family of Mesoporous Molecular Sieves Prepared with Liquid Crystal Templates," *J. Am. Chem. SOC*, vol. 114, no. 27, pp. 10384-10843, 1992.

[38] G. S. Attard, C. G. Göltner, J. M. Corker, S. Henke, and R. H. Templer, "Liquid-Crystal Templates for Nanostructured Metals," *Angeu. Chem. In,. Ed. EngI.*, vol. 36, no. 12, pp. 1315-1317, 1997.

[39] Y. Wan, and D. Zhao, "On the Controllable Soft-Templating Approach to Mesoporous Silicates," *Chemical Reviews,* vol. 107, no. 7, pp. 2821-2860, 2006.

[40] Ö. Çelik, and Ö. Dag, "A New Lyotropic Liquid Crystalline System: Oligo(ethylene oxide) Surfactants with $[M(H_2O)_n]X_m$ Transition Metal Complexes," *Angew. Chem. Int. Ed. ,* vol. 40, no. 20, pp. 3799-3803, 2001.

[41] Ö. Dag, I. Soten, Ö. Çelik, S. Polarz, N. Coombs, and G.A. Ozin, "Solventless Acid-Free Synthesis of Mesostructured Titania: Nanovessels for Metal Complexes and Metal Nanoclusters," *Advanced Functional Materials,* vol. 13, no. 1, pp. 30-36, 2003.

[42] B. Jiang, C. Li, Ö. Dag, H. Abe, T. Takei, T. Imai, Md. S. A. Hossain, Md. T. Islam, K. Wood, J. Henzie, and Y. Yamauchi, "Mesoporous Metallic Rhodium Nanoparticles," *Nature Communications,* vol. 8, 2017.

[43] E. B. Olutaş, F. M. Balcı, and Ö. Dag, "Strong Acid–Nonionic Surfactant Lyotropic Liquid-Crystalline Mesophases as Media for the Synthesis of Carbon Quantum Dots and Highly Proton Conducting Mesostructured Silica Thin Films and Monoliths," *Langmuir,* vol. 31, pp. 10265–10271, 2015.

[44] Ö. Dag, S. Alayoğlu, C. Tura, and Ö. Çelik, "Lyotropic Liquid-Crystalline Phase of Oligo(ethylene oxide) Surfactant/Transition Metal Salt and the Synthesis of Mesostructured Cadmium Sulfide," *Chem. Mater.,* vol. 15, pp. 2711-2717, 2003.

[45] E. Yılmaz, Investigation of Lithium Salts-Nonionic Surfactant Lyotropic Liquid Crystalline Mesophases in a Dye Sensitized Solar Cell as Gel Electrolytes, Ankara: Bilkent University, 2015.

[46] C. Karakaya, Y. Türker, and Ö. Dag, "Molten-Salt-Assisted Self-Assembly (MASA)-Synthesis of Mesoporous Metal Titanate-Titania, Metal Sulfide-Titania, and Metal Selenide-Titania Thin Films," *Adv. Funct. Mater.*, vol. 23, pp. 4002–4010, 2013.

[47] H. Yang, N. Coobms, and G. A. Ozin, "Morphogenesis of Shapes and Surface Patterns in Mesoporous Silica," *Nature,* vol. 386, pp. 692-695, 1997.

[48] C. G. Göltner, S. Henke, M. C. Weissenberger, and M. Antonietti, "Mesoporous Silica from Lyotropic Liquid Crystal Polymer Templates," *Angew. Chem. Int. Ed.*, vol. 37, no. 5, pp. 613-616, 1998.

[49] B. T. Yonemoto, G. S. Hutchings, and F. Jiao, "A General Synthetic Approach for Ordered Mesoporous Metal Sulfides," *J. Am. Chem. Soc.*, vol. 136, no. 25, pp. 8895–8898, 2014.

[50] C. Karakaya, Y. Türker, C. Albayrak, and Ö Dag, " Assembly of Molten Transition Metal Salt-Surfactant in a Confined Space for Synthesis of Mesoporous Metal Oxide-Rich Metal Oxide-Silica Thin Films,"*Chem. Mater.*, vol. 23, pp. 3062–3071, 2011.

[51] M. A. Carreon, and V. V. Guliants, "Ordered Meso- and Macroporous Binary and Mixed Metal Oxides," *Eur. J. Inorg. Chem.,* vol. 2005, no. 1, pp. 27–43 , 2004.

[52] J. H. Ding, and D. L. Gin, "Catalytic Pd Nanoparticles Synthesized Using a Lyotropic Liquid Crystal Polymer Template," *Chem. Mater.,* vol. 12, pp. 22-24, 2000.

[53] T. Kijima, T. Yoshimura, M. Uota, T. Ikeda, D. Fujikawa, S. Mouri, and S. Uoyama, "Noble-Metal Nanotubes (Pt, Pd, Ag) from Lyotropic Mixed-Surfactant Liquid-Crystal Templates," *Angew. Chem.* , vol. 116, pp. 230-234, 2004.

[54] D. Blunk, P. Bierganns, N. Bongartz, R. Tessendorf, and C. Stubenrauch, "New Speciality Surfactants with Natural Structural Motifs," *New Journal of Chemistry*, vol. 30, pp. 1705–1717, 2006.

[55] H. Cölfen, and M. Antonietti, "Mesocrystals: Inorganic Superstructures Made by Highly Parallel Crystallization and Controlled Alignment," *Angew. Chem. Int. Ed*, vol. 44, pp. 5576 – 5591, 2005.

[56] M. Niederberger, and H. Cölfen, "Oriented Attachment and Mesocrystals: Non-classical Crystallization Mechanisms Based on Nanoparticle Assembly," *Phys. Chem. Chem. Phys.*, vol. 8, pp. 3271–3287, 2006.

[57] S. D. Bella, and J. M. Garcia-Ruiz, "Textures in Induced Morphology Crystal Aggregates of $CaCO_3$: Sheaf of Wheat Morphologies," *Journal of Crystal Growth*, vol. 79, no. 1-3, pp. 236-240, 1986.

[58] E. V. Sturm and H. Cölfen , "Mesocrystals: Past, Presence, Future," *Crystals,* vol. 7, no. 207, pp. 1-17, 2017.

[59] C. Albayrak, G. Barım, and Ö. Dag, "Lyotropic Liquid Crystal to Soft Mesocrystal Transformation in Hydrated Salt–Surfactant Mixtures," *Chem. Eur. J.* , vol. 19, pp. 15026–15035, 2013.

[60] A. Clearfield, "Role of Ion Exchange in Solid-State Chemistry," *Chem. Rev.* , vol. 88, pp. 125-148, 1988.

[61] G.G. Hollmana, G. Steenbruggena, and M. Janssen-Jurkovičová, "A two-step Process for the Synthesis of Zeolites from Coal Fy Ash," *Fuel,* vol. 78, pp. 1225–1230 , 1999.

[62] D. H. Son, S. M. Hughes, Y. Yin, and A. P. Alivisatos, "Cation Exchange Reactions in Ionic Nanocrystals," *Science,* vol. 306, pp. 1009-1012, 2004.

[63] D. Ha, A. H. Caldwell, M. J. Ward, S. Honrao, K. Mathew, R. Hovden, M. K. A. Koker, D. A. Muller, R. G. Hennig, and R. D. Robinson, "Solid−Solid Phase Transformations Induced through Cation Exchange and Strain in 2D Heterostructured Copper Sulfide Nanocrystals," *Nano Lett.,* vol. 14, pp. 7090−7099, 2014.

[64] J. B. Rivesta, and P. K. Jain, "Cation Exchange on the Nanoscale: an Emerging Technique for New Material Synthesis, Device Fabrication, and Chemical Sensing," *Chem. Soc. Rev.,* vol. 42, pp. 89-96 , 2013.

[65] H. Lin, J. Cao, B. Luo, B. Xu, and S. Chen, "Synthesis of Novel Z-scheme AgI/Ag/AgBr Composite with Enhanced Visible Light Photocatalytic Activity," *Catalysis Communications* , vol. 21, pp. 91-95, 2012.

[66] Q. Zhu, W. Wang, L. Lin, G. Gao, H. Guo, H. Du, and A. Xu, "Facile Synthesis of the Novel Ag_3VO_4/AgBr/Ag Plasmonic Photocatalyst with Enhanced Photocatalytic Activity and Stability," *J. Phys. Chem. C* , vol. 117, pp. 5894−5900, 2013.

[67] J. Yu, J. Zhang, and S. Liu , "Ion-Exchange Synthesis and Enhanced Visible-Light Photoactivity of CuS/ZnS Nanocomposite Hollow Spheres," *J. Phys. Chem. C* , vol. 114, pp. 13642–13649, 2010.

[68] X. Zou, P. Wang, C. Li, Jun Zhao, D. Wang, T. Asefa, and G. Li, "One-pot Cation Exchange Synthesis of 1D Porous CdS/ZnO Heterostructures for Visible-Light-Driven H_2 Evolution," *Journal of Materials Chemistry A,* vol. 2, pp. 4682–4689 , 2014.

[69] E. Tunkara, and Ö. Dag, "Salt-Acid-Surfactant Lyotropic Liquid Crystalline Mesophases: Synthesis of Highly Transparent Mesoporous Calcium Hydroxyapatite Thin Films," *European Journal of Inorganic Chemistry*, vol. 2016, no. 13-14, pp. 2114-2121, 2015.

[70] G. Botelho, J.C. Sczancoski, J. Andres, L. Gracia, and E. Longo, "Experiemntal and Theoretical Study ob Structure, Optical Properties, and Growth of Metallic Silver Nanostructures in Ag_3PO_4," *J. Phys. Chem. C,* vol. 119, pp. 6293-6306, 2015.

[71] H.B. Ortíz-Oliveros, R.Ma. Flores-Espinosa, E. Ordoñez-Regil, and S.M. Fernández-Valverde, "Synthesis of a-Ti$(HPO_4)_2H_2O$ and sorption of Eu (III)," *Chemical Engineering Journal*, vol. 236, pp. 398–405, 2014.

[72] P. L. Stanghellini, E. Boccaleri, E. Diana, G. Alberti, and R. Vivani, "Vibrational Study of Some Layered Structures Based on Titanium and Zirconium Phosphates," *Inorg. Chem.*, vol. 43, pp. 5698−5703, 2004.

[73] B. B. Sahu, and K. Parida, "Cation Exchange and Sorption Properties of Crystalline α-Titanium(IV) Phosphate," *Journal of Colloid and Interface Science*, vol. 248, pp. 221–230 , 2002.

[74] S. C. Carmen, L.I. Simona, L. C. Phillippe, V. C. Liliana, P. Daniela, "Antibacterial Activity of Silver-Doped Hydroxyapatite Nanoparticles Against Gram-Positive and Gram-Negative Bacteria," *Nano Research Letters*, 2012.

[75] G. Naja, P. Bouvrette , S. Hrapovic, and J. H. T. Luong, "Raman-based Detection of Bacteria Using Silver Nanoparticles Conjugated with Antibodies," *Analyst*, vol. 132, pp. 679-686, 2007.

[76] N. Canbolat, "Wikimedia Commons," 11 11 2015. [Online]. Available: https://commons.wikimedia.org/wiki/File:Nuve6.jpg. [Accessed 08 05 2018].

[77] W. Xu, S. Zhu, Y. Liang, Z. Li, Z. Cui, X. Yang, and A. Inoue, "Nanoporous CuS with Excellent Photocatalytic Property," *Scientific Reports* , vol. 5, 2015.